OULU 2022
C 833

ACTA UNIVERSITATIS OULUENSIS

Laddu Praneeth Roshan Jayasinghe

COORDINATED MULTIANTENNA INTERFERENCE MITIGATION TECHNIQUES FOR FLEXIBLE TDD SYSTEMS

UNIVERSITY OF OULU GRADUATE SCHOOL;
UNIVERSITY OF OULU,
FACULTY OF INFORMATION TECHNOLOGY AND ELECTRICAL ENGINEERING

ACTA UNIVERSITATIS OULUENSIS
C Technica 833

LADDU PRANEETH ROSHAN JAYASINGHE

COORDINATED MULTIANTENNA INTERFERENCE MITIGATION TECHNIQUES FOR FLEXIBLE TDD SYSTEMS

Academic dissertation to be presented, with the assent of the Doctoral Programme Committee of Information Technology and Electrical Engineering of the University of Oulu, for public defence in the Wetteri auditorium (IT115), Linnanmaa, on 29 June 2022, at 12 noon

UNIVERSITY OF OULU, OULU 2022

Acta Univ. Oul. C 833, 2022

Supervised by
Professor Antti Tölli
Professor Matti Latva-aho

Reviewed by
Professor Tommy Svensson
Professor Dirk Slock

Opponent
Docent Mikael Coldrey

ISBN 978-952-62-3349-9 (Paperback)
ISBN 978-952-62-3350-5 (PDF)

ISSN 0355-3213 (Printed)
ISSN 1796-2226 (Online)

Cover Design
Raimo Ahonen

PUNAMUSTA
TAMPERE 2022

Jayasinghe, Laddu Praneeth Roshan, Coordinated multiantenna interference mitigation techniques for flexible TDD systems.
University of Oulu Graduate School; University of Oulu, Faculty of Information Technology and Electrical Engineering
Acta Univ. Oul. C 833, 2022
University of Oulu, P.O. Box 8000, FI-90014 University of Oulu, Finland

Abstract

This dissertation presents cooperative beamformer techniques and possible practical implementations to mitigate the sophisticated interference scenarios in dynamic time-division-duplexing (TDD) systems and integrated access and backhaul (IAB) networks. Greater emphasis is placed on the distributed resource allocation to facilitate simultaneous uplink (UL) and downlink (DL) data transmission by employing multiple-input multiple-output (MIMO) beamformer techniques and bi-directional signalling schemes with different objectives to optimize network utilities while acknowledging important practical considerations and future traffic demand.

The first half of this thesis focuses on dynamic TDD systems, in which available resources per cell can be freely allocated to either UL or DL depending on the instantaneous traffic demand. Hence, complicated UL-DL and DL-UL interference scenarios arise due to simultaneous UL and DL data transmission in adjacent cells. Primary attention is given to mitigation of catastrophic interference exposure in dynamic TDD systems by employing MIMO based decentralized iterative beamforming techniques with traffic-aware network optimization objectives, supported with minimal information exchange among the coordinated base stations (BSs) and user-equipments (UEs). Bi-directional forward-backward training via spatially precoded over-the-air pilot signalling is used to facilitate coordinated beamforming. Novel bi-directional beamformer training strategies and methods for direct estimation (DE) of the stream specific beamformers are developed for each intermediate beamformer update, using overlapping and non-orthogonal pilots.

The latter half of this thesis considers an IAB network consisting of a BS, IAB-relays, and UEs. Both BS and IAB-relay provide access to UEs while BS and relays exchange UEs data via a wireless in-band backhaul using the same frequency-time resources shared with access links. A flexible TDD-based IAB network is considered where IAB-relays and BS are assigned to different UL or DL transmission modes to circumvent conventional half-duplex loss at the IAB-relay. An iterative beamformer design is proposed to jointly handle the resulting cross-channel interference over two consecutive data delivery intervals required for transmission and reception between the BS and UEs via half-duplex IAB-relays. Dynamic traffic behaviour is dealt with via weighted queue minimization objective for which user-specific UL/DL queues are also introduced at IAB-relays to guarantee reliable end-to-end data delivery. Bi-directional forward-backward training via spatially precoded over-the-air pilot signalling allows decentralized beamformer design across all the nodes. A novel user assignment method is proposed to allocate users into BS or IAB-relays considering long-term channel statistics and practical IAB limitations.

Keywords: coordinated beamforming, direct estimation, dynamic or flexible TDD, integrated access and backhaul, pilot decontamination, weighted queue minimization, weighted sum rate maximization

Jayasinghe, Laddu Praneeth Roshan, Koordinoidut moniantennihäiriön vaimennustekniikat joustaville TDD-järjestelmille.
Oulun yliopiston tutkijakoulu; Oulun yliopisto, Tieto- ja sähkötekniikan tiedekunta
Acta Univ. Oul. C 833, 2022
Oulun yliopisto, PL 8000, 90014 Oulun yliopisto

Tiivistelmä

Tämä väitöskirja esittelee yhteistoiminnallisia keilanmuodostustekniikoita ja mahdollisia käytännön toteutuksia monimutkaisten häiriöskenaarioiden lieventämiseksi dynaamisissa aikajakoduplekssointijärjestelmissä (TDD) ja integroiduissa pääsy- ja backhaul-verkoissa (IAB). Enemmän painoarvoa on annettu hajautettuun resurssien allokoi, joka mahdollistaa samanaikaisen uplink (UL) ja downlink (DL) tiedonsiirron käyttämällä moniantennijärjestelmän (MIMO) keilanmuodostustekniikat ja kaksisuuntaiset signalointimenetelmät, joilla on eri tavoitteet verkon apuohjelmien optimoimiseksi, samalla kun otetaan huomioon tärkeät käytännön näkökohdat ja tuleva dataliikenteen kysyntä.

Tämän opinnäytetyön ensimmäinen puolisko keskittyy dynaamisiin TDD-järjestelmiin, joissa käytettävissä olevat resurssit solua kohden voidaan allokoida vapaasti joko UL:lle tai DL:lle riippuen hetkellisestä liikennetarpeesta. Tästä syystä syntyy monimutkaisia UL-DL- ja DL-UL-häiriöskenaarioita, jotka johtuvat samanaikaisesta UL- ja DL-tiedonsiirrosta viereisissä soluissa. Ensisijainen huomio kiinnitetään katastrofaalisen häiriöaltistuksen lieventämiseen dynaamisissa TDD-järjestelmissä käyttämällä MIMO-pohjaista hajautettuja iteratiivisia keilanmuodostustekniikoita liikennetietoisilla verkon optimointitavoitteilla, joita tuetaan minimaalisella tiedonvaihdolla koordinoitujen tukiasemien (BSs) ja käyttäjälaitteiden välillä (UEs). Kaksisuuntaista eteenpäin-taakse-koulutusta spatiaalisesti esikoodatun over-the-air-pilottisignaloinnin avulla käytetään koordinoidun säteenmuodostuksen helpottamiseksi. Uusia kaksisuuntaisia keilanmuodostajien koulutusstrategioita ja menetelmiä keilanmuodostajien suoraa estimointia (DE) varten kehitetään jokaista välikeilanmuodostajan päivitystä varten käyttämällä päällekkäisiä ja ei-ortogonaalisia pilotteja.

Tämän väitöskirjan jälkimmäinen puolisko käsittelee IAB-verkkoa, joka koostuu BS:stä, IAB-releistä ja UE:ista. Sekä BS että IAB-rele tarjoavat pääsyn UE:ihin, kun taas BS ja releet vaihtavat UE:iden dataa langattoman kaistan sisäisen backhaul-yhteyden kautta käyttämällä samoja taajuus-aikaresursseja, jotka jaetaan pääsylinkkien kanssa. Joustavaa TDD-pohjaista IAB-verkkoa harkitaan, jossa IAB-välittimet ja BS on määritetty eri UL- tai DL-lähetystiloihin, jotta voidaan kiertää IAB-releen tavanomaiset half-duplex-häviöt. Iteratiivista keilanmuodostajan rakennetta ehdotetaan käsittelemään samanaikaisesti tuloksena olevaa kanavien välistä häiriötä kahdella peräkkäisellä tiedonsiirtovälillä, jotka tarvitaan lähetykseen ja vastaanottoon BS:n ja UE:iden välillä half-duplex IAB-releiden kautta. Dynaamista liikennekäyttäytymistä käsitellään painotetulla jonojen minimointitavoitteella, jota varten IAB-releissä otetaan käyttöön myös käyttäjäkohtaisia UL/DL-jonoja luotettavan päästä-päähän tiedonsiirron takaamiseksi. Kaksisuuntainen eteenpäin-taakse-koulutus spatiaalisesti esikoodatun over-the-air pilottisignaloinnin avulla mahdollistaa hajautetun keilanmuodostajan suunnittelun kaikissa solmuissa. Uutta käyttäjämääritysmenetelmää ehdotetaan käyttäjien allokoimiseksi BS- tai IAB-välitteisiin ottaen huomioon pitkän aikavälin kanavatilastot ja käytännön IAB-rajoitukset.

Asiasanat: dynaaminen tai joustava TDD, integroitu pääsy ja takaisinkytkentä, koordinoitu säteenmuodostus, painotettu jonominimointi, painotettu summan maksimointi, pilottien puhdistaminen, suora arviointi

To My Family.

Preface

The research studies included in this doctoral thesis were conducted at the Centre for Wireless Communications (CWC) and the communications Engineering Department, University of Oulu, Finland, during 2014-2020. While working towards this thesis, I have gained immense personal and scientific benefits from all my superiors, industry partners and colleagues, all of whom I would like to thank.

First, I am very much grateful to my principal supervisor Professor Antti Tölli, for allowing me to pursue doctoral studies under his supervision. The continued support, encouragement, and guidance from him over the years have been invaluable, and I wish to thank him for that. Secondly, I am very grateful and want to thank my second supervisor, Professor Matti Latva-Aho, for the enormous support he has given to me during my masters and doctoral student period by supervising and taking care of my financial needs. In addition, I wish to thank the thesis reviewers, Professor Tommy Svensson from the Chalmers University of Technology, Sweden, and Professor Dirk Slock from EURECOM, France, for having the patience to read my thesis and for providing constructive comments. I also thank Professor Markku Juntti for being an excellent supervisor for my master thesis.

During the years with the CWC, I have had the privilege to contribute to multiple CWC projects such as the 5Gto10G (5G radio access solutions to 10 GHz and beyond frequency bands), and the high5 projects. I would like to thank the managers of these projects and Adjunct Professor Pekka Pirinen. A special thank you goes to him for being such a flexible person and for the guidance and support he provided as the follow-up group chairperson. As well as this, special thanks goes to Professor Nandana Rajatheva and Dr. Satya Joshi for the constant support provided during my study, and to my research collaborators, Dr. Jarkko Kaleva, Bikshapathi Gauda and Dr. Ganesh Venkataraman. The projects were funded by the European Commission, the Finnish Funding Agency for Technology and Innovation (Tekes), and Nokia Networks. These institutes I would like to acknowledge. I was also fortunate to receive personal research grants for doctoral studies from the following Finnish foundations: the Infotech Oulu Doctoral Program, theNokia Foundation, Tekniikan Edistämissäätiö, the University of Oulu Foundation, as well as the Riitta and Jorma J. Takanen Foundation.

During my doctoral studies, I have had the pleasure to be surrounded by my cheerful colleagues at the CWC including (in alphabetical order) Ayswarya, Dileep, Gawshi, Heshani, Hirley, Hussein, Inosha, Ivana, Krishna, Madushanka, Manosha, Mojtaba, Narimaan, Nalin, Oskari, Pawani, Prashant, Sadeep, Samad, Shehab, Sumudu, Uditha, Yushan. I very much enjoyed our daily exchange of ideas and thoughts, and the fun moments together. I am also very grateful to the CWC administrative staff, in particular Hanna Saarela, Jari Sillanpää, Kirsi Ojutkangas, Renata Sebö, Anu Niskanen and many others.

During my stay in Oulu, I had the privilege to make some very good family friends, including Professor Rajatheva & family, Sandun, Tharanga, Buddhika, Dilani, Chamari, Dimuthu, Bidushi, vishmika, Dileepa, Dinesh, Sahan, Nuwanthika, Nipuni, Indika, Dilin, Tharaka, Thushan, Archana, Nuwan, Akila, Ganewaththe and I give a special thank you to all my friends from Sri Lanka for their support and encouragement during these years.

I want to express my unreserved gratitude to my loving father Sarath Jayasinghe and my loving mother Shanthi de Zoysa for their love, kindness and for always encouraging me to move forward. I thank my elder brother Keeth, for being a great role model and for challenging me to pursue all those great goals in life. The sacrifices you have made during my life are priceless. I would also like to thank my sister-in-law Bhagya and nephews Sahas and Ayodh for their unconditional support and joy brought to my life. In addition, I would like to thank my loving brother Bhagya and sisters Madhasha, Pradeesha and my family members Prabhath, Lakshika, Sanduneth, Anuhas, Tharuth and Thehas for their love and support. I am also grateful to my loving grandparents Rathnasiri/ Rathnawathi, and parents-in-law Jayantha/ Meththa, and wife's sisters Dilakshi and Vidushi for their love and blessings. Last, but not least, I thank my wife, Anagi for always being by my side, loving, supporting, and believing in me.

Espoo, May 24, 2022 Praneeth Jayasinghe

List of abbreviations

Symbols and functions

$A_k^{(\mathrm{dl})}$	Average number of packets arrival at DL UE k
$A_k^{(\mathrm{ul})}$	Average number of packets generated at UL UE k
A_{dl}	Data stream indexing set for the downlink transmissions
A_{ul}	Data stream indexing set for the uplink and downlink transmissions
$a_k^{(\mathrm{dl})}$	The multiplexed rate portion for DL UE k over the backhaul
$a_k^{(a)}$	The multiplexed rate portion for each UE k over the backhaul
$a_k^{(\mathrm{ul})}$	The multiplexed rate portion for UL UE k over the backhaul
A_i	The number of UEs exceeding the spatial multiplexing capabilities of BS-RN link
B	Set of BS in dynamic TDD system
B_{U}	Set of uplink base stations
B_{D}	Set of downlink base stations
$\mathbf{b}_{k,l}$	The pilot training sequence for l^{th} data stream of DL/UL user k
B_{R}	Set of RNs in the IAB network
$\mathbf{b}_{k,l}^{(a,s)}$	The pilot training sequences for l^{th} data stream corresponding to UE (UL or DL) k at timeslot s
$\mathbf{b}_{i,l}^{(a)}$	The pilot training sequences for l^{th} data stream corresponding to RN i for UL or DL data
$\mathbf{b}_{j,n}^{(\mathrm{dl},1)}$	The pilot training sequences for n^{th} data stream corresponding to DL UE j at timeslot 1
$\mathbf{b}_{i,n}^{(\mathrm{dl})}$	The pilot training sequences for n^{th} data stream corresponding to RN i for DL data
$\mathbf{C}_{i_k}$	A symmetric matrix with the size of $S \times S$, which is given by $\mathbf{C}_{i_k} = \sum_{\{j,l\} \in \mathsf{A}_{\mathrm{dl}}} \mathbf{b}_{j,l} \mathbf{b}_{j,l}^{\mathrm{H}}$
$\mathbf{C}$	UE allocation matrix
$c_{i,k}$	Elements in UE allocation matrix
$\mathbf{C}^{(n)}$	UE allocation matrix in the nth iteration
$c_{i,k}^{(n)}$	Elements in UE allocation matrix in the nth iteration
$d_{j,l}^{(\mathrm{dl})}$	Transmitted data symbols to DL UE j in l^{th} spatial stream

$d_{j,l}^{(\mathrm{ul})}$	Transmitted data symbols from UL UE j in l^{th} spatial stream
$\hat{d}_{k,l}^{(a)}$	The estimated data at RX k for l^{th} spatial stream corresponding to UL or DL transmission
$\hat{d}_{k,l}^{(\mathrm{dl})}$	The estimated data at DL UE k received via l^{th} spatial stream
$\hat{d}_{k,l}^{(\mathrm{ul})}$	The estimated data at UL BS corresponding to UE k and l^{th} spatial stream
$d_{j,n}^{(\mathrm{dl},1)}$	Transmitted data symbols to DL UE j in n^{th} spatial stream during 1st timeslot
$d_{j,n}^{(\mathrm{ul},1)}$	Transmitted data symbols from UL UE j in n^{th} spatial stream during 1st timeslot
$d_{i,n}^{(\mathrm{dl})}$	Transmitted data symbols to DL UEs by BS/RN i in n^{th} spatial stream
$d_{j,n}^{(\mathrm{dl},2)}$	Transmitted data symbols to DL UE j in n^{th} spatial stream during 2nd timeslot
$d_{j,n}^{(\mathrm{ul},2)}$	Transmitted data symbols from UL UE j in n^{th} spatial stream during 2nd timeslot
$d_{i,n}^{(\mathrm{ul})}$	Transmitted data symbols to UL UEs by BS/RN i in n^{th} spatial stream
$d_{k,l}^{(a,s)}$	Transmitted data symbols to/from UE k in l^{th} spatial stream during the timeslot s
$\hat{d}_{k,l}^{(\mathrm{dl},1)}$	The estimated data at DL UE k for l^{th} spatial stream and 1st timeslot
$\hat{d}_{k,l}^{(\mathrm{ul},1)}$	The estimated data at UL BS for UE k and l^{th} spatial stream and 1st timeslot
$\hat{d}_{i,l}^{(\mathrm{dl})}$	The estimated data at RN i for DL backhaul data and l^{th} spatial stream
$\hat{d}_{k,l}^{(\mathrm{ul},2)}$	The estimated data at UL BS for UE k and l^{th} spatial stream and 2nd timeslot
$\hat{d}_{k,l}^{(\mathrm{dl},2)}$	The estimated data at DL UE k for l^{th} spatial stream and 2nd timeslot
$\hat{d}_{i,l}^{(\mathrm{ul})}$	The estimated data at RN i for UL backhaul data and l^{th} spatial stream
$\hat{d}_{k,l}^{(a,s)}$	The estimated data corresponding to UL/DL UE k and l^{th} spatial stream during the timeslot s
D_i	The rank of the BS-RN channel for backhaul link i
f_{D}	The maximum Doppler shift
$\mathbf{f}_{i_k,j,l}^{(\mathrm{dl})}$	Estimate of the UE (stream) specific pilots
G_p	The set of users shared the pilot p
$g_{i,k}$	The individual utility value for assigning an UE k to a particular BS or RN i

$\mathbf{H}_{i_j,k}^{(\text{dl})}$	The channel matrix between the DL BS i_j and the UE k
$\mathbf{H}_{j,k}^{(\text{ul-dl})}$	The interference channel matrix between the UL UE j and the DL UE k.
$\mathbf{H}_{i,j}^{(\text{ul})}$	The channel matrix between user j and UL BS i
$\mathbf{H}_{i_j,i}^{(\text{dl-ul})}$	The interference channel matrix between the DL BS i_j serving user j and the UL BS i
$\mathbf{H}_{i,k}$	The channel matrix between BS/RN i and UE k
$\tilde{\mathbf{H}}_{j,k}$	The UE-UE interference channel matrix between UE j and UE k
$\hat{\mathbf{H}}_{1,i}$	The channel matrix between the BS and RN i
i_k	The serving BS of the user k
I_j	The path gain between interfering user j and BS i_k
J_0	A Constant value equal to $\log_2(\beta)$ and β is a predefined constant
J_1	Fisrt order part after Taylor series approximation of the auiliary constraint
J_2	Zero order part after Taylor series approximation of the auiliary constraint
K	Number of UEs in the dynamic TDD system
K_i	The number of users served by each BS i
K_1	Fisrt order part after Taylor series approximation of the auiliary constraint
K_2	Zero order part after Taylor series approximation of the auiliary constraint
$\mathbf{K}_k$	Additional interference term DE estimation
$\bar{\mathbf{K}}_k$	Additional interference term SSE estimation
$k_{\max}$	Maximum number of users that are assigned to the same pilot.
L_k	The maximum number of spatial data streams allocated to UE k
$\bar{L}_i$	The maximum number of spatial data streams between the BS and RN i is
$\mathbf{M}_k^{(a)}$	The received signal covariance matrix for UE k
$\mathbf{M}_k^{(\text{dl})}$	The received signal covariance matrix at DL UE k
$\mathbf{M}_k^{(\text{ul})}$	The received signal covariance matrix at UL BS for UE k
M_i	Number of antennas at the BS i
$\mathbf{m}_{j,l}^{(\text{dl})}$	The transmit precoder for l^{th} spatial data stream of the DL UE j
$\mathbf{m}_{j,l}^{(\text{ul})}$	The transmit precoder for l^{th} spatial data stream of the UL UE j
$\mathbf{m}_{k,l}^{(a)}$	The transmit precoder for l^{th} spatial data stream of the UE k
$\bar{\mathbf{m}}_{k,l}^{(a)}$	The transmit precoder estimated in the previous iteration
$\mathbf{m}_{k,l}^{(\text{dl},1)}$	Transmit precoder for DL UE k via l^{th} spatial stream at 1st timeslot
$\mathbf{m}_{k,l}^{(\text{ul},1)}$	Transmit precoder for UL UE k via l^{th} spatial stream at 1st timeslot
$\mathbf{m}_{k,l}^{(\text{ul},2)}$	Transmit precoder for UL UE k via l^{th} spatial stream at 2nd timeslot

$\mathbf{m}_{k,l}^{(\mathrm{dl},2)}$	Transmit precoder for DL UE k via l^{th} spatial stream at 2nd timeslot
$\mathbf{m}_{k,l}^{(a,s)}$	Transmit precoder for UE k via l^{th} spatial stream at the timeslot s
M	Set of all transmit precoders
$\mathbf{M}_k^{(\mathrm{dl},1)}$	the received signal covariance matrices for DL UE k at 1st timeslot
N	Number of BSs in the dynamic TDD system
N_k	Number of antennas at the UE k
N_0	Gaussian noise variance
$\mathbf{N}_{i_k}^{(\mathrm{dl})}$	The estimation noise matrix for all pilot symbols
$\mathbf{N}_k^{(\mathrm{ul})}$	The estimation noise matrix at UL UE k.
$\mathbf{N}_k^{(\mathrm{dl})}$	The estimation noise matrix for all pilot symbols at DL UE k
$\mathbf{N}_{i_k}^{(\mathrm{ul})}$	The estimation noise matrix for all pilot symbols at UL BS i_k
$\mathbf{N}_k$	The estimation noise matrix for all pilot symbols
$P_i^{(dl)}$	The maximum transmit powers available at the i-th DL BS
$P_k^{(ul)}$	The maximum transmit powers available the k-th UL UE
$Q_k^{(a)}$	The number of queued packets for/at UE k
$Q_k^{(\mathrm{dl})}$	The number of queued packets destined for DL user k
$Q_k^{(\mathrm{ul})}$	The number of queued packets at UL user k
$\bar{Q}_k^{(\mathrm{ul})}$	The number of queued packets destined for UL user k at serving RN
$\bar{Q}_k^{(\mathrm{dl})}$	The number of queued packets destined for DL user k at serving RN
$R_k^{(a)}$	Data transmission rate to user k
$R_{k,l}^{(a)}$	Data rate over the lth spatial stream to user k
$\mathbf{R}_k^{(a)}$	The received training matrices
$\mathbf{R}_k^{(\mathrm{dl})}$	The received precoded pilot training matrix of user k at DL BS i_k
$\mathbf{R}_k^{(\mathrm{ul})}$	The received precoded pilot training matrix at UL user k
$\mathbf{R}_{k,1}^{(\mathrm{dl})}$	The received pilot training matrix at DL BS i_k in Strategy B
$\mathbf{R}_{k,1}^{(\mathrm{ul})}$	The received pilot training matrix at UL UE k in Strategy B
$\mathbf{R}_{k,1}^{(a)}$	The received training matrices for Strategy B
$\mathbf{R}_{k,2}^{(a)}$	The received training matrices for Strategy C
$R_{k,l}^{(\mathrm{dl},1)}$	The number of transmitted bits over the l^{th} spatial stream from DL UE k in the 1st timeslot
$R_{k,l}^{(\mathrm{dl},2)}$	The number of transmitted bits over the l^{th} spatial stream from DL UE k in the 2nd timeslot
$R_{i,l}^{(\mathrm{dl})}$	The number of transmitted bits over the l^{th} spatial stream for RN i to serve DL UEs

$R_{k,l}^{(a,s)}$	The number of transmitted bits over the l^{th} spatial stream to/from UE k at the timeslot s
$R_{i,l}^{(a)}$	The number of transmitted bits over the l^{th} spatial stream for RN i to serve DL/UL UEs
$R_{k,l}^{(\mathrm{ul},2)}$	The number of transmitted bits over the l^{th} spatial stream from UL UE k in the 2nd timeslot
$R_{k,l}^{(\mathrm{ul},1)}$	The number of transmitted bits over the l^{th} spatial stream from UL UE k in the 1st timeslot
$R_{i,l}^{(\mathrm{ul})}$	The number of transmitted bits over the l^{th} spatial stream for RN i from UL UEs
R_{G_p}	The cost function for the pilot assignment
$\mathbf{R}_k^{(a,s)}$	The received precoded training matrices at UE k at timeslot s
$\mathbf{R}_i^{(a,s)}$	The received precoded training matrices at BS/RN i at timeslot s
$\mathbf{R}_1^{(\mathrm{dl},1)}$	The received precoded training matrices at BS k in the 1st timeslot
R_{ac}	The actual achievable sum rate
R_{sum}	The achieved sum rate
S	Length of the pilot sequence
S_k	The path gain between user k serving BS i_k
$S_{i,k}$	The path gain between BS/RN i and UE k
$t_{k,l}^{(a)}$	Auxiliary variable corresponding the l^{th} spatial data stream of the UE k
$\bar{t}_{k,l}^{(a)}$	The point of approximation
$t_{k,l}^{(a,s)}$	Auxiliary variable corresponding the l^{th} spatial data stream of the UE k for the timeslot s
$t_{i,l}^{(a)}$	Auxiliary variable corresponding the l^{th} spatial data stream of the BS/RN i
$\mathbf{T}_k^{(\mathrm{dl})}$	The received precoded pilot training matrix at DL user k
$\mathbf{T}_k^{(\mathrm{ul})}$	The received precoded pilot training matrix for UL user k at BS
$\mathbf{T}_k^{(a)}$	The received precoded pilot training matrix at/for user k
$\mathbf{T}_k^{(\mathrm{dl},1)}$	The received precoded pilot training matrix at DL user k for 1st timeslot
$\mathbf{T}_k^{(a,s)}$	The received precoded pilot training matrix at/for user k for the timeslot s
$\bar{t}_{k,l}^{(a,s)}$	The point of approximation
T	Set of auxiliary variables
T	Duration of the TDD frame

t_S	The signalling rate
U_i	The set of UEs served by each BS i
$\mathbf{u}_{k,l}^{(dl)}$	Linear receiver employs at DL UE k
$\mathbf{u}_{k,l}^{(ul)}$	Linear receiver employs at UL BS i_k
$\mathbf{u}_{k,l}^{(a)}$	The linear receiver for l^{th} spatial data stream of the UE k
$\tilde{\mathbf{u}}_{k,l}^{(a)}$	The linear MMSE receiver employed for data detection
$\mathbf{u}_{k,l}^{(dl,1)}$	Linear receiver employs at DL UE k in 1st timeslot
$\mathbf{u}_{k,l}^{(ul,1)}$	Linear receiver employs at UL BS for UE k in 1st timeslot
$\mathbf{u}_{k,l}^{(dl,2)}$	Linear receiver employs at DL UE k in 2nd timeslot
$\mathbf{u}_{k,l}^{(ul,2)}$	Linear receiver employs at UL BS for UE k in 2nd timeslot
$\tilde{\mathbf{u}}_{k,l}^{(dl,1)}$	The linear MMSE receiver employed for data detection at DL UE k in 1st timeslot
$\mathbf{v}_{i,l}^{(dl)}$	Transmit precoder for RN i at BS, via l^{th} spatial stream
$\mathbf{v}_{i,l}^{(ul)}$	Transmit precoder of the RN i to BS, via l^{th} spatial stream
$v_i^{(a)}$	The scaled dual variable corresponding to equality constraint
$\mathbf{v}_{i,l}^{(a)}$	Transmit precoder for/at RN i at/for BS, via l^{th} spatial stream
$\mathbf{w}_{i,l}^{(dl)}$	Linear receiver employs at RN i to decode backhaul data from BS via l^{th} spatial stream.
$\mathbf{w}_{i,l}^{(ul)}$	Linear receiver employs at BS to decode backhaul data from RN i via l^{th} spatial stream.
W	The set of all receive beamformers
$\mathbf{x}_k^{(dl)}$	The received signal at the DL user k
$\mathbf{x}_i^{(ul)}$	The received signal at the UL BS i
$\mathbf{x}_i^{(ul,1)}$	The received signal at RN i in 1st timeslot
$\mathbf{x}_1^{(ul,2)}$	The received signal at BS in 2nd timeslot
$\mathbf{x}_k^{(dl,1)}$	The received signal at DL UE k in 1st timeslot
$\mathbf{x}_k^{(dl,2)}$	The received signal at DL k in 2nd timeslot
Y_k	The set of users with shortest UE-UE distance to user k
$\mathbf{z}_k^{(dl)}$	Complex white Gaussian noise vector at the DL user k
$\mathbf{z}_i^{(ul)}$	Complex white Gaussian noise vector at the UL BS i
$\mathbf{z}_k$	Complex white Gaussian noise vector at user k
α_k	User prioritize weights
β	A predifined constant introduced with auxiliary MSE constraint
β_i	Complex path amplitude of the ith component

$\delta_{i_k,j,l}$	The estimation noise and pilot contamination corresponding to pilot sequence $\mathbf{b}_{j,l}$ at BS i_k.
Δ	The number bisection iterations required to satisfy the power constraint
$\varepsilon_{k,l}^{(a,s)}$	MSE for UL/DL data detection for UE k, data stream l in timeslot s
$\varepsilon_{i,l}^{(a)}$	MSE for UL/DL data detection at BS/RN i for data stream
$\varepsilon_{k,l}^{(\mathrm{dl},1)}$	MSE for DL data detection for UE k, data stream l in 1st timeslot
$\Psi_k^{(\mathrm{dl})}$	The queue deviation metric for all DL UE queues at the BS
$\Psi_k^{(\mathrm{ul})}$	The queue deviation metric for UL UE k
$\bar{\Psi}_k^{(\mathrm{dl})}$	The queue deviation metric for DL UE k at the RN i_k
$\bar{\Psi}_k^{(\mathrm{ul})}$	The queue deviation metric for UL UE k at the RN i_k
$\tilde{\Psi}_k^{(a)}$	Vector with elements $\alpha_k^{1/q}\Psi_k^{(a)}$
$\tilde{\bar{\Psi}}_k^{(a)}$	Vector with elements $\alpha_k^{1/q}\bar{\Psi}_k^{(a)}$
$\omega_{k,l}^{(a,s)}$	Dual variable for UE k, data stream l and timeslot s
$\omega_{k,l}^{(\mathrm{dl},1)}$	Dual variable for DL UE k for data stream l in 1st timeslot
$\omega_{i,l}^{(\mathrm{dl})}$	Dual variable for DL RN i for data stream l in 1st timeslot
$\omega_{k,l}^{(\mathrm{ul},1)}$	Dual variable for UL UE k for data stream l in 1st timeslot
$\bar{\omega}_{k,l}^{(a,s)}$	Dual variable value from previous iteration
$\mathbf{\Phi}_1^{(\mathrm{dl},1)}$	The weighted transmit co-variance matrix
$\gamma_{k,l}^{(a)}$	SINR at RX node for DL/UL data transmission
$\gamma_{k,l}^{(\mathrm{dl})}$	SINR at DL UE k
$\gamma_{k,l}^{(\mathrm{ul})}$	SINR at UL BS for UL UE k
$\varepsilon_{k,l}^{(a)}$	The MSE for l^{th} stream of for UE k corresponding to UL/DL data detection
$\tilde{\varepsilon}_{k,l}^{(a)}$	The MSE when MMSE receiver is employed
ε_{ik}	Error bound associated with $\mathbf{E}_{ik}$ in the ellipsoidal uncertainty model
η	Weight of the LoS component $\overline{\mathbf{H}}_2$
$\theta_{r,i}$	Angle of arrival for ith dominant path
$\lambda_k^{(a)}$	Number of packets arrivals in bits per seconds for UE k
$\lambda_k^{(\mathrm{dl})}$	Number of packets arrivals in bits per seconds for DL UE k
$\lambda_k^{(\mathrm{ul})}$	Number of packets arrivals in bits per seconds for UL UE k
$\nu_k^{(a)}$	Dual variable corresponding to the power constraint for UE k
$\nu_k^{(\mathrm{dl})}$	Dual variable corresponding to the power constraint at DL BS i_k
$\nu_k^{(\mathrm{ul})}$	Dual variable corresponding to the power constraint at UL UE k
$\nu_1^{(\mathrm{dl},1)}$	Dual variable corresponding to the power constraint at BS

$\mathbf{\Phi}_k^{(a)}$	The weighted transmit covariance matrix for UE k
$\mathbf{\Phi}_k^{(\mathrm{dl})}$	The weighted transmit covariance matrix for DL UE k
$\mathbf{\Phi}_k^{(\mathrm{ul})}$	The weighted transmit covariance matrix for UL UE k
$\bar{\mathbf{\Phi}}_{k,1}^{(\mathrm{dl})}$	The estimated weighted transmit covariance matrix for DL UE k at BS
$\bar{\mathbf{\Phi}}_{k,1}^{(\mathrm{ul})}$	The estimated weighted transmit covariance matrix for UL UE k
$\bar{\mathbf{\Phi}}_{k,1}^{(a)}$	The estimated weighted transmit covariance matrix
$(\bar{\mathbf{\Phi}}_k^{(\mathrm{dl})})_{\mathrm{SSE}}$	The SSE estimated weighted transmit covariance matrix
$(\bar{\mathbf{\Phi}}_k^{(\mathrm{dl})})_{\mathrm{DE}}$	The DE estimated weighted transmit covariance matrix
$\Psi_k^{(a)}$	The queue deviation for the DL/UL UE k
$\tilde{\mathbf{\Psi}}^{(a)}$	The prioritized queue deviation vector for all the DL/UL UEs
$\tilde{\Psi}_k^{(a)}$	Vector elements in the prioritized queue deviation vector.
$\tilde{\mathbf{\Psi}}^{(\mathrm{dl})}$	The prioritized queue deviation vector for all the DL UEs
$\tilde{\mathbf{\Psi}}^{(\mathrm{ul})}$	The prioritized queue deviation vector for all the UL UEs
σ	Weight of the scattering component $\widetilde{\mathbf{H}}_2$ in the AF MIMO system
ξ	Variable introduced for aggressive convergence
ζ	A small constant
θ	A constant > 1
τ	Time instance
τ_0	The duration for a one precoder/decoder iteration
ζ_i	Penalty value limiting the allocation
$\bar{\omega}_{k,l}$	Denotes fixed $\omega_{k,l}^{(a)}$ from the previous iteration.
$\omega_{k,l}$	Dual variable
ρ	Step size %item[$\mathbf{\Omega}_{i_k}$]
$\mathbf{\Omega}_k$	The cross pilot interference

Mathematical Operators

$\mathbf{I}_N$	$N \times N$ identity matrix
$\lvert x \rvert$	Absolute value of the complex number x
$(x)^+$	Positive part of scalar x, i.e., $\max(0,x)$
$\lfloor x \rfloor$	Largest integer less than or equal to x
$\lvert\lvert \mathbf{x} \rvert\rvert_q$	ℓ_q-norm of complex vector $\mathbf{x}$
$x \in \mathscr{S}$	x is a member of set $\mathscr{S}$

$\mathbf{X}^H$	Hermitian of matrix $\mathbf{X}$
$\mathbf{X}^*$	Conjugate of matrix $\mathbf{X}$
$\mathbf{X}^T$	Transpose of matrix $\mathbf{X}$
$\mathbf{X}^{-1}$	Inverse of matrix $\mathbf{X}$
$\mathbf{X}^\dagger$	Pseudo-inverse of matrix $\mathbf{X}$
$(\mathbf{X})_{i,j}$	Element at the ith row and the jth column of matrix $\mathbf{X}$
$\|\|\mathbf{X}\|\|_F$	Frobenius norm of $\mathbf{X}$
$\mathrm{Tr}(\mathbf{X})$	Trace of matrix $\mathbf{X}$
$\det(\mathbf{X})$	Determinant of matrix $\mathbf{X}$
$\mathbb{C}$	Set of complex numbers
$\mathbb{C}^n$	Set of complex n-vectors
$\mathbb{C}^{m\times n}$	Set of complex $m \times n$ matrices
$\mathscr{CN}(x,y)$	Circularly symmetric complex Gaussian random variable with mean x and variance y
$\mathscr{CN}(\mathbf{x},\mathbf{Y})$	Circularly symmetric complex Gaussian vector distribution with mean $\mathbf{x}$ and covariance matrix $\mathbf{Y}$
$\sim$	Distributed according to
$\mathbb{E}(\cdot)$	Expectation
$\mathbb{E}_d(\cdot)$	Expectation over data symbols
$\mathbb{E}_\tau(\cdot)$	Expectation over time
$\Re(z)$	Real part of z
$\log_2(\cdot)$	Logarithm in base 2
$\ln(\cdot)$	Natural logarithm
$\max(\cdot)$	Maximum
$\min(\cdot)$	Minimum
$\mathbf{Pois}(\cdot)$	Poisson arrival process

Acronyms

3GPP	3rd Generation Partnership Project
5G	5th Generation
AO	Alternating optimization
BS	Base station
BIT	Bi-directional training
CSI	Channel state information

DE	Direct estimation
DF	Decode-and-forward
DL	Downlink
eMBB	Enhanced Mobile Broadband
EE	Energy efficiency
F-B	Forward-Backward
GP	Guard period
HD	Half-duplex
IAB	Integrated Access and Backhaul
i.i.d.	Independent and identically distributed
KKT	Karush-Kuhn-Tucker
LoS	Line of sight
LTE	Long Term Evolution
LTE-M	Long Term Evolution for Machines
MIMO	Multiple input multiple output
MMSE	Minimum mean square error
MSE	Mean square error
mMTC	Massive Machine Type Communications
mm-Wave	Milimeter wave
NB-IoT	NarrowBand-Internet of Things
NR	New radio
OTA	Over-the-air
PNC	Physical layer network coding
QoS	Quality of service
QWSR	Queue weighted sum rate
RN	Relay node
SCA	Successive convex approximation
SER	Symbol error rate
SI	Self-interference
SINR	Signal-to-interference-plus-noise ratio
SMSE	Sum mean square error
SNR	Signal to noise ratio
TDD	Time division duplex
TWR	Two way relaying
UE	User equipment

UL	Uplink
URLLC	Ultra-Reliable Low Latency Communications
WMSE	Weighted MSE
WSMSE	Weighted sum mean square error
WSR	Weighted sum rate

Contents

1 Introduction

1.1 Background and introduction

During the last couple of decades, radical technological transformations have occurred worldwide, primarily due to the progression of the semiconductor industry, computers, smartphones, artificial intelligence, the internet and wireless communication [1, 2, 3, 4]. In particular, wireless communication has paved the way for the development of numerous other technologies and applications. Furthermore, the demand for mobile data traffic has increased exponentially over the past decade and is expected to increase further in the upcoming years [5, 6]. Notably, 5th generation (5G) technology-based wireless networks are expected to provide extremely high data rates, significant capacity enhancements, high reliability, and ultra-low latency communication by aiming to meet the demands of new application scenarios [7, 8, 9, 10].

At the commencement of 5G standardization activities, three main application scenarios were defined to be accomplished from 5G. These were enhanced mobile broadband (eMBB), ultra-reliable low-latency communications (URLLC), and massive machine type communications (mMTC) [11, 12, 13, 14]. The aim of 5G eMBB is to deliver high capacity, throughput, and data rates, whereas URLLC is expected to provide highly reliable and low latency data communication for critical industrial applications and autonomous vehicles. The 5G mMTC standard is designed to improve the capabilities of long-term evolution for machines (LTE-M) and narrowband internet of things (NB-IoT) such as battery life, coverage, and device density by connecting many devices to 5G base stations (BSs). Researchers and 3rd generation partnership project (3GPP) delegates have examined different approaches to meet these requirements, including applying larger bandwidths, multiple antenna techniques, new physical layer designs, and flexible frame structures, etc [10, 15, 16, 17].

The first phase of the 5G launch began in mid-2019 based on 3GPP Release 15, with the main objective of providing greater capacity and higher data rates for mobile broadband [18]. In general, these targets can be fundamentally attained using broader bandwidth and spectrally efficient methods, such as densification of the access network and the use of multiple antenna beamformer techniques. Moreover, the 5G spectrum consists of both licensed and unlicensed frequencies, with time-division-duplexing (TDD) and frequency-division-duplexing (FDD) methods to increase the capacity and

coverage of mobile networks. For capacity and data rate enhancements, TDD operates at 2.5-5.0 GHz and millimetre-wave (mm-Wave) 24–39 GHz, while FDD operates below 2.7 GHz to offer wide coverage, low latency, and high-reliability [7]. Moreover, multiple-input-multiple-output (MIMO) beamforming is theoretically shown to deliver higher spectral efficiency and greater coverage while improving the link performance by mitigating catastrophic interference [19, 20]. The most notable difference between 5G and LTE is the emphasis on beamforming and the prevalence of TDD, due to antennas being smaller at higher frequencies, making massive MIMO deployments more convenient and TDD more suitable for eMBB deployment. [21, 22].

Traditionally, mobile networks have primarily been FDD, in part because FDD is more suitable for networks of macrocells deployed with a wide coverage area and partly because FDD was traditionally designed for symmetric traffic using paired spectrum [23]. Nevertheless, it is crucial to consider the traffic asymmetry between downlinks (DL) and uplinks (UL) in order to optimize networks in 5G and beyond. In this respect, TDD systems have become increasingly important as they are inherently more spectrally efficient than FDD systems. Consequently, TDD technology has been embraced for TD-LTE and 5G networks operating at 2.5-5 GHz and mm-Wave frequencies. These developments were driven mainly by the desire to avoid paying patent royalties for competing with FDD-based standards and the ability to use an unpaired spectrum [7, 24, 25].

In 5G, TDD becomes even more compelling for a number of reasons. First, a large number of small cells with a short-range are required in order to achieve the desired spectral efficiency. Promisingly, TDD-based small cell deployments offer better performance where the transmit powers, mobile speeds, and channel propagation delays are relatively low. The second key technical concept is the use of large (distributed) antenna arrays in order to simultaneously serve multiple user-equipments (UEs) and suppress many undesired interference sources [26, 27, 28, 29]. Again, such an approach is better matched to TDD networks as TDD offers reciprocity-based channel acquisition and facilitates efficient downlink beamforming without explicit feedback from users to circumvent problems due to limited pilot resources [26, 30]. Finally, as networks become more data-centric and thus less symmetric in their traffic, TDD allows for resources to be dynamically adapted between the UL and DL by changing the number of time slots allocated to each direction within the TDD frame.

5G with TDD has strict requirements for synchronization and timing alignment of DL and UL among inter-operators and cells as there is a possibility of having BS-BS

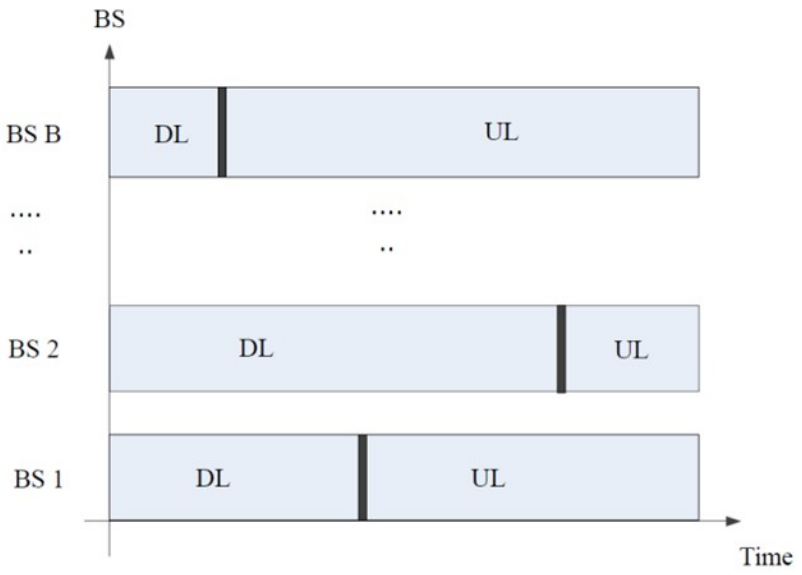

Fig. 1. Asymmetric traffic handling in Dynamic TDD systems by allocating UL-DL resources asynchronously over the network.

and UE-UE interference due to timing misalignment [31, 32]. Interference such as this is remarkably similar to interference observed in dynamic TDD systems, in which resource allocation between UL and DL can be done asynchronously. In phase 2 of 5G, dynamic TDD is under consideration, which is well suited for small cell scenarios because the amount of instantaneous UL and DL traffic can vary significantly with time and between adjacent cells [33]. Nevertheless, dynamic TDD requires novel schemes for training, channel feedback, dynamic resource allocation and interference management. Until recently, how dynamic TDD interacts with such schemes has not been thoroughly studied.

Fig.1 illustrates an example of UL/DL resource allocation within a dynamic TDD network. Besides the normal UL-to-UL and DL-to-DL types of interference, dynamic TDD in multi-cell operation may also cause UL-to-DL interference (UE-UE) and DL-to-UL interference (BS-BS). [33, 34, 35, 36]. In order to mitigate or even avoid this interference, resource allocation and beamforming can both be carried out collectively by a coordinating group of cells that consist of both UEs and BSs. Such coordination, in turn, requires acquiring channel state information (CSI) of the transmitter to receiver links. The channel reciprocity can be utilized to acquire the CSI of the UE-BS links;

however, the particular challenge of the dynamic TDD approach is the acquisition of the CSI between the mutually interfering UE terminals [37, 38, 39]. In order to support such functionality, the UEs should start performing similar functions as BSs have traditionally done, i.e., being more aware of the neighbourhood and measuring the other nodes in the near vicinity and exchanging control information among different nodes, etc. In particular, UEs must provide UE-to-UE CSI via explicit feedback or over-the-air (OTA) signalling mechanisms that rely on precoded uplink pilots [26, 40]. The frame structure in 5G offers larger flexibility in symbol allocation between uplink and downlink, which encourages traffic-aware dynamic TDD operation, and also mini-slots structures can be utilized to facilitate the OTA signalling framework [16, 41, 36]. Hence, an application-specific frame can be employed to support beamforming functionality on dynamic TDD, by dividing the TDD frame into two portions: 1. Beamformer signalling and 2. Data transmission. TDD frames should be long enough to facilitate multiple OTA bidirectional signalling iterations to obtain sufficiently converged beamformers while keeping the training overhead at modest levels. Implementing the above TDD frame structure is possible with the approved 3GPP NR standard, as detailed in [36].

To meet ever-growing traffic demands, small cells ought to be densely deployed by the next generation of cellular systems [42, 43]. A fibre-based backhaul is expensive to connect these small cells to the core network, and a separate wireless radio backhaul is not always practical if the site space is limited. Therefore, a high-speed wireless backhaul makes more sense since it is more cost-effective, flexible, and easier to deploy [44, 45, 46]. Furthermore, small cells will be able to benefit from the large bandwidth of 5G, which makes it an attractive backhaul solution. Due to these factors, the second phase of 5G studies focused on studying integrated access and backhaul (IAB) systems under the new radio (NR) technologies mentioned in the 3GPP specification [47, 48, 49, 50, 51].

In IAB or a self-backhauling system which is shown in Fig.2, the backhaul and access use the same time and frequency resources [47, 52]. It is important to note that IAB supports simultaneous UL and DL transmissions; the available resources per TDD frame can be freely allocated between UL and DL transmission depending on traffic demands and user distribution within the network. As a consequence of such traffic-aware flexible TDD based IAB networks, managing dynamic traffic in small cells and mitigating interference are the challenges that arise in them. To counteract the additional UL-to-DL and DL-to-UL interference that can arise in a dynamic setting, BSs

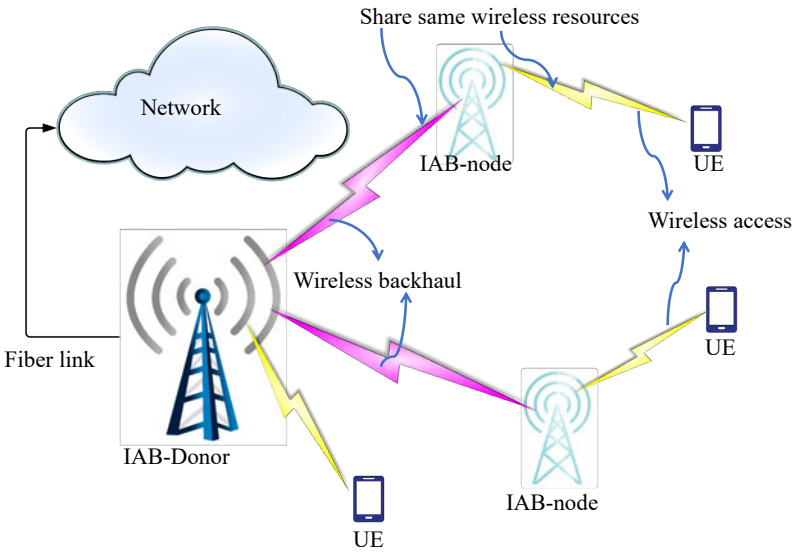

Fig. 2. An example of an IAB system sharing wireless resources for backhauling and access.

should use advanced coordinated resource allocation and beamforming methods where the transmissions within a coordinated set of cells are designed jointly.

1.2 Literature review

The relevant state of the art which is associated with the scope of this thesis is presented in this section. The *Dynamic TDD* system and prior works are described in Section 1.2.1. In Section 1.2.2, literature is presented on *Integrated and Access*. These provide the background to the detailed analysis considered in Chapters 2-3.

1.2.1 Dynamic TDD

Mobile data traffic is expected to grow exponentially in the coming years due to ever-increasing smartphone usage, and massive demand for online video and cloud services [5, 18, 53]. During the COVID-19 pandemic, mobile data traffic spiked significantly as a result of the development of the concept of remote working [54]. Thus, future

wireless mobile networks should be able to handle the growing traffic demands that are asymmetrical and bursty. Small-cell deployment has been identified as a key research direction to fulfil these requirements [55, 56, 57, 58]. A large number of small cells with a very small coverage area can be used in addition to the traditional macro/micro cells to deliver mobile data in high mobile data traffic areas [34, 59, 60]. TDD based small-cell deployments are very useful in such circumstances, where the transmit powers, mobile speeds and channel propagation delays are relatively low. Furthermore, asymmetric mobile data traffic can be efficiently handled with TDD by allocating resources in UL and DL directions based on the instantaneous traffic demand. Hence, TDD based small-cell networks provide several benefits, such as reduced complexity CSI estimation using channel reciprocity, flexible handling of dynamic traffic and easy frequency re-use planning [33, 61, 30].

In a small cell network, imposing the same fixed UL/DL configuration over the network would greatly limit the overall resource utilization as the adjacent cells potentially have different instantaneous UL/DL traffic demands. Dynamic TDD can be used to overcome this problem by adjusting the UL/DL mode asynchronously based on the traffic state of each individual cell [33, 62]. More importantly, the 3GPP NR standard has given special consideration to fully dynamic or flexible TDD, which is an essential aspect of 5G [16, 63]. It is therefore necessary for the new 5G air interfaces to meet the physical layer latency requirements without imposing limitations on UL/DL slot assignment [64].

Interference management in dynamic TDD systems becomes more challenging as complicated interference scenarios arise due to simultaneous UL and DL data transmission in adjacent cells [65]. Specifically, the DL BS transmission may interfere with the UL reception (BS-BS interference) and the UL UE transmission may interfere with DL reception (UE-UE interference). Previous studies on dynamic TDD have focused on complicated time slot allocation algorithms that mitigate this cross-link interference [27, 66, 67, 68, 69]. In addition to increased spectral efficiency and improved reliability, spatial processing via MIMO systems provides additional degrees of freedom to mitigate the detrimental interference both at the transmitter and receiver [70, 71]. Hence, the interference management in dynamic TDD based small-cell deployments is more efficient when both BSs and UEs are equipped with multiple antennas.

While the channel reciprocity can be utilized to acquire the CSI of the UE-BS and BS-BS links, a specific challenge of the dynamic TDD approach is to acquire the CSI

between the mutually interfering UEs. Explicit feedback of the UE-UE channels in addition to a full CSI exchange between BSs would be required to enable an optimal beamformer design which renders the centralized design impractical. However, the coordinated beamformer design for dynamic TDD systems can be carried out in a decentralized manner with the help of bi-directional forward-backward (F-B) training via spatially precoded OTA pilot signalling [37, 39, 36]. In this case, it is essential to have fast beamformer convergence to implement these systems in practice with fading channels and to minimize the training overhead [36].

Accurate CSI estimation is essential for any beamformer design. Hence, we need to employ distinguishable pilot sequences to estimate corresponding channels at the relevant nodes. However, the number of orthogonal pilot sequences that can be used for CSI estimation is constrained due to the limited coherence time and coherence bandwidth of the wireless channel [26, 72]. Consequently, in dense networks, the number of orthogonal pilots is not sufficient to distinguish all possible channels. Hence, we must reuse pilot sequences or employ non-orthogonal pilots to estimate the CSI. This, on the other hand, causes the so-called pilot contamination effect, where the desired channel is polluted by other channels [26, 73, 74]. Therefore, beamformer or CSI estimation should be robust against any pilot contamination effect.

The vast majority of dynamic TDD studies are focused on the development of distributed dynamic time slot allocation algorithms to alleviate cross-slot interference. For example, in [27, 66, 67, 68, 69] different centralized and decentralized strategies for allocating time slots are addressed and compared. Small cell dynamic TDD transmissions have been investigated for heterogeneous networks by utilizing a cell clustering and power control based interference cancellation scheme in [75]. An energy efficiency (EE) beamformer design was proposed in [76], with the cloud radio access network assumption, which requires centralized processing. Furthermore, the dynamic TDD system was analysed using a game-theoretic model in [65], for UL/DL optimization.

In the context of synchronous UL/DL[1] TDD networks, numerous centralized and decentralized beamformer designs with different coordination assumptions have been considered to optimize network utilities such as weighted sum rate (WSR) maximization, EE, weighted queue minimization (WQM), and weighted sum mean square error (WSMSE) minimization, e.g., in [37, 77, 78, 79, 80, 81, 82, 83, 84, 85, 86]. Several cross-layer resource allocation problems are discussed in [77, 78], and various

[1] Synchronous UL/DL refers to the transmission of UL/DL over a multi-cell network synchronously

decentralized solutions are presented with a variety of assumptions and configurations. In [79], distributed transmit beamforming was studied for the cognitive radio network. In [80, 81], the WSR maximization is carried out via WSMSE minimization and alternating optimization of the transmit precoders and receive beamformers. Expected WSR is maximized for the noisy MIMO K-cell interfering broadcast channel (IBC) in [82] by exploiting the relationship between WSR and WMSE assuming partial CSI availability at the transmitter and perfect CSI at the receiver. A systematic comparison of distributed beamforming optimization algorithms in terms of performance, complexity, information exchange, and convergence properties was carried out in [83]. A low-complexity approximate beamforming technique with a fast converging iterative algorithm was proposed in [84] for maximizing EE in multiuser downlink systems. Furthermore, the authors in [37] proposed a distributed CSI acquisition framework and novel fast converging strategies for the iterative WSMSE based approach in a realistic multi-cell environment. Further convergence improvements for the WSR problem based on successive convex approximation (SCA) methods were proposed in [85], along with the additional per-user quality of service (QoS)/rate constraints. Recently, a traffic-aware transceiver design for weighted queue minimization has been investigated in [86]. Similar to [37, 80, 81, 85], the decentralized solution in [86] was based on the iterative evaluation of Karush-Kuhn-Tucker (KKT) conditions of the optimization problem. The resulting beamformer structures were shown to be very similar to those corresponding to other optimization objectives such as WSR maximization, WSMSE minimization, etc. However, most of these studies assumed perfect channel estimation in their designs.

Practical implementation of coordinated precoding and CSI acquisition have been investigated in, e.g., [37, 39, 87, 88, 89]. Therein, bidirectional F-B training using spatially precoded pilots is employed to provide an implicit exchange of intermediate beamformers between BSs and UEs, assuming that enough orthogonal pilots are available for stream specific precoded pilots. Moreover, the pilot contamination effect and possible ways to mitigate this impact have been studied by employing precoded pilot estimation techniques and different pilot allocation/reuse methods, e.g., in [90, 73, 91, 92, 93, 94, 95, 96, 97]. Blind pilot decontamination without coordination between cells is considered in [90], where the authors proposed a channel predicting approach by utilizing the properties of random matrix theory. Bjornson *et al.* [73, 91] investigated pilot contamination in massive MIMO systems and performed a mathematical analysis to find asymptotic limitations and develop an engineering solution for pilot assignment. Further, in [73], it is discovered that pilot contamination generally

does not cause a fundamental upper limit on the spectral efficiency in massive MIMO, due to the fact that the users' angular spread does not overlap. In [92], the achievable rates in a contaminated multi-user MIMO system were analysed, and decontamination based on MMSE estimation in [93] was discussed. In [94], pilot sequence hopping is performed at each transmission slot to reduce pilot contamination, and Kalman filtering is also applied to enhance the channel estimation. A recent study in [97] exploited channel sparsity to tackle pilot contamination in a cell-free massive MIMO system, in there consider semi-blind methods for joint channel estimation and data detection.

An interesting approach to mitigating pilot contamination was proposed in [39], where a direct least squares (LS) beamformer estimation from the contaminated UL/DL pilots was investigated. In [98], the authors show how pilot precoding and combining can accommodate a large number of UEs in one cell and significantly improve channel estimation quality. Moreover, there have been a few studies to mitigate pilot contamination by using pilot reuse algorithms with the use of channel statistics. For example, in [95], spatial correlation properties are utilized for reusing the pilot resources among users with sufficient angular separation. An analysis of open-loop power control and pilot sequence reuse schemes within a group of cells was investigated in [99]. An algorithm for scheduling pilots in conjunction with beamforming based on an optimization framework was proposed in [96]. However, none of these studies considers dynamic TDD settings.

1.2.2 Integrated access and backhaul

Small cell deployment has been recognized as a key research direction to fulfil ever-growing traffic demand in the next generation of cellular systems [5, 34, 100]. However, connecting these small cell BSs to the core network using optical fibre links/backhaul can be onerous and complex [101]. Current developments of mm-Wave communication have enabled the possibility to use a high-speed wireless backhaul to densified small-cell networks, which can be more cost-effective, flexible, and easier to deploy [102]. These networks are referred to as IAB systems or self-backhaul systems.

A self-backhauling or IAB network consists of three components, which in 3GPP standardization have been coined as IAB-donor (referred to as BS), IAB-nodes (i.e., relay nodes (RNs)), and UEs [47]. Relay nodes assist the BS to provide wireless access to UEs while the BS offers both direct access for UEs to the core network and wireless backhauling functionality to RNs. Moreover, IAB offers the flexibility to use the same

wireless resources for access and backhaul data transmissions simultaneously in both UL and DL directions based on the traffic requirements. Therefore, IAB plays a vital role in wireless communication networks to expand coverage and improve the throughput with lower transmit power requirements and with minimal planning and implementation cost. Consequently, IAB systems have received significant attention in the 3GPP NR specifications [47, 48, 49, 103].

IAB network is a cooperative relaying network with some advanced capabilities. Cooperative relaying can be used to improve the reliability, throughput, and coverage of communication with lower power requirements [104, 105, 106, 107, 108]. Higher layer (layer 2 or layer 3) relaying protocol such as decode-and-forward (DF) protocol is more suited for the IAB network as the relay node (RN) must be capable of simultaneously handling multiple UL and DL UEs. Furthermore, it is essential to have user-specific queues for both UL and DL UEs at RNs to guarantee end-to-end data delivery. Full-duplex (FD) relaying with DF protocol at the RN has been considered in some recent studies on IAB functionality [109, 110, 111]. Even though FD relaying facilitates both backhaul and access data transmission simultaneously, the practical implementation is still challenging due to excessive complexity and production costs [112, 113]. Moreover, two-way half-duplexed (HD) relaying protocol has emerged as a potential alternative to FD relaying protocol, which utilizes the spectrum more efficiently and considerably reduces the conventional HD loss [114, 115, 116]. In the two-way HD relaying protocol, both BS and UEs (served by RN) transmit backhaul and access data to the RN in the first timeslot (multiple access stage) while in the next timeslot, the RN broadcasts receive messages to BS and UEs (broadcasting stage), thus both UL and DL UE data are served within two consecutive time intervals. As the current 3GPP NR study encourages application-specific flexible frame structures, by employing flexible TDD based resource scheduling, IAB networks can support two-way HD relaying [16]. Nevertheless, it is challenging to handle complicated cross-link interference scenarios introduced in the IAB system. MIMO systems provide more spatial degrees of freedom to mitigate interference in complex interference-limited systems [117]. Hence, the interference in IAB networks can be efficiently mitigated by employing multiple antennas at each node.

It is essential to collect required CSI, either centralized or decentralized, to design beamformers for the IAB system. In a flexible TDD-based IAB, the channel reciprocity can be used to acquire the CSI between each node via reverse link pilot measurements. A specific challenge with the considered flexible-TDD (where both UL and DL transmissions co-exist) arrangement is the CSI acquisition of the cross-link interference channels,

e.g., among mutually interfering user terminals. Explicit feedback of the UE-to-UE and RN-to-UE channels to the BS would be required to enable optimal beamformer design, which would make the centralized implementation infeasible in practice. However, the decentralized coordinated beamformer design can be made possible by employing bi-directional F-B training via spatially precoded OTA pilot signalling [37, 39, 36]. In practice, the number of orthogonal pilot sequences is limited as their availability for CSI estimation depends on the coherence time and coherence bandwidth of the wireless channel [26, 72]. Smart pilot reuse schemes or robust estimation techniques with non-orthogonal pilots can be employed to carry out the beamformer design by adequately mitigating the pilot contamination effect [89].

The recent advances of self-interference (SI) cancellation techniques have motivated to carry out research on FD in-band communication [118, 119], also applied to self-backhauling networks [109, 110, 111, 74, 120, 121]. For example, in [109], downlink spectrum allocation schemes were studied for FD small cell networks in both centralized and decentralized manners by considering in-band FD, out-band FD, and hybrid schemes. In [110, 111], robust beamformer designs were proposed for an FD MIMO relaying system assuming imperfect CSI estimation. In addition, in [74], the resource allocation/optimization with mm-Wave and massive MIMO techniques was investigated. Authors in [120] have considered FD relaying for heterogeneous networks, and the two-way FD relaying has been proposed and compared with the existing FD and HD relaying schemes in [121]. The majority of these studies compared results with the conventional HD system, which is 50 per cent inefficient. As an alternative to FD systems, there are numerous studies on two-way HD relaying in [114, 115, 116, 117, 122, 123, 124, 125], which have shown that two-way HD relaying improves the spectral efficiency significantly compared to the conventional HD system. Most of these studies have considered physical-layer network coding (PNC) and beamforming techniques to assist the two-way relaying. In addition, there have been two recent studies on IAB that investigated the optimization of uplink power control, topology, and routing by using genetic algorithm-based techniques [126, 127].

There have been numerous studies on multi-user MIMO based beamformer designs for optimizing network utilities such as WSR, WMMSE, and WQM in both centralized and decentralized manners with different coordination assumptions [37, 80, 81, 86]. Furthermore, the practical implementation of the coordinated precoding and CSI acquisition by employing bi-directional OTA signalling has been studied in, e.g., [37, 39, 89]. Different techniques were investigated in [39, 90, 93, 95, 128] to mitigate the pilot

contamination effect at the CSI estimation process. In particular, a practical approach based on direct LS beamformer estimation from the contaminated UL/DL pilots was investigated in [39].

1.3 Aims, contributions and outline of this thesis

The aim of this thesis is to investigate certain flexible TDD-based heterogeneous networks, such as dynamic TDD systems and IAB systems, which are crucial when designing future wireless systems. In particular, a greater emphasis is placed on developing new algorithms for training, channel feedback, resource allocation, and interference management in such networks.

In the first part of this thesis, the focus is on a multi-cell, multi-user network that operates in a traffic-aware, dynamic TDD mode. There, the UL-DL timeslot allocation is different from one cell to another. Later in this thesis, the focus is directed at a flexible TDD-based IAB system, in which the BS and IAB-relays operate in different UL-DL modes. The following is the outline of this thesis, which summarizes the major contributions of each chapter.

Chapter 2 is based on the results which have been documented in [129, 130, 131, 132, 133], which presents a detailed analysis of dynamic TDD networks, in which the available resources per cell can be freely allocated to either UL or DL depending on the instantaneous traffic demand. Particular interest is given to complicated UL-DL and DL-UL interference scenarios that arise due to simultaneous UL and DL data transmission in adjacent cells. Then, decentralized iterative beamformer designs are proposed for several traffic-aware network optimization objectives such that only minimal information exchange is required among the coordinated BSs and UEs. Chapter 2 further focuses on bi-directional F-B training via spatially precoded over-the-air pilot signalling to facilitate coordinated beamforming. The aforementioned allows BSs and UEs to iteratively optimize their respective transmitters/receivers based on only locally measured reverse link pilot measurements. Later in the chapter, novel bi-directional beamformer training strategies and methods for direct estimation (DE) of the stream specific beamformers are developed for each intermediate beamformer update in a limited and noisy pilot environment. The proposed signalling and DE schemes allow for non-orthogonal and overlapping pilots, which considerably reduces the resource coordination effort. Later in the chapter, the decontamination ability of the proposed strategies with limited pilot resources is analysed using numerical examples

and the proposed training and estimation framework is compared to the traditional stream-specific channel estimation method and an uncoordinated system.

Chapter 3 is based on the results of which have been detailed in [134, 135], and it studies the IAB network, which consists of one BS, several RNs, and UEs, in which BS and RNs exchange UE data via a wireless in-band backhaul while sharing the same frequency-time resources with access links. Further in the study, a flexible TDD-based IAB network is considered where RNs and BS are assigned to distinct UL or DL transmission modes to mitigate conventional HD loss at RNs. An iterative beamformer design is proposed to manage the resulting cross-channel interference and to allocate a wireless backhaul and access resources jointly over two consecutive data delivery intervals required for communications between the BS and UEs through HD RNs. Dynamic traffic behaviour is handled via weighted queue minimization objective, and user-specific UL/DL queues are also introduced at RNs to guarantee reliable end-to-end data delivery. Bi-directional F-B training via spatially precoded over-the-air pilot signalling is employed to allow decentralized beamformer design across all the nodes. A novel user allocation method is proposed to assign UEs to BS or RNs based only on long-term channel statistics and some practical IAB limitations. The numerical examples are carried out to compare the proposed flexible IAB system and conventional HD relaying system.

Chapter 4 concludes this thesis and discusses several potential future directions based on this work.

1.4 The author's contribution to the publications

This thesis is based, in part, on two journal articles [133, 134] and five conference articles [129, 130, 131, 132, 135] that have been already published. The author of this thesis had the primary responsibility of comprehending the original ideas, derivation of the equations, developing the simulation software, producing the numerical results, and writing the articles. Co-authors provided comments, criticism, support during the process.

In addition to the papers above, the author has published three journal articles [108, 136, 137] and six conference articles [138, 139, 140, 141, 142, 143] that are not included in this thesis.

2 Bi-directional beamformer training for dynamic TDD networks

2.1 Introduction

Motivated by the concerns in Section 1.2.1, we study several decentralized beamformer designs with different optimization objectives for multi-cell multi-user MIMO dynamic TDD systems. We consider WQM, and its special cases, queue weighted sum rate (QWSR) maximization and sum mean square error (SMSE) minimization objectives with power constraints at DL BSs and UL UEs. First, we improve the convergence properties of the WQM approach presented in [86] by reformulating it similar to [85], and the problem is solved via iterative evaluation of KKT conditions leading to a distributed algorithm. Then, to facilitate practical implementation, we employ OTA signalling architecture as in [37, 39, 36]. More specifically, we employ precoded pilots to exchange the intermediate beamformers in both backward and forward directions iteratively. We consider a TDD frame to carry out both OTA bi-directional signalling and data transmission. Moreover, several bi-directional training iterations can be embedded into a TDD frame before the data transmission. A methodology was proposed in [36], to implement this TDD frame structure by adapting standardization works on 3GPP NR [16]. As the number of OTA signalling rounds is increased, the time remaining for the actual data transmission becomes shorter. Hence, the impact of OTA training overhead is investigated via numerical simulations.

Moreover, we propose three different direct beamformer estimation methods to alleviate the pilot contamination effect. In these methods, we use the received precoded pilot information to estimate intermediate beamformers directly using LS based estimation without separately decorrelating individual pilot sequences. We refer to these approaches as DE methods. The DE approaches are compared with conventional stream-specific estimation (SSE) method, where the beamformers are constructed from the estimated equivalent (precoded) channel vectors. In both techniques, precoded pilot sequences are used to implicitly exchange information on beamformers and user-specific weights. However, when non-orthogonal pilots are used for the beamformer signalling, the DE approach provides a better estimation due to the LS based estimation gain. Furthermore, the superiority of the DE method (versus SSE) is demonstrated analytically.

Finally, to enhance the decontamination further, we consider a traditional pilot reuse approach for alleviating pilot overlap. A simple (but centralized) pilot reuse approach is proposed for a complicated dynamic TDD setup based on large-scale fading information of the BS-UE and UE-UE channels.

The following are the major contributions of this chapter:

- A fast converging iterative decentralized beamformer design is proposed for a dynamic TDD system with the WQM objective.
- The proposed design is adapted to QWSR maximization and SMSE minimization objectives as special cases of a WQM design.
- OTA bi-directional signalling architecture is proposed to implement beamformer designs in practice.
- Three DE-based beamformer estimation strategies are proposed to mitigate the pilot contamination.
- The superiority of DE over SSE is proven analytically.
- A centralized pilot reuse algorithm is proposed to a dynamic TDD setting.
- The performance of the proposed methods is studied with numerical examples.

This chapter is based on of our previously published journal [133] and conference papers [129, 130, 131, 132].

2.2 System model

We consider a multi-cell multi-user MIMO system operating in dynamic TDD mode. The multi-cell network consists of N BSs and K UEs. We denote the set of BS indices as $\mathsf{B} = \{1,\ldots,N\}$, while the set of UEs served by each BS i is denoted by U_i. The number of users served by each BS i is denoted by $K_i = |\mathsf{U}_i|$. Additionally, the serving BS of the user k is denoted as i_k. Each UE k employs N_k antenna elements, whereas each BS i employs M_i antenna elements. In a given time, a subset of base stations $\mathsf{B}_\mathrm{U} \subseteq \mathsf{B}$ serves the uplink traffic and the rest of the base stations $\mathsf{B}_\mathrm{D} = \mathsf{B} \setminus \mathsf{B}_\mathrm{U}$ serve the DL traffic. The maximum number of spatial data streams allocated to UE $k \in \mathsf{U}_i$ is denoted by $L_k \leq \min(M_i, N_k)$. For notational simplicity, we define two sets $\mathsf{A}_\mathrm{dl} = \{j, l | j \in \mathsf{U}_i, l = 1,\ldots,L_j, i \in \mathsf{B}_\mathrm{D}\}$ and $\mathsf{A}_\mathrm{ul} = \{j,l | j \in \mathsf{U}_i, l = 1,\ldots,L_j, i \in \mathsf{B}_\mathrm{U}\}$. Here, A_ul and A_dl represent data stream indexing sets for the uplink and downlink transmissions, respectively. Furthermore, we assume the channels to be reciprocal in the UL and DL. The dynamic TDD model is illustrated in Fig. 3.

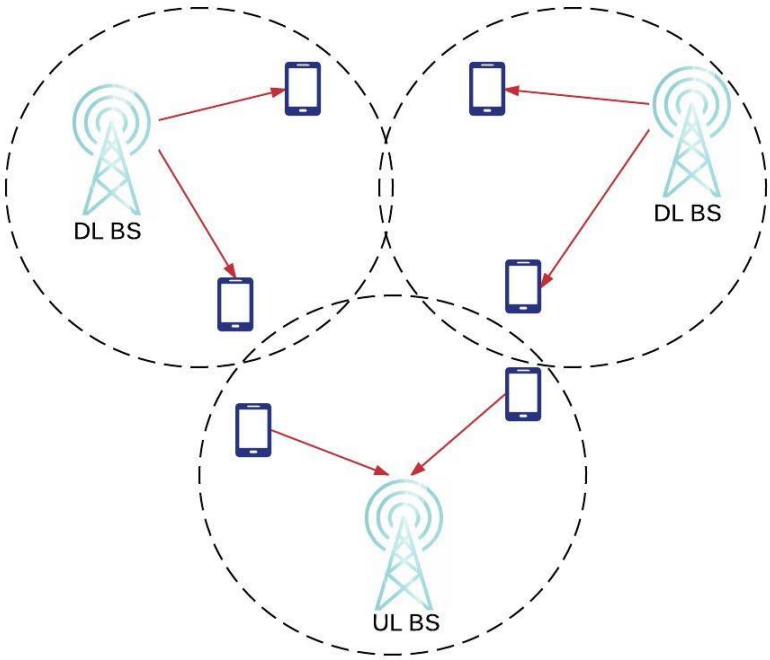

Fig. 3. Dynamic TDD system (Reprinted, with permission, from [133] ©2018 IEEE).

The received signal $\mathbf{x}_k^{(\mathrm{dl})} \in \mathbb{C}^{N_k}$ at the DL user k can be expressed as

$$\mathbf{x}_k^{(\mathrm{dl})} = \sum_{\{j,l\}\in \mathsf{A}_{\mathrm{dl}}} \mathbf{H}_{i_j,k}^{(\mathrm{dl})} \mathbf{m}_{j,l}^{(\mathrm{dl})} d_{j,l}^{(\mathrm{dl})} + \sum_{\{j,l\}\in \mathsf{A}_{\mathrm{ul}}} \mathbf{H}_{j,k}^{(\text{ul-dl})} \mathbf{m}_{j,l}^{(\mathrm{ul})} d_{j,l}^{(\mathrm{ul})} + \mathbf{z}_k^{(\mathrm{dl})}, \tag{1}$$

where $\mathbf{H}_{i_j,k}^{(\mathrm{dl})} \in \mathbb{C}^{N_k \times M_{i_j}}$ is the channel matrix between the DL BS i_j and the UE k, $\mathbf{H}_{j,k}^{(\text{ul-dl})} \in \mathbb{C}^{N_k \times N_j}$ is the interference channel matrix between the UL UE j and the DL UE k. The transmit precoder for l^{th} spatial data stream of the DL UE $j \in \mathsf{U}_i$ is denoted as $\mathbf{m}_{j,l}^{(\mathrm{dl})} \in \mathbb{C}^{M_i}$ and the transmit precoder for l^{th} spatial data stream of the UL UE $j \in \mathsf{U}_i$ is $\mathbf{m}_{j,l}^{(\mathrm{ul})} \in \mathbb{C}^{N_j}$. Transmitted data symbols to DL UE j in l^{th} spatial stream and transmitted data symbols from UL UE j in l^{th} spatial stream are denoted as $d_{j,l}^{(\mathrm{dl})}$ and $d_{j,l}^{(\mathrm{ul})}$, respectively. Here, the transmit data symbols are assumed to be independent and identically distributed with $\mathbb{E}\{|d_{j,l}^{(\mathrm{dl})}|^2\} = 1$ and $\mathbb{E}\{|d_{j,l}^{(\mathrm{ul})}|^2\} = 1$. We assume complex white Gaussian noise vector $\mathbf{z}_k^{(\mathrm{dl})} \in \mathbb{C}^{N_k}$ with variance N_0 per element. Similarly, the

received signal $\mathbf{x}_i^{(\mathrm{ul})} \in \mathbb{C}^{M_i}$ at the uplink BS i is given by

$$\mathbf{x}_i^{(\mathrm{ul})} = \sum_{\{j,l\}\in \mathsf{A}_{\mathrm{ul}}} \mathbf{H}_{i,j}^{(\mathrm{ul})} \mathbf{m}_{j,l}^{(\mathrm{ul})} d_{j,l}^{(\mathrm{ul})} + \sum_{\{j,l\}\in \mathsf{A}_{\mathrm{dl}}} \mathbf{H}_{i_j,i}^{(\mathrm{dl\text{-}ul})} \mathbf{m}_{j,l}^{(\mathrm{dl})} d_{j,l}^{(\mathrm{dl})} + \mathbf{z}_i^{(\mathrm{ul})}, \tag{2}$$

where $\mathbf{H}_{i,j}^{(\mathrm{ul})} \in \mathbb{C}^{M_i \times N_j}$ is the channel matrix between user j and UL BS i, $\mathbf{H}_{i_j,i}^{(\mathrm{dl\text{-}ul})} \in \mathbb{C}^{M_i \times M_{i_j}}$ is the interference channel matrix between the DL BS i_j serving user j and the UL BS i. Additionally, we consider $\mathbf{z}_i^{(\mathrm{ul})} \in \mathbb{C}^{M_i}$ to be complex white Gaussian noise vector with variance N_0 per element. Note that, due to the channel reciprocity, $\mathbf{H}_{i,j}^{(\mathrm{ul})} = \mathbf{H}_{i,j}^{(\mathrm{dl})^{\mathrm{T}}}$.

To estimate the received data through l^{th} spatial stream, DL UE k employs a linear receiver $\mathbf{u}_{k,l}^{(\mathrm{dl})} \in \mathbb{C}^{N_k}$. Similarly, the UL BS i_k employs a linear receiver $\mathbf{u}_{k,l}^{(\mathrm{ul})} \in \mathbb{C}^{M_{i_k}}$ to decode the received data from UL user k through the spatial stream l. Then, the estimated data at a RX[2] node, corresponding to UL/DL data transmission can be written in a common form as $\hat{d}_{k,l}^{(a)}$. Here, for DL UE k, the estimated data is given as $\hat{d}_{k,l}^{(\mathrm{dl})} = \mathbf{u}_{k,l}^{(\mathrm{dl})^{\mathrm{H}}} \mathbf{x}_k^{(\mathrm{dl})}$ whereas for UL BS i_k, the estimated data transmitted by UE k is given as $\hat{d}_{k,l}^{(\mathrm{ul})} = \mathbf{u}_{k,l}^{(\mathrm{ul})^{\mathrm{H}}} \mathbf{x}_{i_k}^{(\mathrm{ul})}$. From here on, for simplicity, a generic supercript 'a' is introduced to represent both 'DL' and 'UL' directions.

The mean squared error (MSE) for l^{th} stream of for UE k corresponding to UL/DL data detection is defined as[3]

$$\varepsilon_{k,l}^{(a)} = \mathbb{E}_d[|d_{k,l}^{(a)} - \hat{d}_{k,l}^{(a)}|^2] = 1 - 2\Re(\mathbf{u}_{k,l}^{(a)^{\mathrm{H}}} \mathbf{H}_{i_k,k}^{(a)} \mathbf{m}_{k,l}^{(a)}) + \mathbf{u}_{k,l}^{(a)^{\mathrm{H}}} \mathbf{M}_k^{(a)} \mathbf{u}_{k,l}^{(a)}, \tag{3}$$

where $\mathbf{M}_k^{(a)}$ is the received signal covariance matrix for UE k. This is given for DL UE k as

$$\begin{aligned} \mathbf{M}_k^{(\mathrm{dl})} = \mathbb{E}_d[\mathbf{x}_k^{(\mathrm{dl})} \mathbf{x}_k^{(\mathrm{dl})^{\mathrm{H}}}] = & \sum_{\{j,l\}\in \mathsf{A}_{\mathrm{dl}}} \mathbf{H}_{i_j,k}^{(\mathrm{dl})} \mathbf{m}_{j,l}^{(\mathrm{dl})} (\mathbf{H}_{i_j,k}^{(\mathrm{dl})} \mathbf{m}_{j,l}^{(\mathrm{dl})})^{\mathrm{H}} \\ & + \sum_{\{j,l\}\in \mathsf{A}_{\mathrm{ul}}} \mathbf{H}_{j,k}^{(\mathrm{ul\text{-}dl})} \mathbf{m}_{j,l}^{(\mathrm{ul})} (\mathbf{H}_{j,k}^{(\mathrm{ul\text{-}dl})} \mathbf{m}_{j,l}^{(\mathrm{ul})})^{\mathrm{H}} + \mathsf{N}_0 \mathbf{I} \end{aligned} \tag{4}$$

and for UL UE k at BS i_k (note that in UL, the $\mathbf{M}_k^{(\mathrm{ul})}$ is the same for all $k \in \mathsf{U}_{i_k}$) as

$$\begin{aligned} \mathbf{M}_k^{(\mathrm{ul})} = \mathbb{E}_d[\mathbf{x}_{i_k}^{(\mathrm{ul})} \mathbf{x}_{i_k}^{(\mathrm{ul})^{\mathrm{H}}}] = & \sum_{\{j,l\}\in \mathsf{A}_{\mathrm{ul}}} \mathbf{H}_{i_k,j}^{(\mathrm{ul})} \mathbf{m}_{j,l}^{(\mathrm{ul})} (\mathbf{H}_{i_k,j}^{(\mathrm{ul})} \mathbf{m}_{j,l}^{(\mathrm{ul})})^{\mathrm{H}} \\ & + \sum_{\{j,l\}\in \mathsf{A}_{\mathrm{dl}}} \mathbf{H}_{i_j,i_k}^{(\mathrm{dl\text{-}ul})} \mathbf{m}_{j,l}^{(\mathrm{dl})} (\mathbf{H}_{i_j,i_k}^{(\mathrm{dl\text{-}ul})} \mathbf{m}_{j,l}^{(\mathrm{dl})})^{\mathrm{H}} + \mathsf{N}_0 \mathbf{I}. \end{aligned} \tag{5}$$

[2]RX is used to refer DL UE for DL transmission or UL BS for UL transmission.

[3]$\mathbb{E}_d\{.\}$ is the expectation operation over transmit data symbols.

$$\gamma_{k,l}^{(\mathrm{dl})} = \frac{\left|\mathbf{u}_{k,l}^{(\mathrm{dl})\mathrm{H}}\mathbf{H}_{i_k,k}^{(\mathrm{dl})}\mathbf{m}_{k,l}^{(\mathrm{dl})}\right|^2}{\mathsf{N}_0\|\mathbf{u}_{k,l}^{(\mathrm{dl})}\|^2 + \sum\limits_{\substack{\{j,n\}\in\mathsf{A}_{\mathrm{dl}}\\ \{j,n\}\neq\{k,l\}}} |\mathbf{u}_{k,l}^{(\mathrm{dl})\mathrm{H}}\mathbf{H}_{i_j,k}^{(\mathrm{dl})}\mathbf{m}_{j,n}^{(\mathrm{dl})}|^2 + \sum\limits_{\{j,n\}\in\mathsf{A}_{\mathrm{ul}}} |\mathbf{u}_{k,l}^{(\mathrm{dl})\mathrm{H}}\mathbf{H}_{j,k}^{(\mathrm{ul\text{-}dl})}\mathbf{m}_{j,n}^{(\mathrm{ul})}|^2} \tag{8}$$

$$\gamma_{k,l}^{(\mathrm{ul})} = \frac{\left|\mathbf{u}_{k,l}^{(\mathrm{ul})\mathrm{H}}\mathbf{H}_{i_k,k}^{(\mathrm{ul})}\mathbf{m}_{k,l}^{(\mathrm{ul})}\right|^2}{\mathsf{N}_0\|\mathbf{u}_{k,l}^{(\mathrm{ul})}\|^2 + \sum\limits_{\substack{\{j,n\}\in\mathsf{A}_{\mathrm{ul}}\\ \{j,n\}\neq\{k,l\}}} |\mathbf{u}_{k,l}^{(\mathrm{ul})\mathrm{H}}\mathbf{H}_{i_k,j}^{(\mathrm{ul})}\mathbf{m}_{j,n}^{(\mathrm{ul})}|^2 + \sum\limits_{\{j,n\}\in\mathsf{A}_{\mathrm{dl}}} |\mathbf{u}_{k,l}^{(\mathrm{ul})\mathrm{H}}\mathbf{H}_{i_j,i_k}^{(\mathrm{dl\text{-}ul})}\mathbf{m}_{j,n}^{(\mathrm{dl})}|^2} \tag{9}$$

The linear minimum MSE (MMSE) receiver employed for data detection can be obtained from (3) as

$$\tilde{\mathbf{u}}_{k,l}^{(a)} = (\mathbf{M}_k^{(a)})^{-1}\mathbf{H}_{i_k,k}^{(a)}\mathbf{m}_{k,l}^{(a)}. \tag{6}$$

When the MMSE receiver is employed, the corresponding MSE can be obtain as

$$\tilde{\varepsilon}_{k,l}^{(a)} = 1 - \tilde{\mathbf{u}}_{k,l}^{(a)\mathrm{H}}\mathbf{H}_{i_k,k}^{(a)}\mathbf{m}_{k,l}^{(a)}, \tag{7}$$

which is called the MMSE value of the estimated received data corresponding to the UL/DL data transmission of user k from spatial stream l. Finally, assuming independent detection of data streams, we can write the signal-to-interference-plus-noise ratio (SINR) $\gamma_{k,l}^{(a)}$ at RX node for DL/UL data transmission as in (8) and (9).

2.3 Decentralized beamformer design

The main problem in centralized dynamic TDD beamformer design is to acquire the CSI at the centralized node. That is, all the DL BS-UE channels, UL BS-UE channels, cross-UE channels and cross-BS channels should be available at the centralized unit. This is a tedious task as there are lots of cross-UE channels to be estimated and reported. Hence, decentralized beamformer design is more suited for dynamic TDD networks, where we can overcome the channel estimation problem by using a bi-directional OTA signalling framework [36]. In this section, we study an iterative decentralized beamformer design for dynamic TDD. First, we generalize the WQM solution from [86] to cover the dynamic TDD setting. Furthermore, we reformulate the problem for improved convergence using the ideas from [85] that were originally applied to WSR maximization. Second, we consider some special cases of WQM to obtain a beamformer

design for QWSR maximization and SMSE minimization. In this Section, we consider only the algorithmic solution for the distributed framework. Practical implementation and related imperfections are presented in latter sections.

2.3.1 Weighted queue minimization

Here, weighted ℓ_q-norm queue minimization of the UL and DL users is considered with sum transmit power constraints at the transmitters. Let $Q_k^{(\mathrm{dl})}$ denote the number of queued packets destined for DL user k and $Q_k^{(\mathrm{ul})}$ denote the number of queued packets at UL user k at a given scheduling instant. Additionally, we model the traffic generation in the network using Poisson arrival process, where $\lambda_k^{(\mathrm{dl})}(\tau) \sim \mathbf{Pois}(A_k^{(\mathrm{dl})})$ is the generated traffic for DL user k in time instance τ. Similarly, $\lambda_k^{(\mathrm{ul})}(\tau) \sim \mathbf{Pois}(A_k^{(\mathrm{ul})})$ defines the generated traffic at UL user k at time instance τ. Here, $A_k^{(\mathrm{dl})} = \mathbb{E}_\tau\{\lambda_k^{(\mathrm{dl})}\}$ and $A_k^{(\mathrm{ul})} = \mathbb{E}_\tau\{\lambda_k^{(\mathrm{ul})}\}$ are the average number of packet arrivals in bits for the corresponding UL/DL users. Then, the total number of queued packets at $(\tau+1)$th time instant destined/available to user k is given by

$$Q_k^{(a)}(\tau+1) = \left[Q_k^{(a)}(\tau) - R_k^{(a)}(\tau)\right]^+ + \lambda_k^{(a)}(\tau), \tag{10}$$

where $[x]^+ \triangleq \max\{x,0\}$ and $R_k^{(a)}$ is the transmission rate to user k with $a = \{\mathrm{UL},\mathrm{DL}\}$. Here, $R_k^{(a)} = \sum_{l=1}^{L_k} R_{k,l}^{(a)}$, where $R_{k,l}^{(a)}$ denotes the number of transmitted bits over the lth spatial stream to user k. For SINR $\gamma_{k,l}^{(a)}$, the maximum rate is bounded by $R_{k,l}^{(a)} \leq \log_2(1+\gamma_{k,l}^{(a)})$. Now, we can define the queue deviation metric for the DL and UL as

$$\Psi_k^{(a)} = Q_k^{(a)} - R_k^{(a)} = Q_k^{(a)} - \sum_{l=1}^{L_k} \log_2(1+\gamma_{k,l}^{(a)}). \tag{11}$$

In order to simplify the notation, let $\tilde{\boldsymbol{\Psi}}^{(a)}$ denote a vector with elements $\tilde{\Psi}_k^{(a)} \triangleq \alpha_k^{1/q}\Psi_k^{(a)}$. Here, α_k is the weighting factor, used to prioritize users based on their corresponding QoS requirements. The WQM problem can be formulated as

$$\min_{\mathbf{m}_{k,l}^{(a)},\mathbf{u}_{k,l}^{(a)}} \quad \|\tilde{\boldsymbol{\Psi}}^{(\mathrm{dl})}\|_q + \|\tilde{\boldsymbol{\Psi}}^{(\mathrm{ul})}\|_q \tag{12a}$$

$$\text{s. t.} \quad \sum_{k\in\mathsf{U}_i}\sum_{l=1}^{L_k} \|\mathbf{m}_{k,l}^{(\mathrm{dl})}\|^2 \leq P_i^{(\mathrm{dl})} \quad \forall i \tag{12b}$$

$$\sum_{l=1}^{L_k} \|\mathbf{m}_{k,l}^{(\mathrm{ul})}\|^2 \leq P_k^{(\mathrm{ul})} \quad \forall k, \tag{12c}$$

where optimization variables are transmit precoders $\mathbf{m}_{k,l}^{(a)}$ and receive combiners $\mathbf{u}_{k,l}^{(a)}$. Additionally, $P_i^{(dl)}$ and $P_k^{(ul)}$ are the maximum transmit powers available at the i-th DL BS and the k-th UL UE, respectively. Note that (12a) includes an implicit rate constraint $Q_k^{(a)} - \sum_{l=1}^{L_k} R_{k,l}^{(a)} \geq 0$ on the maximum number of transmitted bits for each user as governed by the number of backlogged packets [86]. The ℓ_q norm is used to provide a trade off between the fairness and sum queue minimization.

At RX, we employ MMSE receivers. Hence, we obtain the following relation between the MSE and the SINR [37]

$$\tilde{\varepsilon}_{k,l}^{(a)} = (1 + \gamma_{k,l}^{(a)})^{-1}. \tag{13}$$

Therefore, we can write the user-specific rates using the user-specific MSE values as $R_k^{(a)} = \sum_{l=1}^{L_k} - \log_2(\tilde{\varepsilon}_{k,l}^{(a)})$. Now, we introduce auxiliary MSE constraint as in [85] to (12) and re-write the optimization problem as

$$\min_{\mathbf{m}_{k,l}^{(a)}, \mathbf{u}_{k,l}^{(a)}, t_{k,l}^{(a)}} \quad \sum_{a \in \{\text{UL,DL}\}} \sum_{k} \alpha_k \Big(Q_k^{(a)} - \sum_{l=1}^{L_k} t_{k,l}^{(a)} \log_2(\beta) \Big)^q \tag{14a}$$

$$\text{s. t.} \quad \varepsilon_{k,l}^{(a)} \leq \beta^{-t_{k,l}^{(a)}} \tag{14b}$$

$$\text{(12b), (12c),} \tag{14c}$$

where β is a predefined constant to adjust the approximation function such that $\beta > 0$ [85]. By introducing these MSE constraints, our objective becomes a convex function of auxiliary variables $t_{k,l}^{(a)}$. However, the constraint (14b) is still in a non-convex form. The non-convexity in (14b) can be handled iteratively by using the first-order Taylor series approximation similar to [85]

$$\beta^{-t_{k,l}^{(a)}} = -K_1 t_{k,l}^{(a)} + K_2, \tag{15}$$

where $K_1 = \beta^{-\bar{t}_{k,l}^{(a)}} \log(\beta)$ and $K_2 = \beta^{-\bar{t}_{k,l}^{(a)}} + \bar{t}_{k,l}^{(a)} K_1$. Here, $\bar{t}_{k,l}^{(a)}$ is the point of approximation. By employing the above approximation for the MSE constraints, we can re-write

the equivalent optimaization problem as

$$\min_{\mathbf{m}_{k,l}^{(a)},\mathbf{u}_{k,l}^{(a)},t_{k,l}^{(a)}} \quad \sum_{a\in\{\mathrm{UL,DL}\}}\sum_{k}\alpha_k\Big(Q_k^{(a)}-\sum_{l=1}^{L_k}t_{k,l}^{(a)}\log_2(\beta)\Big)^q \tag{16a}$$

$$\text{s. t.} \quad 1-2\Re(\mathbf{u}_{k,l}^{(a)\mathrm{H}}\mathbf{H}_{i_k,k}^{(a)}\mathbf{m}_{k,l}^{(a)}) + \mathbf{u}_{k,l}^{(a)\mathrm{H}}\mathbf{M}_k^{(a)}\mathbf{u}_{k,l}^{(a)} \le -K_1 t_{k,l}^{(a)} + K_2 \tag{16b}$$

$$(12b),\ (12c). \tag{16c}$$

Finally, the optimization problem (16) can be solved using alternating optimization (AO) between the transmit and receive beamformers, where we adopt an approach based on the KKT optimality conditions [85, 86]. Due to the independent nature of the optimization variables, the solution can be decoupled to calculate at RX and TX[4] nodes iteratively. Therefore, we define tasks for each coordinated nodes to implement this distributed iterative solution. For example, the RX node performs the task *'Receiver update'* and the TX node performs the task *'Transmitter update'* as mentioned below.

Receiver update

Here, we present the beamformer design steps that should be performed at the RX node . To do this, all the transmit precoders should be made available at the RX node. We begin by fixing the transmit precoders and solving for the receive beamformers and the other variables (auxiliary and dual). First, we calculate MMSE receivers $\mathbf{u}_{k,l}^{(a)}$ using (6). Next, the corresponding MSE $\varepsilon_{k,l}^{(a)}$ is obtained from (7). Then, the MSE bounds can be solved with respect to fixed MSE $\varepsilon_{k,l}^{(a)}$ as

$$t_{k,l}^{(a)} = \bar{t}_{k,l}^{(a)} + \frac{1}{\log(\beta-\xi)}\Big(1-\varepsilon_{k,l}^{(a)}\bar{t}_{k,l}^{(a)}\Big), \tag{17}$$

where $\bar{t}_{k,l}^{(a)}$ denotes $t_{k,l}^{(a)}$ from the previous iteration, $\xi = \frac{\beta-\theta}{n^\zeta}$, $\zeta \in \mathsf{R}$ is chosen to be an approximately small constant and $\theta > 1$. Here, the multiplier $\frac{1}{\log(\beta-\rho)}$ can be considered a step size and ξ is used for more aggressive convergence as detailed in [85]. Then, dual variables $\omega_{k,l}^{(a)}$ corresponding to (15) are obtained as

$$\omega_{k,l}^{(a)} = (1-\rho)\bar{\omega}_{k,l}^{(a)} + \rho\Big[\frac{\alpha_k q\log_2(\beta)}{K_1}\Big(Q_k^{(a)}-\sum_{l=1}^{L_k}t_{k,l}^{(a)}\log_2(\beta)\Big)^{(q-1)}\Big]^+, \tag{18}$$

[4]TX is used to refer to DL BS for the DL transmission or UL UE for the UL transmission.

where $\bar{\omega}_{k,l}^{(a)}$ denotes fixed $\omega_{k,l}^{(a)}$ from the previous iteration. Here, $\rho \in (0,1)$ controls the convergence and is used to prevent over-allocation. From here on, we refer to $\omega_{k,l}^{(a)}$ as user specific weight. The calculated MMSE receivers and user-specific weights information must be conveyed to /made available at coordinating TX nodes, in order to perform *'Transmitter update'* task.

Transmitter update

In the next step, we fix the MMSE receivers and solve for the transmit precoders. At this point, we assume all the MMSE receiver information and user-specific weights available at the TX node (to be detailed in Section 3.4.1). The transmit beamformers $\mathbf{m}_{k,l}^{(a)}$ can be derived from the first-order optimality conditions of (14) as

$$\mathbf{m}_{k,l}^{(a)} = \left(\mathbf{\Phi}_k^{(a)} + \nu_k^{(a)}\mathbf{I}\right)^{-1} \omega_{k,l}^{(a)} \mathbf{H}_{i_k,k}^{(a)\mathrm{H}} \mathbf{u}_{k,l}^{(a)}, \tag{19}$$

where $\mathbf{\Phi}_k^{(a)}$ and $\nu_k^{(a)}$ are the weighted transmit covariance matrix and the dual variable corresponding to power constraint at the transmiter (UL UE k or DL BS i_k). For DL BS i_k, $\mathbf{\Phi}_k^{(\mathrm{dl})}$ $\forall\, k \in \mathsf{U}_{i_k}$ is given by

$$\begin{aligned}\mathbf{\Phi}_k^{(\mathrm{dl})} = &\sum_{\{j,l\}\in\mathsf{A}_{\mathrm{dl}}} \omega_{j,l}^{(\mathrm{dl})} \mathbf{H}_{i_k,j}^{(\mathrm{dl})\mathrm{H}} \mathbf{u}_{j,l}^{(\mathrm{dl})} (\mathbf{H}_{i_k,j}^{(\mathrm{dl})\mathrm{H}} \mathbf{u}_{j,l}^{(\mathrm{dl})})^{\mathrm{H}} \\ &+ \sum_{\{j,l\}\in\mathsf{A}_{\mathrm{ul}}} \omega_{j,l}^{(\mathrm{ul})} \mathbf{H}_{i_j,i_k}^{(\mathrm{dl\text{-}ul})\mathrm{H}} \mathbf{u}_{j,l}^{(\mathrm{ul})} (\mathbf{H}_{i_j,i_k}^{(\mathrm{dl\text{-}ul})\mathrm{H}} \mathbf{u}_{j,l}^{(\mathrm{ul})})^{\mathrm{H}}.\end{aligned} \tag{20}$$

Similarly, for UL user k, $\mathbf{\Phi}_k^{(\mathrm{ul})}$ is given by

$$\begin{aligned}\mathbf{\Phi}_k^{(\mathrm{ul})} = &\sum_{\{j,l\}\in\mathsf{A}_{\mathrm{ul}}} \omega_{j,l}^{(\mathrm{ul})} \mathbf{H}_{i_j,k}^{(\mathrm{ul})\mathrm{H}} \mathbf{u}_{j,l}^{(\mathrm{ul})} (\mathbf{H}_{i_j,k}^{(\mathrm{ul})\mathrm{H}} \mathbf{u}_{j,l}^{(\mathrm{ul})})^{\mathrm{H}} \\ &+ \sum_{\{j,l\}\in\mathsf{A}_{\mathrm{dl}}} \omega_{j,l}^{(\mathrm{dl})} \mathbf{H}_{j,k}^{(\mathrm{ul\text{-}dl})\mathrm{H}} \mathbf{u}_{j,l}^{(\mathrm{dl})} (\mathbf{H}_{j,k}^{(\mathrm{ul\text{-}dl})\mathrm{H}} \mathbf{u}_{j,l}^{(\mathrm{dl})})^{\mathrm{H}}.\end{aligned} \tag{21}$$

The transmit beamformers can be efficiently solved from (19) by a bisection search over the dual variables $\nu_k^{(\mathrm{dl})}$ and $\nu_k^{(\mathrm{ul})}$ to satisfy the power constraints $\sum_{k\in\mathsf{U}_i}\sum_{l=1}^{L_k} \|\mathbf{m}_{k,l}^{(\mathrm{dl})}\|^2 \leq P_i^{(\mathrm{dl})}$ and $\sum_{l=1}^{L_k} \|\mathbf{m}_{k,l}^{(\mathrm{ul})}\|^2 \leq P_k^{(\mathrm{ul})}$, respectively.

Here, we employed an alternating optimization approach to calculate the precoders and decoders. Hence, the beamformers are not optimal as they are optimized for their fixed counterparts. Thus, we need to repeat the precoder/decoder optimization

until the estimated beamformers and/or the optimization objective have converged. This procedure is summarized in Algorithm 1. Note that the centralized unit can obtain the same solution by considering this distributed implementation as independent subproblems, which can be solved in parallel. However, for dynamic TDD setting, we are more interested in the decentralized solution. Moreover, the detailed signalling structure to facilitate the iterative algorithm is explained in Section 2.4.

Algorithm 1 Iterative Beamformer Design

1: Initializing feasible transmit beamformers $\mathbf{m}_{k,l}^{(a)}$. ▷ TX
2: Distribute initial transmit beamformers and prioritizing weights α_k to all RX. ▷ TX
3: **repeat**
4: Estimate MMSE receivers $\mathbf{u}_{k,l}^{(a)}$ from (6). ▷ RX
5: Estimate auxiliary variables $t_{k,l}^{(a)}$, and user specific weights $\omega_{k,l}^{(a)}$ using (17) and (18). ▷ RX
6: Distribute all MMSE receivers and user specific weights to all TX. ▷ RX
7: Estimate transmit precoders $\mathbf{m}_{k,l}^{(a)}$ from (19). ▷ TX
8: Distribute all transmit precoders to all RX. ▷ TX
9: **until** convergence.

2.3.2 Queue weighted sum rate maximization

In this section, we consider a special case of WQM assuming $Q_k^{(a)}$ is large and $q = 2$. Consequently, (14) is reduced to the following equivalent QWSR maximization problem

$$\max_{\mathbf{m}_{k,l}^{(a)}, \mathbf{u}_{k,l}^{(a)}} \quad \sum_{a \in \{\mathrm{UL,DL}\}} \sum_{k} \sum_{l=1}^{L_k} \alpha_k Q_k^{(a)} R_{k,l}^{(a)} \tag{22}$$

$$\text{s.t} \quad \text{(12b), (12c).}$$

We can follow the same procedure as in WQM to obtain an iterative beamformer design for the QWSR maximization problem. Since we assume the queue size to be large, we do not need to control the over-allocation of assigned rates as in (18). Therefore, the user-specific weights $\omega_{k,l}^{(a)}$ are given simply as

$$\omega_{k,l}^{(a)} = \frac{\alpha_k \log_2(\beta) Q_k^{(a)}}{K_1}. \tag{23}$$

The other beamformer and auxiliary variable updates are the same as in WQM. Note that when $Q_k^{(a)} = 1 \forall k$, QWSR objective is equivalent to WSR. Note that when $\beta = 2$, the beamformer estimation procedure is equivalent to the WSMSE based approach.

2.3.3 Sum MSE minimization

The WQM problem can be approximated by a simple SMSE minimizing beamformer design provided that the system operates in a high SNR regime with equal user priorities, the queue sizes are large with $q = 1$, and there are enough spatial degrees of freedom available such that all users can be served concurrently. The SMSE minimization problem can be formulated as

$$\begin{aligned} \underset{\mathbf{m}_{k,l}^{(a)}\mathbf{u}_{k,l}^{(a)}}{\text{min.}} \quad & \sum_{a\in\{\text{UL,DL}\}} \sum_{k} \sum_{l=1}^{L_k} \varepsilon_{k,l}^{(a)} \\ \text{s.t} \quad & \text{(12b), (12c).} \end{aligned} \tag{24}$$

In this special case, the weight updates are not required and the optimal TX and RX beamformers (given fixed RX and TX beamformers) are solved directly from (19) and (6), respectively.

2.4 Training and signalling

In the previous section, we considered iterative beamformer designs for WQM, QWSR, and SMSE objectives. In this section, we introduced possible approaches to implement these algorithms in practice. In all of the proposed iterative beamformer algorithms, we need to iteratively exchange or make available the intermediate beamformers and user-specific weights between the coordinated nodes. However, in a dynamic TDD setup, we do not have the luxury to use a backhaul based approach as UEs also play a role in beamformer estimation. Hence, we employ F-B OTA training for the implicit information exchange [37, 36].

In the considered F-B OTA training scheme, we employ precoded (and weighted) pilot sequences in the forward and backward directions. Here, the forward direction refers to transmitters sending their training sequences, while the backward direction refers to receivers sending their training sequences. The bi-directional training allows a fully distributed coordinated computation of transmit/receive beamformers without full CSI exchange over a backhaul. Furthermore, bi-directional signalling is embedded into

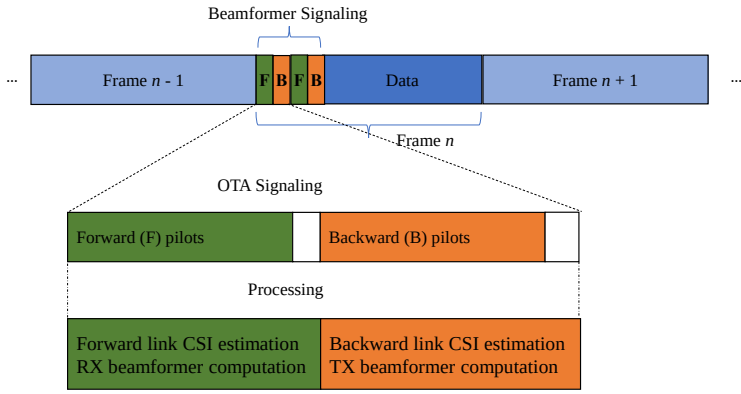

Fig. 4. TDD frame structure (Reprinted, with permission, from [133] ©2018 IEEE)..

each TDD frame to facilitate fast iterative information exchange, as shown in Fig. 4 [36]. The nodes estimate their precoder/decoder based on the received forward/backward training sequences. Then, the estimated precoder/decoder is used for precoding the next iteration forward/backward training. Using this approach, we are able to practically implement the proposed beamformer designs.

It is possible to implement TDD frame structure in Fig. 4 (Scheduling block), with the approved 3GPP NR standard [16]. The beamformer signalling part can be implemented by concatenating multiple minislots together with the required guard period (GP) [36], then multiple slots can be aggregated for data transmission. Moreover, each F-B iteration adds signalling overhead to the system. Hence, it is better to have a larger scheduling block to minimize the signalling overhead. However, it is constrained by coherence time and the traffic burstiness of the system. Note that the TDD frame should be synchronous over the UL/DL cells during the beamformer signalling. However, if the user scheduling remains the same for multiple TDD frames, and if the channel is slowly fading, the B-F training phase can use the beamformers from the previous frame as the starting point. Then, we can have less F-B iterations per TDD frame.

In a dense dynamic TDD network, a large number of orthogonal pilots would be required for ideal pilot estimation. In general, this is not possible due to the limited number of orthogonal resources. Therefore, we have to reuse the pilot sequences or employ non-orthogonal pilots during the training. Thus, the desired channel can be polluted by other user channels. This scenario is known as pilot contamination.

Hence, it is essential to study the dynamic TDD system under imperfect OTA signalling conditions. Pilot contamination can be demoted in several ways, such as allocating pilots to minimize the pilot overlap and using clever channel estimation algorithms [90, 73, 92, 93, 95]. In the following subsections, we study various approaches to mitigate the pilot contamination while supporting the original beamformer design objectives. First, we consider three LS based strategies for direct beamformer estimation using only the precoded pilot information. Then, to further enhance the pilot decontamination, we propose the pilot reuse method based on the large-scale fading information. Additionally, we analytically compare the proposed DE method with the SSE method to prove the superior decontamination capability of the DE approach.

2.4.1 Pilot decontamination by direct beamformer estimation

Here, we investigate the OTA signalling architecture under imperfect pilot conditions by assuming that the pilot training sequences used by each UE/BS are non-orthogonal, and only the pilot training sequences of the associated in-cell users are known to each UE/BS. As we employ non-orthogonal overlapping pilots, the effective channels are contaminated by interfering pilot training sequences. Therefore, they cannot be perfectly distinguished from each other. Without this information, we cannot directly construct $\mathbf{\Phi}_k^{(\mathrm{dl})}$ in (20) at the DL BS i_k or $\mathbf{\Phi}_k^{(\mathrm{ul})}$ in (21) at the UL UE k in order to estimate their transmit precoders. To overcome this problem, we introduce three different strategies to facilitate the direct precoder/decoder estimation by using the received precoded training information directly without separately estimating all individual pilots (channels). In Table 1, the signalling requirements for the forward/backward training are summarized for the proposed schemes: Strategy A, Strategy B and Strategy C. Strategy A is proposed to implement exact beamformer design at both RX and TX with the minimum number OTA signalling (one forward and one backward training iteration per one beamformer signalling round). Hence, a separate (quantized) feedback link is required to transmit additional scalar weight information. Alternatively, we propose two designs: Strategy B and Strategy C. Both schemes use only the OTA signalling to exchange required information. In Strategy B, similar to Strategy A, we try to construct the beamformer design with the minimum number of OTA signalling. However, one backward training is not enough to fully reconstruct the required weighted covariance matrix at the TX node. Hence, Strategy B follows an approximated beamformer design. To overcome the limitation of Strategy B and for the full construction of the beamformer design,

Table 1. Precoded pilots/feedback used in each strategy (Reprinted, with permission, from [133] ©2018 IEEE).

Strategy	Forward training	Backward training		Feedback
		1st	2nd	
Strategy A	$\mathbf{m}_{k,l}^{(a)}$	$\sqrt{\omega_{k,l}^{(a)}}\mathbf{u}_{k,l}^{(a)}$	NA	$\sqrt{\omega_{k,l}^{(a)}}$
Strategy B	$\mathbf{m}_{k,l}^{(a)}$	$\mathbf{u}_{k,l}^{(a)}$	NA	NA
Strategy C	$\mathbf{m}_{k,l}^{(a)}$	$\sqrt{\omega_{k,l}^{(a)}}\mathbf{u}_{k,l}^{(a)}$	$\omega_{k,l}^{(a)}\mathbf{u}_{k,l}^{(a)}$	NA

we propose Strategy C with two backward training resources. Further details on each strategy are presented below.

2.4.2 Strategy A

In this strategy, we employ two training signals and one feedback message for each precoder/decoder iteration. First, forward pilots are transmitted by precoding the training sequence with the transmit beamformers $\mathbf{m}_{k,l}^{(a)}$. Then, the RXs estimate their MMSE receivers $\mathbf{u}_{k,l}^{(a)}$ and the corresponding user-specific weights $\omega_{k,l}^{(a)}$ by using the received pilot training matrices. Next, the RX nodes use weighted MMSE receivers $\sqrt{\omega_{k,l}^{(a)}}\mathbf{u}_{k,l}^{(a)}$ as the precoders for backward training pilots. At the same time, the RXs transmit the square root of user-specific weights $\sqrt{\omega_{k,l}^{(a)}}$ through the feedback channel. Both, the backward pilot information and feedback information are used to estimate the transmit precoder $\mathbf{m}_{k,l}^{(a)}$ at the TX node. In the following, the direct beamformer estimation procedure for Strategy A is described in more detail.

Transmit precoder estimation

Let $\mathbf{b}_{k,l} \in \mathbb{C}^S$ denote the pilot training sequence for l^{th} data stream of DL/UL user k, where S is the length of the pilot sequence. For backward training, the pilots are precoded with $\sqrt{\omega_{k,l}^{(a)}}\mathbf{u}_{k,l}^{(a)}$. Then, the received precoded pilot training matrix of user k at DL BS i_k (note that the $\mathbf{R}_k^{(\text{dl})}$ is the same for all $k \in \mathsf{U}_{i_k}$) is given by

$$\mathbf{R}_k^{(\text{dl})} = \sum_{\{j,l\}\in\mathsf{A}_{\text{dl}}} \sqrt{\omega_{j,l}^{(\text{dl})}}\mathbf{H}_{i_k,j}^{(\text{dl})^{\text{H}}}\mathbf{u}_{j,l}^{(\text{dl})}\mathbf{b}_{j,l}^{\text{H}} + \sum_{\{j,l\}\in\mathsf{A}_{\text{ul}}} \sqrt{\omega_{j,l}^{(\text{ul})}}\mathbf{H}_{i_j,i_k}^{(\text{dl-ul})^{\text{H}}}\mathbf{u}_{j,l}^{(\text{ul})}\mathbf{b}_{j,l}^{\text{H}} + \mathbf{N}_{i_k}^{(\text{dl})}, \quad (25)$$

where $\mathbf{N}_{i_k}^{(\mathrm{dl})} \in \mathbb{C}^{M_{i_k} \times S}$ is the estimation noise matrix for all pilot symbols. Similarly, the received pilot training matrix at UL user k, during the first backward training, is given by

$$\mathbf{R}_k^{(\mathrm{ul})} = \sum_{\{j,l\} \in \mathsf{A}_{\mathrm{ul}}} \sqrt{\omega_{j,l}^{(\mathrm{ul})}} \mathbf{H}_{i_j,k}^{(\mathrm{ul})^{\mathrm{H}}} \mathbf{u}_{j,l}^{(\mathrm{ul})} \mathbf{b}_{j,l}^{\mathrm{H}} + \sum_{\{j,l\} \in \mathsf{A}_{\mathrm{dl}}} \sqrt{\omega_{j,l}^{(\mathrm{dl})}} \mathbf{H}_{j,k}^{(\mathrm{ul\text{-}dl})^{\mathrm{H}}} \mathbf{u}_{j,l}^{(\mathrm{dl})} \mathbf{b}_{j,l}^{\mathrm{H}} + \mathbf{N}_k^{(\mathrm{ul})}, \quad (26)$$

where $\mathbf{N}_k^{(\mathrm{ul})} \in \mathbb{C}^{N_k \times S}$ is the estimation noise matrix.

At DL BS i_k, we recover a noisy version of $\mathbf{\Phi}_k^{(\mathrm{dl})}$ $\forall\, k \in \mathsf{U}_{i_k}$ in (20) directly using the received composite channel information $\mathbf{R}_k^{(\mathrm{dl})}$ as,

$$\bar{\mathbf{\Phi}}_k^{(\mathrm{dl})} = \mathbf{R}_k^{(\mathrm{dl})} \mathbf{R}_k^{(\mathrm{dl})^{\mathrm{H}}} = \mathbf{\Phi}_k^{(\mathrm{dl})} + \mathbf{\Omega}_{i_k}, \quad (27)$$

where $\mathbf{\Omega}_{i_k}$ includes all the cross-terms in (25) due to non-orthogonal pilots as well as noise. With orthogonal pilots, $\mathbf{\Omega}_{i_k}$ would contain only estimation noise. The structure and significance of $\mathbf{\Omega}_{i_k}$ is examined in more detail in Section 2.4.5. Similarly, we can approximately construct $\mathbf{\Phi}_k^{(\mathrm{ul})}$ in (21) at UL user k directly using the received composite channel information $\mathbf{R}_k^{(\mathrm{ul})}$ as

$$\bar{\mathbf{\Phi}}_k^{(\mathrm{ul})} = \mathbf{R}_k^{(\mathrm{ul})} \mathbf{R}_k^{(\mathrm{ul})^{\mathrm{H}}} = \mathbf{\Phi}_k^{(\mathrm{ul})} + \mathbf{\Omega}_k, \quad (28)$$

where $\mathbf{\Omega}_k$ indicates the cross pilot interference.

With the knowledge of the received training matrices $\mathbf{R}_k^{(a)}$, user-specific weights $\sqrt{\omega_{k,l}^{(a)}}$ (received via the feedback channel) and own training sequences $\mathbf{b}_{k,l}$, we can locally estimate the transmit beamformers in a closed form expressions as

$$\mathbf{m}_{k,l}^{(a)} = \left(\mathbf{R}_k^{(a)} \mathbf{R}_k^{(a)^{\mathrm{H}}} + \mathbf{I} \nu_k^{(a)} \right)^{-1} \sqrt{\omega_{k,l}^{(a)}} \mathbf{R}_k^{(a)} \mathbf{b}_{k,l}, \quad (29)$$

where the optimal $\nu_k^{(\mathrm{dl})}$ and $\nu_k^{(\mathrm{ul})}$ are found by a bisection search to satisfy the power constraints $\sum_{k \in \mathsf{U}_i} \sum_{l=1}^{L_k} \|\mathbf{m}_{k,l}^{(\mathrm{dl})}\|^2 \leq P_i^{(\mathrm{dl})}$ and $\sum_{l=1}^{L_k} \|\mathbf{m}_{k,l}^{(\mathrm{ul})}\|^2 \leq P_k^{(\mathrm{ul})}$, respectively. In ideal conditions with orthogonal pilots and a very high pilot SNR (or very large S), (29) would be equal to (19).

Receive beamformer and weights estimation

In the forward training, the pilots are precoded with the transmit precoders $\mathbf{m}_{k,l}^{(a)}$. Then, the received precoded pilot training matrix at DL user k is given by,

$$\mathbf{T}_k^{(\mathrm{dl})} = \sum_{\{j,l\} \in \mathsf{A}_{\mathrm{dl}}} \mathbf{H}_{i_j,k}^{(\mathrm{dl})} \mathbf{m}_{j,l}^{(\mathrm{dl})} \mathbf{b}_{j,l}^{\mathrm{H}} + \sum_{\{j,l\} \in \mathsf{A}_{\mathrm{ul}}} \mathbf{H}_{j,k}^{(\mathrm{ul\text{-}dl})} \mathbf{m}_{j,l}^{(\mathrm{ul})} \mathbf{b}_{j,l}^{\mathrm{H}} + \mathbf{N}_k^{(\mathrm{dl})}, \quad (30)$$

where $\mathbf{N}_k^{(\mathrm{dl})} \in \mathbb{C}^{N_k \times S}$ is the estimation noise matrix for all pilot symbols. Similarly, the received precoded pilot training matrix at UL BS i_k is given by

$$\mathbf{T}_k^{(\mathrm{ul})} = \sum_{\{j,l\} \in \mathsf{A}_{\mathrm{ul}}} \mathbf{H}_{i_k,j}^{(\mathrm{ul})} \mathbf{m}_{j,l}^{(\mathrm{ul})} \mathbf{b}_{j,l}^{\mathrm{H}} + \sum_{\{j,l\} \in \mathsf{A}_{\mathrm{dl}}} \mathbf{H}_{i_j,i_k}^{(\mathrm{dl\text{-}ul})} \mathbf{m}_{j,l}^{(\mathrm{dl})} \mathbf{b}_{j,l}^{\mathrm{H}} + \mathbf{N}_{i_k}^{(\mathrm{ul})}, \tag{31}$$

where $\mathbf{N}_{i_k}^{(\mathrm{ul})} \in \mathbb{C}^{M_{i_k} \times S}$ is the estimation noise matrix. Then, by using the received composite channel information $\mathbf{T}_k^{(a)}$ and own pilot training sequence $\mathbf{b}_{k,l}$ we can directly estimate the MMSE receivers as

$$\mathbf{u}_{k,l}^{(a)} = \left(\mathbf{T}_k^{(a)} \mathbf{T}_k^{(a)^{\mathrm{H}}} + \mathsf{N}_0 \mathbf{I} \right)^{-1} \mathbf{T}_k^{(a)} \mathbf{b}_{k,l}. \tag{32}$$

Additionally, the RX MSE can be estimated as

$$\varepsilon_{k,l}^{(a)} = 1 - \mathbf{u}_{k,l}^{(a)\mathrm{H}} \mathbf{T}_k^{(a)} \mathbf{b}_{k,l}. \tag{33}$$

Finally, we can estimate $\omega_{k,l}^{(a)}$ using (18) or (23) based on our optimization objective. Note that here we assume that, for any particular user, the forward and backward sequences are the same. However, the forward/backward pilots can also be designed separately.

2.4.3 Strategy B

In contrast to Strategy A, Strategy B does not require feedback channel to exchange the user-specific weights. Similar to Strategy A, the forward training pilots are precoded with the transmit precoders $\mathbf{m}_{k,l}^{(a)}$. Then, the RX nodes estimate the MMSE receivers $\mathbf{u}_{k,l}^{(a)}$. Next, the estimated MMSE receivers are used to precode the backward training pilots. The information received from the backward training pilots is enough to reconstruct the $\mathbf{\Phi}_k^{(a)}$ at TX k/i_k. However, by using locally evaluated user-specific weights, we can only approximately estimate the transmit precoders.

Transmit precoder estimation

In the backward training, the pilots are precoded with the MMSE receivers $\mathbf{u}_{k,l}^{(a)}$ without weights $\omega_{k,l}^{(a)}$. The received pilot training matrix at DL BS $i_k, \forall\, k \in \mathsf{U}_{i_k}$ is, then, given by

$$\mathbf{R}_{k,1}^{(\mathrm{dl})} = \sum_{\{j,l\} \in \mathsf{A}_{\mathrm{dl}}} \mathbf{H}_{i_k,j}^{(\mathrm{dl})^{\mathrm{H}}} \mathbf{u}_{j,l}^{(\mathrm{dl})} \mathbf{b}_{j,l}^{\mathrm{H}} + \sum_{\{j,l\} \in \mathsf{A}_{\mathrm{ul}}} \mathbf{H}_{i_j,i_k}^{(\mathrm{dl\text{-}ul})^{\mathrm{H}}} \mathbf{u}_{j,l}^{(\mathrm{ul})} \mathbf{b}_{j,l}^{\mathrm{H}} + \mathbf{N}_{i_k}^{(\mathrm{dl})}. \tag{34}$$

Similarly, the received pilot training matrix at UL user k, during the first backward training, is given by

$$\mathbf{R}_{k,1}^{(\mathrm{ul})} = \sum_{\{j,l\}\in \mathsf{A}_{\mathrm{ul}}} \mathbf{H}_{i_j,k}^{(\mathrm{ul})^{\mathrm{H}}} \mathbf{u}_{j,l}^{(\mathrm{ul})} \mathbf{b}_{j,l}^{\mathrm{H}} + \sum_{\{j,l\}\in \mathsf{A}_{\mathrm{dl}}} \mathbf{H}_{j,k}^{(\mathrm{ul\text{-}dl})^{\mathrm{H}}} \mathbf{u}_{j,l}^{(\mathrm{dl})} \mathbf{b}_{j,l}^{\mathrm{H}} + \mathbf{N}_k^{(\mathrm{ul})}. \tag{35}$$

Then, we can estimate the user weights $\omega_{k,l}^{(a)}$ *locally* by using the first set of received composite channel $\mathbf{R}_{k,1}^{(a)}$ and training sequence $\mathbf{b}_{k,l}$ at TX k/i_k. To do this, first, we estimate MSE $\varepsilon_{k,l}^{(a)}$ locally as

$$\varepsilon_{k,l}^{(a)} = 1 - (\mathbf{R}_{k,1}^{(a)} \mathbf{b}_{k,l})^{\mathrm{H}} \bar{\mathbf{m}}_{k,l}^{(a)}, \tag{36}$$

where $\bar{\mathbf{m}}_{k,l}^{(a)}$ is the transmit precoder estimated in the previous iteration or the initial condition. Then, we can estimate $\omega_{k,l}^{(a)}$ using (18) or (23). Finally, we construct $\bar{\mathbf{\Phi}}_{k,1}^{(\mathrm{dl})}$, at DL BS i_k, as

$$\begin{aligned}
\bar{\mathbf{\Phi}}_{k,1}^{(\mathrm{dl})} &\triangleq \mathbf{R}_{k,1}^{(\mathrm{dl})} (\mathbf{I} + \sum_{j\in \mathsf{U}_{i_k}} \sum_{l=1}^{L_j} \frac{(\omega_{j,l}^{(\mathrm{dl})} - 1)}{S} \mathbf{b}_{j,l} \mathbf{b}_{j,l}^{\mathrm{H}}) \mathbf{R}_{k,1}^{(\mathrm{dl})^{\mathrm{H}}} \\
&= \sum_{j\in \mathsf{U}_{i_k}} \sum_{l=1}^{L_j} \omega_{j,l}^{(\mathrm{dl})} \mathbf{H}_{i_k,j}^{(\mathrm{dl})^{\mathrm{H}}} \mathbf{u}_{j,l}^{(\mathrm{dl})} (\mathbf{H}_{i_k,j}^{(\mathrm{dl})^{\mathrm{H}}} \mathbf{u}_{j,l}^{(\mathrm{dl})})^{\mathrm{H}} + \sum_{\substack{\{j,l\}\in \mathsf{A}_{\mathrm{dl}} \\ j\notin \mathsf{U}_{i_k}}} \mathbf{H}_{i_k,j}^{(\mathrm{dl})^{\mathrm{H}}} \mathbf{u}_{j,l}^{(\mathrm{dl})} (\mathbf{H}_{i_k,j}^{(\mathrm{dl})^{\mathrm{H}}} \mathbf{u}_{j,l}^{(\mathrm{dl})})^{\mathrm{H}} \\
&\quad + \sum_{\{j,l\}\in \mathsf{A}_{\mathrm{ul}}} \mathbf{H}_{i_j,i_k}^{(\mathrm{dl\text{-}ul})^{\mathrm{H}}} \mathbf{u}_{j,l}^{(\mathrm{ul})} (\mathbf{H}_{i_j,i_k}^{(\mathrm{dl\text{-}ul})^{\mathrm{H}}} \mathbf{u}_{j,l}^{(\mathrm{ul})})^{\mathrm{H}} + \mathbf{\Omega}_{i_k}.
\end{aligned} \tag{37}$$

Similarly, at UL UE k, we construct $\bar{\mathbf{\Phi}}_k^{(\mathrm{ul})}$ as

$$\begin{aligned}
\bar{\mathbf{\Phi}}_{k,1}^{(\mathrm{ul})} &\triangleq \mathbf{R}_{k,1}^{(\mathrm{ul})} (\mathbf{I} + \sum_{l=1}^{L_k} \frac{(\omega_{k,l}^{(\mathrm{dl})} - 1)}{S} \mathbf{b}_{k,l} \mathbf{b}_{k,l}^{\mathrm{H}}) \mathbf{R}_{k,1}^{(\mathrm{ul})^{\mathrm{H}}} \\
&= \sum_{l=1}^{L_k} \omega_{k,l}^{(\mathrm{ul})} \mathbf{H}_{i_k,k}^{(\mathrm{ul})^{\mathrm{H}}} \mathbf{u}_{k,l}^{(\mathrm{ul})} (\mathbf{H}_{i_k,k}^{(\mathrm{ul})^{\mathrm{H}}} \mathbf{u}_{k,l}^{(\mathrm{ul})})^{\mathrm{H}} + \sum_{\substack{\{j,l\}\in \mathsf{A}_{\mathrm{ul}} \\ j\neq k}} \mathbf{H}_{i_j,k}^{(\mathrm{ul})^{\mathrm{H}}} \mathbf{u}_{j,l}^{(\mathrm{ul})} (\mathbf{H}_{i_j,k}^{(\mathrm{ul})^{\mathrm{H}}} \mathbf{u}_{j,l}^{(\mathrm{ul})})^{\mathrm{H}} \\
&\quad + \sum_{\{j,l\}\in \mathsf{A}_{\mathrm{dl}}} \mathbf{H}_{j,k}^{(\mathrm{ul\text{-}dl})^{\mathrm{H}}} \mathbf{u}_{j,l}^{(\mathrm{dl})} (\mathbf{H}_{j,k}^{(\mathrm{ul\text{-}dl})^{\mathrm{H}}} \mathbf{u}_{j,l}^{(\mathrm{dl})})^{\mathrm{H}} + \mathbf{\Omega}_k.
\end{aligned} \tag{38}$$

It is clear that in this estimation scheme, $\bar{\mathbf{\Phi}}_{k,1}^{(\mathrm{ul})}$ does not contain the ideal $\mathbf{\Phi}_k^{(\mathrm{a})}$ from (20)-(21) unlike in (37)-(38). This is mainly due to the unavailability of the user specific weights from the interfered users. This is equivalent to assuming $\omega_{k,l}^{(a)} = 1$ for all

non-local data streams. As in Strategy A, with the knowledge of the received training matrices $\mathbf{R}_{k,1}^{(a)}$ and own training sequences $\mathbf{b}_{k,l}$, we can estimate the transmit beamformers directly in closed form as

$$\mathbf{m}_{k,l}^{(a)} = \left(\bar{\mathbf{\Phi}}_{k,1}^{(a)} + \mathbf{I}\nu_k^{(a)}\right)^{-1} \omega_{k,l}^{(a)} \mathbf{R}_{k,1}^{(a)} \mathbf{b}_{k,l} \tag{39}$$

where the optimal $\nu_k^{(\mathrm{a})}$ is found by a bisection search similar to (29). The receive beamformer estimation procedure for Strategy B is the same as in Strategy A.

2.4.4 Strategy C

In this strategy, we employ three training pilots per beamformer iteration, one in the forward direction and two consecutive training pilots in the backward direction. The forward training procedure is the same as strategies A and B, where we use transmit precoders $\mathbf{m}_{k,l}^{(a)}$ as the pilot precoders. The RXs estimate their MMSE receivers $\mathbf{u}_{k,l}^{(a)}$ and the corresponding user weights $\omega_{k,l}^{(a)}$ from the received pilots. In the backward phase, the first training sequences are precoded with $\sqrt{\omega_{k,l}^{(a)}}\mathbf{u}_{k,l}^{(a)}$ and the second transmission pilot sequences are precoded with $\omega_{k,l}^{(a)}\mathbf{u}_{k,l}^{(a)}$. The estimated pilot training matrices for the first pilot sequence are the same as in Strategy A (25)-(26), denoted by $\mathbf{R}_k^{(a)}$. The training matrix corresponding to the second pilot sequence, denoted by $\mathbf{R}_{k,2}^{(a)}$, is the same except that the weight difference ($\sqrt{\omega_{k,l}^{(a)}}$ is replaced by $\omega_{k,l}^{(a)}$). The backward pilot information is used to estimate the transmit precoder $\mathbf{m}_{k,l}^{(a)}$ as

$$\mathbf{m}_{k,l}^{(a)} = \left(\mathbf{R}_k^{(a)}\mathbf{R}_k^{(a)^{\mathrm{H}}} + \mathbf{I}\nu_k^{(a)}\right)^{-1} \mathbf{R}_{k,2}^{(a)} \mathbf{b}_{k,l}. \tag{40}$$

Other expressions are derived similar to Strategies A and B and are omitted here to avoid repetition.

2.4.5 DE vs SSE

The signalling and training strategies proposed in previous subsections directly estimate the beamformers (DE approach) from the received pilot training matrices. As an alternative implementation, we consider the SSE technique. In the SSE method, we separately estimate each pilot, and the estimated information is used to calculate beamformers and user weights. Therefore, all the coordinating nodes need to know the

pilot sequences used at each node. The SSE approach can be highly vulnerable to pilot contamination, if non-orthogonal pilot sequences are employed for OTA signalling. However, the DE is better suited for noisy environments and more resilient to pilot contamination. In this section, we analyse the DE and SSE estimation inaccuracies by considering the estimation of $\mathbf{\Phi}_k^{(\mathrm{dl})}$ in Strategy A. Additionally, without loss of generality, we examine *DL only* case ($\mathsf{A}_{\mathrm{ul}} = \emptyset$) in order to ease the notational complexity.

In stream specific estimation, we assume that all pilots are first individually estimated. Then, the covariance matrices and beamformers are constructed from those individual parts. The signalling model remains the same, that is, the received training matrix is of form (25). Recalling that $\mathbf{R}_k^{(\mathrm{dl})}$ is the same for all $k \in \mathsf{U}_{i_k}$, from (25), each DL BS $i_k = 1,\ldots,B, k \in \mathsf{U}_{i_k}$ estimates the UE (stream) specific pilots as

$$\mathbf{f}_{i_k,j,l}^{(\mathrm{dl})} = \mathbf{R}_k^{(\mathrm{dl})}\mathbf{b}_{j,l}, \forall (j,l) = \sqrt{\omega_{j,l}^{(\mathrm{dl})}}\mathbf{H}_{i_k,j}^{(\mathrm{dl})\mathrm{H}}\mathbf{u}_{j,l}^{(\mathrm{dl})} + \delta_{i_k,j,l}, \tag{41}$$

where $\delta_{i_k,j,l}$ denotes the estimation noise and pilot contamination corresponding to pilot sequence $\mathbf{b}_{j,l}$ at BS i_k. We can immediately observe a potential downside to this. In order to accomplish (41), BS i_k has to know all pilot sequences $\mathbf{b}_{j,l}$. Additionally, the amount of estimation noise and pilot contamination gradually increases with the number of pilot sequences. Then, by using all the collected stream specific estimates, the matrix $(\bar{\mathbf{\Phi}}_k^{(\mathrm{dl})})_{\mathrm{SSE}}$ for the SSE approach is given by

$$(\bar{\mathbf{\Phi}}_k^{(\mathrm{dl})})_{\mathrm{SSE}} = \sum_{\{j,l\}\in\mathsf{A}_{\mathrm{dl}}} \mathbf{f}_{i_k,j,l}^{(\mathrm{dl})}\mathbf{f}_{i_k,j,l}^{(\mathrm{dl})\mathrm{H}} = \mathbf{\Phi}_k^{(\mathrm{dl})} + \mathbf{K}_k + \bar{\mathbf{K}}_k + \sum_{\{j,l\}\in\mathsf{A}_{\mathrm{dl}}} \mathbf{N}_{i_k}^{(\mathrm{dl})}\mathbf{b}_{j,l}\mathbf{b}_{j,l}^{\mathrm{H}}\mathbf{N}_{i_k}^{(\mathrm{dl})\mathrm{H}} \tag{42}$$

where $\mathbf{K}_k$ and $\bar{\mathbf{K}}_k$ are additional interference terms given in (43) and (44), respectively. In contrast, the estimation expressions $(\bar{\mathbf{\Phi}}_k^{(\mathrm{dl})})_{\mathrm{DE}}$ for the DE approach are given by

$$(\bar{\mathbf{\Phi}}_k^{(\mathrm{dl})})_{\mathrm{DE}} = \mathbf{R}_k^{(\mathrm{dl})}\mathbf{R}_k^{(\mathrm{dl})\mathrm{H}} = \mathbf{\Phi}_k^{(\mathrm{dl})} + \mathbf{K}_k + \mathbf{N}_{i_k}^{(\mathrm{dl})}\mathbf{N}_{i_k}^{(\mathrm{dl})\mathrm{H}} \tag{45}$$

From the expressions in (45) and (42), we can observe that the SSE expression differs from DE case due to additional estimation error term $\bar{\mathbf{K}}_k$ and estimated noise terms $\mathbf{N}_{i_k}^{(\mathrm{dl})}\mathbf{N}_{i_k}^{(\mathrm{dl})\mathrm{H}}$ and $\sum_{\{j,l\}\in\mathsf{A}_{\mathrm{dl}}}\mathbf{N}_{i_k}^{(\mathrm{dl})}\mathbf{b}_{j,l}\mathbf{b}_{j,l}^{\mathrm{H}}\mathbf{N}_{i_k}^{(\mathrm{dl})\mathrm{H}}$. In order to compare the DE and SSE approaches, first, we can see that $\mathbb{E}[\mathbf{N}_{i_k}^{(\mathrm{dl})}\mathbf{N}_{i_k}^{(\mathrm{dl})\mathrm{H}}]$ is a diagonal matrix of size $M_{i_k} \times M_{i_k}$ with each diagonal element equal to $\mathsf{N}_0 S$, i.e.,

$$\mathrm{Tr}(\mathbb{E}[\mathbf{N}_{i_k}^{(\mathrm{dl})}\mathbf{N}_{i_k}^{(\mathrm{dl})\mathrm{H}}]) = M_{i_k}\mathsf{N}_0 S. \tag{46}$$

For the SSE case, we can form a symmetric matrix $\mathbf{C}_{i_k} = \sum_{\{j,l\}\in\mathsf{A}_{\mathrm{dl}}}\mathbf{b}_{j,l}\mathbf{b}_{j,l}^{\mathrm{H}}$ with the size of $S \times S$, where the diagonal terms are equal to K/S. Since the matrix trace is invariant

$$\mathbf{K}_k = \sum_{\substack{\{j,l\}\in \mathsf{A}_{\mathrm{dl}} \\ \{y,z\}\in \mathsf{A}_{\mathrm{dl}} \\ (y\neq j \& z\neq l)}} \sqrt{\omega_{j,l}^{(\mathrm{dl})}\omega_{y,z}^{(\mathrm{dl})}}\mathbf{H}_{i_k,j}^{(\mathrm{dl})^{\mathrm{H}}}\mathbf{u}_{j,l}^{(\mathrm{dl})}\mathbf{b}_{j,l}^{\mathrm{H}}\mathbf{b}_{y,z}(\mathbf{H}_{i_k,y}^{(\mathrm{dl})^{\mathrm{H}}}\mathbf{u}_{y,z}^{(\mathrm{dl})})^{\mathrm{H}}$$
$$+ \sum_{\{j,l\}\in \mathsf{A}_{\mathrm{dl}}} \sqrt{\omega_{j,l}^{(\mathrm{dl})}}\left(\mathbf{H}_{i_k,j}^{(\mathrm{dl})^{\mathrm{H}}}\mathbf{u}_{j,l}^{(\mathrm{dl})}\mathbf{b}_{j,l}^{\mathrm{H}}\mathbf{N}_{i_k}^{(\mathrm{dl})^{\mathrm{H}}} + \mathbf{N}_{i_k}^{(\mathrm{dl})}\mathbf{b}_{j,l}(\mathbf{H}_{i_k,j}^{(\mathrm{dl})^{\mathrm{H}}}\mathbf{u}_{j,l}^{(\mathrm{dl})})^{\mathrm{H}}\right) \tag{43}$$

$$\bar{\mathbf{K}}_k = \sum_{\substack{\{\{j,l\},\{y,z\},\{s,t\}\}\in \mathsf{A}_{\mathrm{dl}} \\ (s\neq j \& t\neq l)}} \sqrt{\omega_{s,t}^{(\mathrm{dl})}\omega_{y,z}^{(\mathrm{dl})}}\mathbf{H}_{i_k,s}^{(\mathrm{dl})^{\mathrm{H}}}\mathbf{u}_{s,t}^{(\mathrm{dl})}\mathbf{b}_{s,t}^{\mathrm{H}}\mathbf{b}_{j,l}\mathbf{b}_{j,l}^{\mathrm{H}}\mathbf{b}_{y,z}(\mathbf{H}_{i_k,y}^{(\mathrm{dl})^{\mathrm{H}}}\mathbf{u}_{y,z}^{(\mathrm{dl})})^{\mathrm{H}}$$
$$+ \sum_{\substack{\{\{j,l\},\{y,z\}\}\in \mathsf{A}_{\mathrm{dl}} \\ (y\neq j \& z\neq l)}} \sqrt{\omega_{y,z}^{(\mathrm{dl})}}\left(\mathbf{H}_{i_k,y}^{(\mathrm{dl})^{\mathrm{H}}}\mathbf{u}_{y,z}^{(\mathrm{dl})}\mathbf{b}_{y,z}^{\mathrm{H}}\mathbf{b}_{j,l}\mathbf{b}_{j,l}^{\mathrm{H}}\mathbf{N}_{i_k}^{(\mathrm{dl})^{\mathrm{H}}} + \mathbf{N}_{i_k}^{(\mathrm{dl})}\mathbf{b}_{j,l}\mathbf{b}_{j,l}^{\mathrm{H}}\mathbf{b}_{y,z}(\mathbf{H}_{i_k,y}^{(\mathrm{dl})^{\mathrm{H}}}\mathbf{u}_{y,z}^{(\mathrm{dl})})^{\mathrm{H}}\right) \tag{44}$$

under cyclic permutations, the following holds

$$\mathrm{Tr}(\mathbb{E}[\sum_{\{j,l\}\in \mathsf{A}_{\mathrm{dl}}} \mathbf{N}_{i_k}^{(\mathrm{dl})}\mathbf{b}_{j,l}\mathbf{b}_{j,l}^{\mathrm{H}}\mathbf{N}_{i_k}^{(\mathrm{dl})^{\mathrm{H}}}]) = M_{i_k}\mathsf{N}_0 K. \tag{47}$$

Assuming a practical scenario where the number of users served is larger than the available pilot resources (sequence length), $K > S$, then

$$\mathrm{Tr}(\mathbb{E}[\sum_{\{j,l\}\in \mathsf{A}_{\mathrm{dl}}} \mathbf{N}_{i_k}^{(\mathrm{dl})}\mathbf{b}_{j,l}\mathbf{b}_{j,l}^{\mathrm{H}}\mathbf{N}_{i_k}^{(\mathrm{dl})^{\mathrm{H}}}]) > \mathrm{Tr}(\mathbb{E}[\mathrm{N}_{i_k}^{(\mathrm{dl})}\mathbf{N}_{i_k}^{(\mathrm{dl})^{\mathrm{H}}}]). \tag{48}$$

Finally, by taking the MSE of estimates (45) and (42), we can obtain the following relationship

$$\mathbb{E}[|(\mathbf{\Phi}_k^{(\mathrm{dl})})_{\mathrm{SSE}} - \mathbf{\Phi}_k^{(\mathrm{dl})}|^2] \succ \mathbb{E}[|(\mathbf{\Phi}_k^{(\mathrm{dl})})_{\mathrm{DE}} - \mathbf{\Phi}_k^{(\mathrm{dl})}|^2] + \bar{\mathbf{K}}_k\bar{\mathbf{K}}_k^{\mathrm{H}}, \tag{49}$$

where the inequality follows from (48) and from the fact that $\bar{\mathbf{K}}_k\bar{\mathbf{K}}_k^{\mathrm{H}}$ is a positive definite matrix. Thus, DE provides better estimation performance than SSE in the MSE sense.

2.4.6 Decontamination via pilot reuse

In this section, we consider a traditional pilot reuse approach to enhance the pilot decontamination further. The main aim is to assess how much additional gain can be achieved by applying a *centralized* pilot assignment as compared to the decentralized direct estimation methods proposed in Section 3.4.1. A simple pilot reuse approach

is proposed for a complicated dynamic TDD setup based only on large-scale fading information of the BS-UE and UE-UE channels. In dynamic TDD networks, finding a proper utility for the pilot assignment is challenging. For example, the received channel information at DL UE k in the forward training phase and received channel information at DL BS i_k in the backward training phase are contaminated with different set of BSs and UEs. Consequently, taking into account the specific challenges associated with the dynamic TDD scenario, we propose a logarithmically weighted interference-to-signal-ratio (ISR) based decontamination scheme.

In the considered heuristic method, the pilot allocation is carried out utilizing the user specific path loss measurements and reports. The basic idea is to reuse the same pilot for two users when they are physically far from each other. In addition to BS-UE path loss measurements, we assume UE-UE received signal strength indicator (RSSI) based measurements are made available at BSs to avoid allocating the same pilots to severely interfering DL and UL users. In order to do this, UE should be able to listen to received signals from both BSs and nearby UEs. Based on the RSSI measurements, UE reports a set of strongest measured RSSI values, both from BSs and UEs to serving BS via a separate control channel.

To assign the pilots, we define a cost function R_{G_p} for every orthogonal pilot $p \in \{1,...,S\}$ that is shared with a set of users $\mathsf{G}_p \subset \mathsf{U}$ as

$$R_{\mathsf{G}_p} = \sum_{k \in \mathsf{G}_p} \log(1 + \sum_{j \in \mathsf{G}_p / \{k\}} I_j / S_k) \tag{50}$$

where S_k is the path gain between user k serving BS i_k, and I_j is the path gain between interfering user j and BS i_k. Logarithmic ISR weighting is used to provide fairness such that weak users (far from BS) are not severely penalized. Every time a pilot is reused, the cost function is increased correspondingly. The resulting ISR value is scaled by 1 to make the utility function always positive. Finally, the minimization problem used for the pilot allocation is formulated as

$$\begin{aligned} &\underset{\mathsf{G}_p \forall p}{\text{minimize}} \quad \sum_{p=1}^{S} R_{\mathsf{G}_p} \\ &s.t \qquad \mathsf{Y}_k \cap \mathsf{G}_p = \emptyset \qquad \forall k, p, \end{aligned} \tag{51}$$

where Y_k is the set of users with the shortest UE-UE distance to user k. Finding an optimal solution for the above integer problem is highly complex for large S and K. Hence, a sub-optimal greedy method is used to solve the problem and the entire process

is summarized in Algorithm 2. First, potential cost values for each pair are computed assuming they share the same pilot. Then, the user pair with the minimum cost is assigned with the same pilot. Consequently, next pilot resources are assigned to the unassigned user pairs with the minimum utility value. Continuing this, up to $2S$ users are assigned. Then, the rest of the unassigned users are allocated to pilots using the same greedy method on the per pilot basis in such a way that the corresponding pilot will not be used more than $K/S+1$ times. Here, the main target is to minimize the total log weighted pilot interference in the system. This may not accurately match the original traffic aware optimization objective in Section 2.3. However, the results show significant sum rate improvement as compared to random pilot assignment.

Algorithm 2 Pilot Reuse Algorithm

1: **Initialize** :
   - Define $k_{\max} = \lceil \frac{K}{S} \rceil$ - maximum number of users that are assigned to the same pilot.
   - Find Y_k for each user k and set $\mathsf{G} = \emptyset$.
2: **First phase:** Assign pilots up to $2S$ users
3: For $a = 1 : K$, For $b = 1 : K$, If $b \notin \mathsf{Y}_a$ do:
4: Calculate $R_{\{a,b\}}$ for $\{a,b\}$ UE pair from (50).
5: End, End, End
6: For $p = 1 : S$ do:
7: Define set $\mathsf{X} = \{\{a,b\} \mid \{a,b\} \subset \mathsf{U} \text{ and } \{a,b\} \not\subset \mathsf{G}\}$
8: $\underset{\forall \{a,b\} \subset \mathsf{X}}{\text{argmin}} \; R_{\{a,b\}} \rightarrow \mathsf{G}_p = \{a,b\}$
9: Update user assignment $\mathsf{G} = \mathsf{G}_1 \cup ... \cup \mathsf{G}_S$
10: End
11: **Last phase:** Assign pilots to unassigned users
12: For $c = 1 : k_{\max} - 2$, For $p = 1 : S$, do:
13: Define set $\mathsf{Z} = \{x \mid \mathsf{Y}_x \cap \mathsf{G}_p = \emptyset \text{ and } x \notin \mathsf{G}\}$
14: $\underset{x \in \mathsf{Z}}{\text{argmin}} \; R_{\mathsf{G}_p \cup \{x\}} \rightarrow \mathsf{G}_p = \mathsf{G}_p \cup \{x\}$
15: Update pilot assignment $\mathsf{G} = \mathsf{G}_1 \cup ... \cup \mathsf{G}_S$
16: End End

2.4.7 Complexity and overhead

It is important to study the complexity and associated overhead of the proposed DE-based strategies. Therefore, in this subsection, we look into those two concerns.

Complexity study

Here, we study the computational complexity of the proposed direct beamformer estimation methods. All strategies have similar computational complexities. Hence, we consider Strategy A in this study. In proposed iterative strategies, the complexity is linearly proportional to the number of OTA signalling rounds. Hence, we focus on one iteration only. There are four types of nodes involved in computing beamformers. The corresponding complexity at each node is as follows:

- DL BS - The dominant operation is the matrix inversion in (29). Additionally, there is a dual variable which we found by a bisection search to satisfy the power constraint. Hence, the complexity is $\mathsf{O}(M_i^3 \times \Delta \times K_i \times L_k)$, where Δ is the number of bisection iterations required to satisfy the power constraint.
- DL UE - Here, the dominant operation is the matrix product operation within the inverse matrix in (32). Hence the complexity is $\mathsf{O}(N_k^2 \times S)$.
- UL BS - The complexity due to operations in (32) is roughly $\mathsf{O}(M_i^2 \times (M_i + S + L_k \times K_i))$.
- UL UE - The dominant complexity comes from the bisection iterations and the matrix inversion in (29). Therefore, the complexity is $\mathsf{O}(N_k^3 \times \Delta \times L_k)$.

It is obvious that BS should have a higher computational capability compared to UEs. For the proposed strategies, for BSs, the maximum complexity requirement arises when it is in DL mode, which is $\mathsf{O}(M_i^3 \times \Delta \times K \times L_k)$ per one beamformer signalling round. Additionally, for UEs, the maximum complexity requirement is $\mathsf{O}(N_k^3 \times \Delta \times L_k)$, which arises when it is in UL mode.

Overhead model

As in Fig. 4, the TDD frame is divided into two portions: 1. beamformer signalling, 2. data transmission. Therefore, the actual achievable rate of the system pretty much

depends on the beamformer training duration. Here, we can model it as

$$R_{\mathrm{ac}} = (1 - \frac{\tau_0}{T}\mathrm{BIT})R_{\mathrm{sum}}, \tag{52}$$

where, R_{ac} is the actual achievable sum rate and R_{sum} is the achieved sum rate from the iterative algorithm after BIT bi-directional precoder/decoder training rounds. The signalling overhead per one signalling round is $\frac{\tau_0}{\mathrm{T}}$, where τ_0 and T are the duration for a one precoder/decoder iteration and the duration of the TDD frame, respectively. Here, we refer to τ_0 as the 'effective overhead duration per F-B training round '. The following tasks are performed during the τ_0

- Tx nodes transmit precoded pilots, which are precoded with transmit beamformers (F-training).
- Rx nodes estimate receiver beamformers and user-specific weights.
- Rx nodes transmit pilots using the estimated receive beamformers as pilot precoders possibly weighted by the user-specific weights as described in Section IV.B-D (B-training). Moreover, in Strategy A, we utilize a separate (quantized) feedback mechanism to exchange the scalar weights.
- Tx nodes estimate transmit precoders.

In addition to the above tasks, a guard period is required when the communication direction changes forward to backward and vice-versa. However, the overhead related for exchanging control messages such as measured RSSI values, explicit information about the queue sizes and prioritize coefficients is not included in this formula as the reporting period for such messages is much longer. In numerical examples, we investigate the optimal number of bi-directional signalling rounds required for a TDD frame with this overhead model.

2.5 Numerical examples

Numerical analyses of the dynamic TDD system were conducted using two different simulation models, a 19-cell wrap-up model, and a standalone model. The following subsections analyse the performance of dynamic TDD with these simulation models.

2.5.1 19-cell wrap-up model

The simulations are carried out for the nineteen cell (= 19) wrap-around model, as illustrated in Fig. 5. The distances between the BSs are considered to be 200 m and the

UEs are randomly placed at the cell edge. For all the simulations, the path loss exponent is fixed to 3.67. The power constraint for DL BSs and UL UEs are normalized such that $P_k^{(\mathrm{ul})} = P_i^{(\mathrm{dl})}/K_i$, i.e., the total cell-specific UL power is equal to the DL power. However, we consider a different power allocation in Fig. 9. Moreover, SNR is defined with respect to the DL cell edge user (SNR = $S_k P_{i_k}^{(\mathrm{dl})}/\mathsf{N}_0$). To simplify the study, all the user priority weights are assumed to be $\alpha_k = 1$. In Fig. 10, we examine time-correlated block fading, which is generated using Jake's Doppler spectrum model with the normalized user terminal velocity $t_S f_D = 0.01$, where t_S and f_D are the signalling rate and the maximum Doppler shift, respectively. For the rest of the figures, we have used an uncorrelated block fading model. We have randomly assigned UL/DL BSs with DL cell probability = 0.5, for all the results except in Fig. 8. User weights $\alpha_k Q_k^{(a)} = 1 \forall k$ are used for all results with WSR maximization. Perfect CSIT is assumed to be available in the simulation results shown in Figs. 6–10. For the practical channel/beamformer estimation results shown in Figs. 11–13, the pilot gain is considered to be 10dB.

The actual achievable sum rate obtained from the WSR maximization objective versus the total overhead due to OTA signalling is shown in the top of Fig. 6. The second figure illustrates the convergence of the beamformer algorithm with respect to the number of beamformer iterations. In this particular example, we assume that a single precoder/decoder iteration consumes 1% ($\frac{\tau_0}{T} = 0.01$) of the frame length. Note that it is possible to have τ_0 smaller than 0.1ms with the proposed TDD frame structure [36]. Hence, we can obtain $\frac{\tau_0}{T} = 0.01$ even with a relatively short coherence time (if the coherence time is 10 ms, we can have a TDD frame with T =10 ms). We can observe that the scenario with $\beta = 30$, $\zeta = 0.05$ and $\theta = e$ has a better converging behaviour in comparison to the WMMSE [81] approach. Additionally, the coordinated system provides considerable gain as compared to the uncoordinated system. The uncoordinated beamformer design is introduced as a reference, where the beamformers are calculated locally without considering the inter-cell interference. This shows the achievable rate peaks, when the overhead is between $0.05 - 0.10$, i.e., BIT $= 5 - 10$ rounds. The achieved gain over the uncoordinated scheme is almost 100% due to the greatly improved interference coordination. For the rest of the figures, we will use parameters $\beta = 30$, $\zeta = 0.05$, $\theta = e$ and BIT $= 5$.

Fig. 7 illustrates the average rate of the dynamic TDD system versus the transmit SNR considering the DL, UL and UL/DL sum rates. Note that the results are shown after 5 precoder/decoder iterations. We can observe that the sum rate improves for both coordinated and uncoordinated systems with SNR up to 5 dB. After that, the

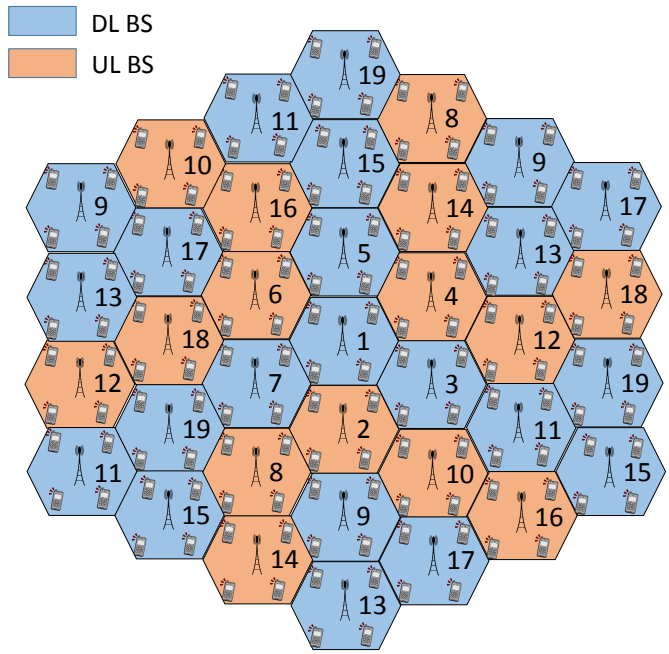

Fig. 5. 19-cell wrap-up model (Reprinted, with permission, from [133] ©2018 IEEE).

uncoordinated system performance degrades due to the strong interference from the other-cell users. However, the proposed coordinated scheme performs well even at a high SNR region. Due to user specific power constraints, each UL user uses all the power for transmit beamforming. This leads to high UL-to-DL interference, which degrades the DL user SINR and rate. Thus, the UL users have a somewhat higher rate at high SNR. Fig. 8, represents the average rate performance of the dynamic TDD system with given DL cell probability. Despite difficult UL-DL interference scenarios, the sum rate is only slightly decreased (around $5-6\%$) with a 0.5 DL cell probability as compared to the DL or UL only cases.

The average rate of the dynamic TDD system against the power disparity between DL and UL transmissions is shown in Fig. 9. Power disparity is defined as $10\log_{10}(P_i^{(\mathrm{dl})}/P_k^{(\mathrm{ul})})$ dB. We change the UL power while keeping DL power fixed to obtain different disparity levels. We can observe that the UL rate degrades and DL rate

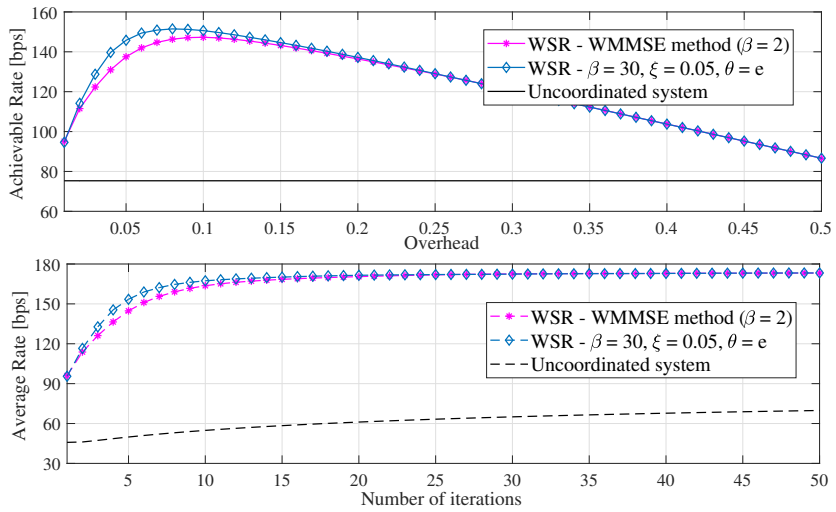

Fig. 6. Overhead and convergence comparison with cell edge SNR = 20 dB, $K = 152$, $K_i = 8$ & $M_i = 8\ \forall i \in \mathrm{B}, N_k = 2\ \forall k$ **(Reprinted, with permission, from [133] ©2018 IEEE).**

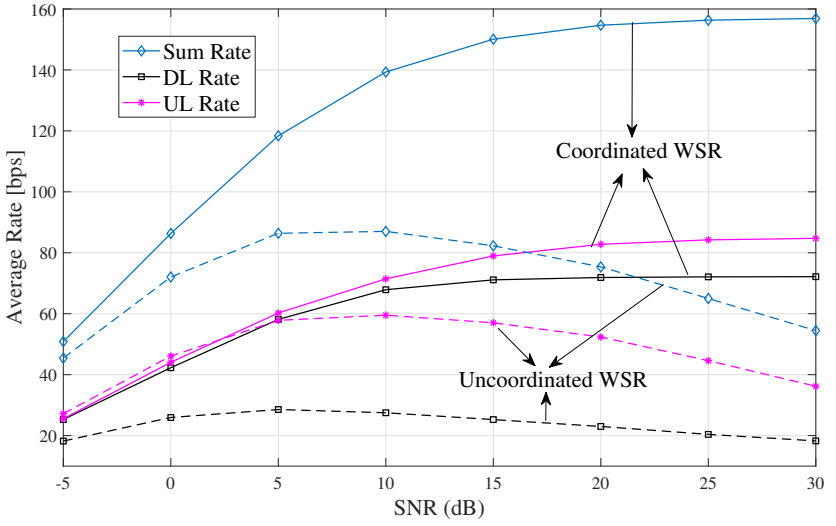

Fig. 7. Comparison of coordinated & uncoordinated WSR designs with $K = 152, K_i = 8$ & $M_i = 8\ \forall i \in \mathrm{B}, N_k = 2\ \forall k$ **(Reprinted, with permission, from [133] ©2018 IEEE).**

increases linearly with the power disparity. Additionally, the UL and DL rates show similar performance when the power disparity is 10dB. Similar to previous cases, the

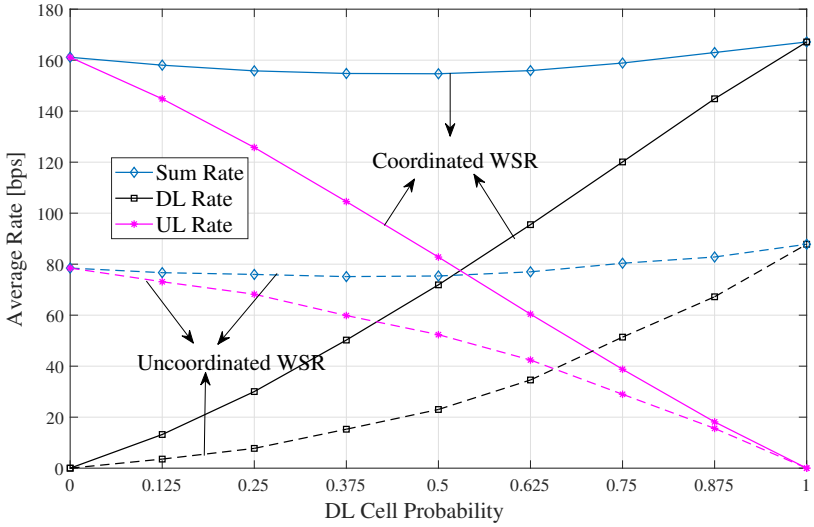

Fig. 8. Dynamic TDD system performance with the DL cell probability at cell edge SNR = 20 dB, $K = 152, K_i = 8$ & $M_i = 8\ \forall i \in \mathrm{B}, N_k = 2\ \forall k$ **(Reprinted, with permission, from [133] ©2018 IEEE).**

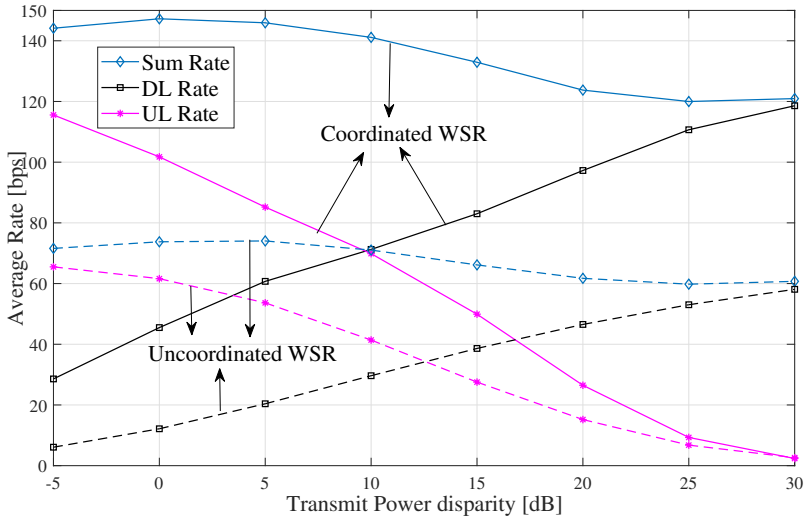

Fig. 9. Dynamic TDD system performance with power disparity between DL and UL transmissions at cell edge SNR = 20 dB, $K_i = 4\ M_i = 8\ \forall i \in \mathrm{B}, N_k = 2\ \forall k$ **(Reprinted, with permission, from [133] ©2018 IEEE).**

coordinated design show a 100% gain in comparison to the uncoordinated case in all disparity levels.

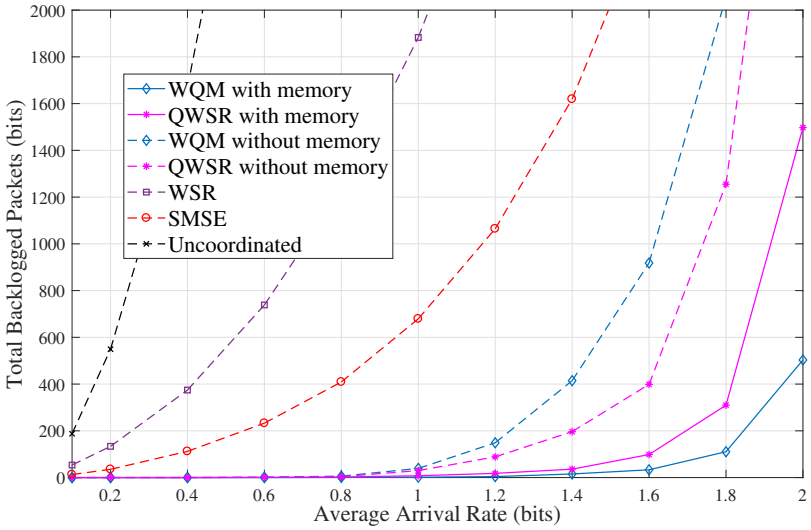

Fig. 10. Total backlogged packets at the system after 1000 timeslots for each optimization objective with cell edge SNR = 20 dB, $K = 38, K_i = 2$ & $M_i = 4\ \forall i \in \mathrm{B}, N_k = 2\ \forall k$ **(Reprinted, with permission, from [133] ©2018 IEEE).**

In Fig. 10, we compare the proposed beamformer objectives with respect to total backlogged packets in the system queues for a given traffic arrival rate. As we study the system for time-correlated fading, we can use beamformers estimated in the previous time slot to initialize the beamformers for the current time slot (with memory). Thus, we can improve the beamformer convergence. Note that this is only useful when our objectives are WQM or QWSR maximization. In other objectives the 'with memory' approach works only when every user has a large queue. Here, WQM provides better performance with memory compared to other methods, due to the improved convergence properties. However, QWSR provides good performance in both the 'with memory' and 'without memory' approaches due to its fast rate of convergence. Interestingly, (W)SR has very poor performance, since it ignores the backlog status in the user queues altogether and tends to assign non-zero weights $\omega_{k,l}^{(a)}$ only to a subset of users with good channel (and interference) conditions. In contrast, using SMSE criterion results in a somewhat more fair resource allocation as $\omega_{k,l}^{(a)} = 1\ \forall\ k,l$. As a result, the traffic aware (WQM, QWSR) beamformer design can handle up to $2-3$ or 10 times larger traffic loads than traditional (W)SR and SMSE criteria or uncoordinated design, respectively.

In Fig. 11, the performance of the proposed bi-directional direct beamformer estimation strategies are illustrated with the SSE approach. In general, we do not assume

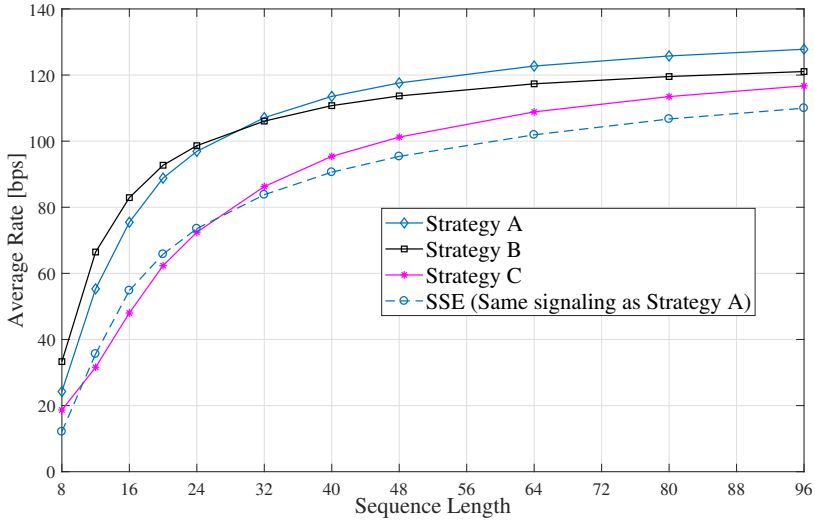

Fig. 11. Comparison of proposed DE strategies with cell edge SNR = 20 dB, $N = 19, K = 76, K_i = 4$ & $M_i = 8\ \forall i \in \mathrm{B}, N_k = 2\ \forall k$ **(Reprinted, with permission, from [133] ©2018 IEEE).**

any pilot coordination between cells. Therefore, the user specific training sequences in both forward and backward directions are non-orthogonal (overlapping). However, the pilots for same cell users can still be made orthogonal. Thus, in Fig. 11 each pilot sequence is interfered by up to 72 partially overlapping pilot sequences. For short sequence lengths, the received precoded pilot matrix is heavily contaminated by pilot interference. In particular, Strategy C does not perform well in these conditions due to a significant mismatch between the received pilot matrices $\mathbf{R}_k^{(a)}$ and $\mathbf{R}_{k,2}^{(a)}$ required to compute the beamformers in (40). Strategy B is less prone to errors in updating the weights $\omega_{k,l}^{(a)}$ as they are estimated only for intra-cell users. Therefore, it performs somewhat better than Strategy A with short sequence lengths. However, its performance saturates with less overlapping pilots as the user weights from other cell users are not available. The proposed strategies A and B start to perform reasonably well when the sequence length is longer than 24. In general, the DE approach provides significantly better performance than the SSE method. Moreover, due to the improved decontamination ability discussed in Section 2.4.5, it is possible to provide the same sum rate as the SSE method with much shorter ($\leq 1/2$) pilot sequence lengths.

Fig. 12 illustrates the added value of centralized pilot allocation given in Algorithm 2 for both DE and SSE methods (both with Strategy A signalling). As expected, the centralized pilot allocation, requiring tight resource coordination (via a backhaul)

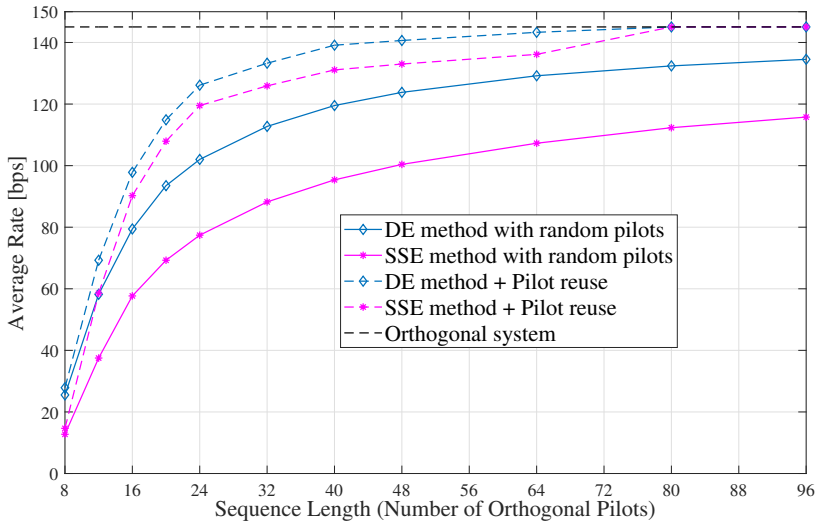

Fig. 12. Impact of the pilot reuse for both DE and SSE methods at cell edge SNR = 20 dB, $K = 76, K_i = 4$ & $M_i = 8\ \forall i \in \mathrm{B}, N_k = 2\ \forall k$ **(Reprinted, with permission, from [133] ©2018 IEEE).**

among adjacent cells, further improves the performance of both beamformer estimation schemes. In particular, the performance of the SSE method is greatly improved due to minimized pilot overlap. However, an uncoordinated random pilot allocation combined with the proposed direct beamformer estimation framework can provide most of these gains while requiring minimum or no coordination. Note that in this example, the number of data streams per user is restricted to 1. Therefore, every stream can be allocated with an orthogonal pilot for the bi-directional training when the pilot length is greater than 76. Finally, in Fig. 13, the performance of the Dynamic TDD system by employing both Strategy A and pilot reuse is illustrated for different UE/BS densities (K_i). There is a significant rate loss for the $K_i = 8$ case, when the number of pilots is less than 20. Therefore, for the number of pilots 8 - 20, the sum rate of the system is in the range of 10% - 60% in comparison to the orthogonal system. However, note that this is due to the severe pilot contamination of the system, where the same pilot will be shared with more than eight users. For all the UE/BS densities, system performance is quite satisfactory when the pilots/user ratio is greater than 25%.

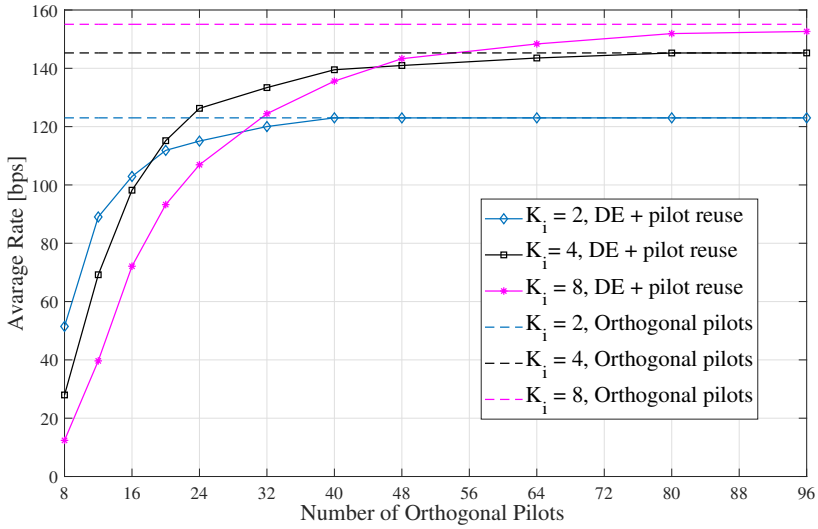

Fig. 13. Pilot decontamination using both DE and pilot reuse at cell edge SNR = 20 dB, $M_i = 8\ \forall i \in \mathsf{B}, N_k = 2\ \forall k$ **(Reprinted, with permission, from [133] ©2018 IEEE).**

2.5.2 Standalone model

In this case, simulations are carried out for the two and three cell scenarios with four users in each cell. The power constraint for the DL transmission is fixed to $P_i^{(\mathrm{dl})} = 10\ \forall i \in \mathsf{B}_D$ and for the UL user power transmission $P_k^{(\mathrm{ul})} = 4\ \forall k \in \mathsf{B}_U$. All the priority weights are assumed to be $\alpha_k = 1$. The number of antennas at each BS is $M_i = 4\ \forall i \in \mathsf{B}$, and the number of antennas at each user terminal is $N_k = 2\ \forall k$. The simulation environment is defined by three types of terminal separations, as shown in Fig. 14. The path loss between the two DL cell edge users (α), UL user to DL user (β) and UL BS to DL BS (δ). Additionally, the path loss from a BS to in-cell users is normalized to be 0 dB. In Figs. 15–17, we consider uncorrelated fading, which is modelled using Clarke's channel model. In Fig. 18, we consider time-correlated block fading, that is by modelling it using Jake's Doppler spectrum model with the normalized user terminal velocity $t_{\mathrm{S}} f_{\mathrm{D}} = 0.01$, where t_{S} and f_{D} are the signalling rate and the maximum Doppler shift, respectively.

The actual sum rate for transmit SNRs 10 dB and 20 dB versus the total overhead for the two cell DL only case id shown in Fig. 15. One BIT iteration is assumed to take two OFDM symbols. Thus, $\gamma = 0.01$ and $\gamma = 0.02$ correspond to frame lengths 200 and 100, respectively. Additionally, the uncoordinated beamformer design is considered

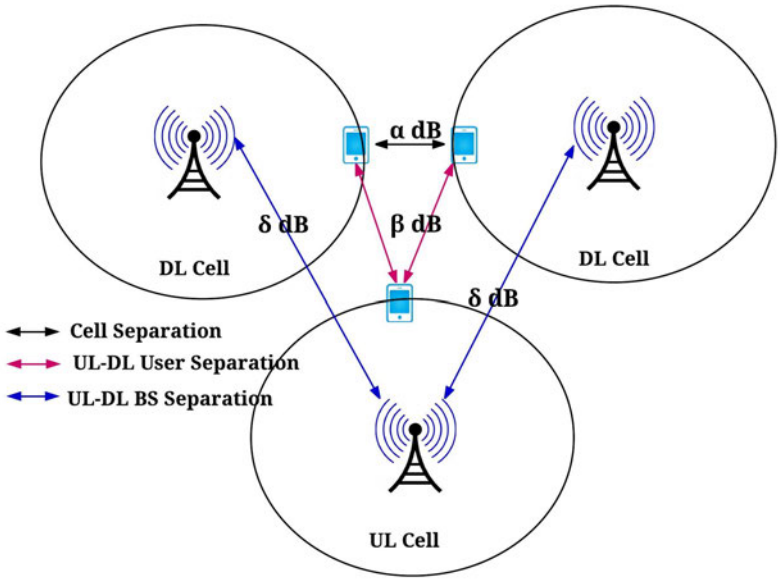

Fig. 14. Terminal separations in dynamic TDD (Reprinted, with permission, from [129] ©2015 IEEE).

the reference case (beamformers calculated locally without considering the inter-cell interference). Algorithm 1 with the bi-directional signalling can be seen to obtain the peak data rate with less than 10% and 15% overhead for the frame length $\gamma = 0.01$ and $\gamma = 0.02$, respectively. The actual sum rate improves significantly compared to the uncoordinated system when the cell separations are equal to $\alpha = 0$ dB, and it provides considerable performance gain even for larger signalling overhead. However, for the low inter-cell interference scenarios (lower transmit SNR with larger cell separation), the uncoordinated system starts to outperform the proposed beamformer design.

Fig. 16 demonstrates the actual sum rate versus the total overhead of the three cell network with two DL BSs and one UL BS. We consider the TDD frame length 200 ($\gamma = 0.01$), and different α, β and δ values. Similar to Fig. 15, the actual sum rate improves significantly for a lower α, β and δ values compared to the uncoordinated system. The peak rate is obtained with less than 12% overhead for all the scenarios and the sum rate improves even with 30% signalling overhead. Therefore, the proposed algorithm performs very well when complex interference conditions are present. Fig. 17 illustrates the average sum rate of the system versus the transmit SNR with a similar

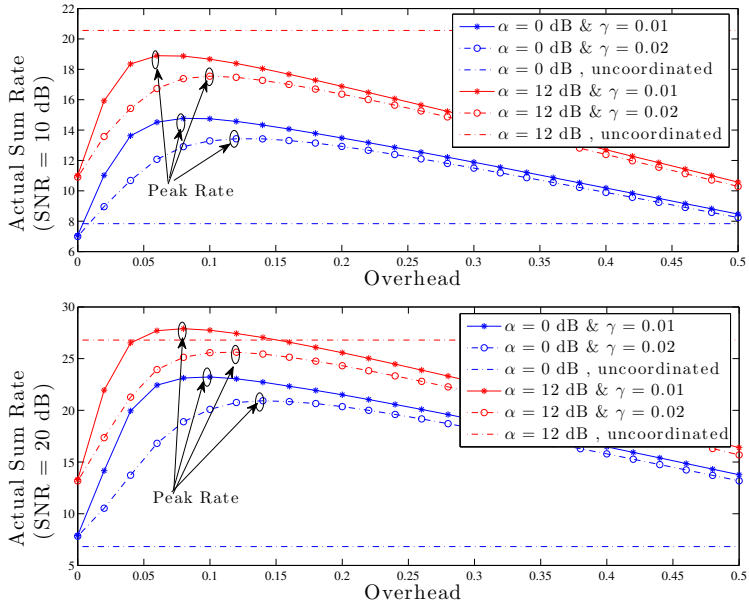

Fig. 15. Actual sum rate vs overhead with different SNR (10, 20 dB) values (Reprinted, with permission, from [129] ©2015 IEEE).

BS allocation as in Fig. 4, where we vary β (3, 6, 9, 12 dB) while α and δ are fixed to observe the impact of the UL user transmission on the sum rate. For lower β and high transmit SNR, UL users dominate the sum rate. This is due to the high UL-to-DL interference, which degrades the DL user SINR. However, for large β, DL user dominates due to less UL-to-DL interference.

When BS/user allocation remains constant for a longer time, we can exploit the fading environment to obtain converged beamformers with less bi-directional signalling iterations, thus improving the system performance. At a given time instant, the precoders are optimized for a fixed channel realization. Thus, as a result of iterative optimization, only the subset of the available users/streams are allocated and the rest of the users/streams remain inactive. By introducing a periodic beamformer re-initialization method for a moderately fast fading scenario, the beamformer allocation is periodically refreshed in order to reflect the changing channel conditions, and hence to improve the

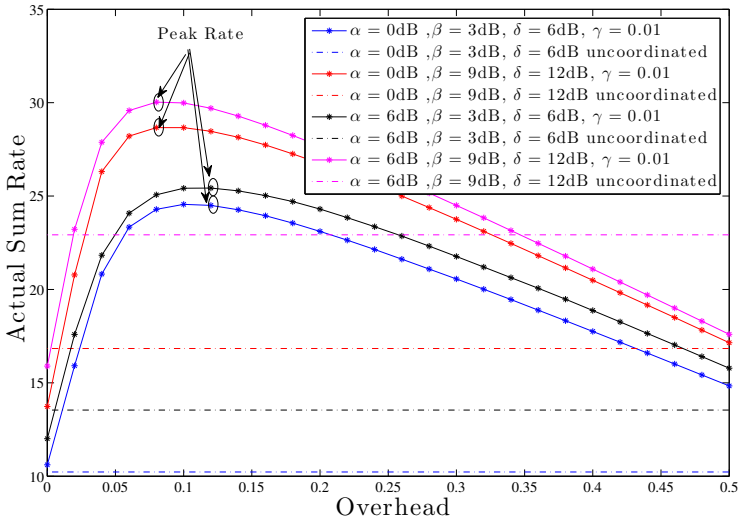

Fig. 16. Actual sum rate vs overhead at SNR = 20 dB, with diferent α, β, δ (Reprinted, with permission, from [129] ©2015 IEEE).

sum throughput of the system. A numerical analysis carried out in Fig. 18 illustrates the advantage of the beamformer re-initialization method.

Fig. 18 illustrates the impact of the periodic beamformer re-initialization on the system performance in a time-correlated channel, we consider the two cell DL only case with 20 dB transmit SNR. The average actual sum rate is obtained over 1000 random channel initializations with 100 correlated channel blocks. Three cases with different BIT iterations (3, 5, 10) are considered with beamformer re-initialization in every 10 TDD frames. The actual sum rate is better in the cases with BIT = 3 and 5. Thus, in a time-correlated channel, the proposed algorithm can be used with periodic re-initialization to improve the performance vastly with using less BIT.

2.6 Summary and discussion

In this chapter, we have investigated multiantenna interference management for dynamic TDD systems with several network optimization objectives. In the considered multi-cell multi-user dynamic TDD network, the available resources per cell can be freely allocated to either UL or DL depending on the instantaneous traffic demand. Thus, complex interference scenarios arise as a result of simultaneous transmission of DL and UL data

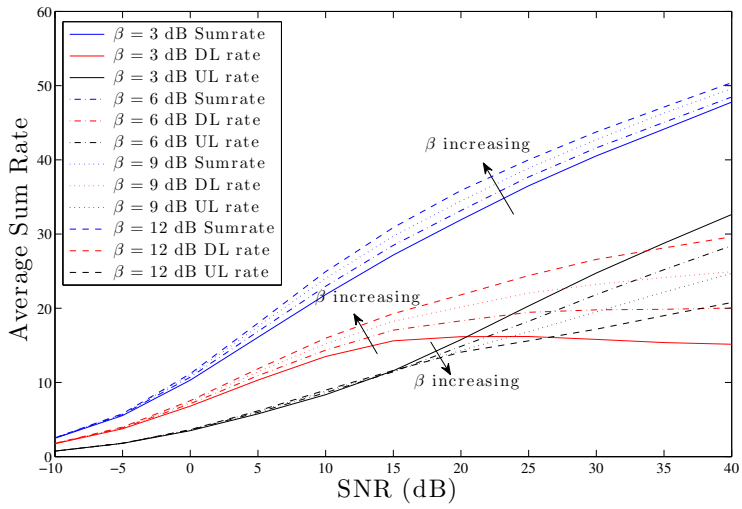

Fig. 17. Average sum rate vs SNR for different β values (Reprinted, with permission, from [129] ©2015 IEEE).

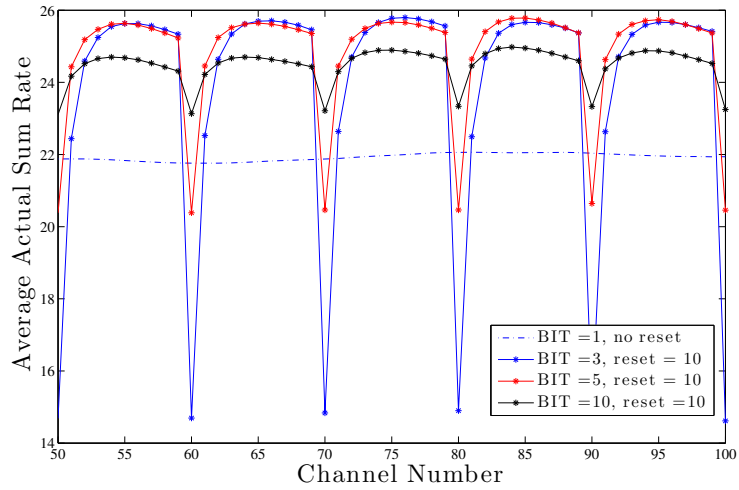

Fig. 18. Average sum rate over a time-correlated channel at SNR = 20 dB with $\gamma = 0.01$ (Reprinted, with permission, from [129] ©2015 IEEE).

in adjacent cells. The centralized beamformer design is also impractical in the dynamic TDD setting since acquiring the CSI between mutually interfering UEs is tedious. However, the coordinated beamformer design for dynamic TDD systems can be carried

out in a decentralized manner with the help of bi-directional F-B training via spatially precoded OTA pilot signalling. Accordingly, decentralized iterative beamformer designs are obtained for WQM, (Q)WSR maximization, and SMSE minimization objectives such that only minimal information exchange is required among BSs and UEs. The original formulation of the weighted ℓ_q-norm queue minimization problem was in non-convex form and NP-hard. After reformulating and introducing auxiliary MSE constraints, this was solved iteratively by using KKT conditions along with the AO method.

A novel bi-directional signalling scheme was embedded into the TDD frame to facilitate OTA signalling for the iterative algorithm. The TDD frame consisted of two portions: beamformer signalling information and data. A bi-directional OTA signalling and training framework was developed to iteratively optimize the transmit and receive beamformers both in UL and DL. A distributed fast converging beamformer design based on the WQM criterion was shown to be the best approach for handling both dynamic traffic variation and difficult interference scenarios. Novel bi-directional beamformer training strategies and methods for direct estimation (DE) of the stream-specific beamformers are developed for each intermediate beamformer update in a limited and noisy pilot environment. Three DE strategies were proposed to alleviate the contamination due to non-orthogonal and overlapping pilot allocations. Strategies A and B were shown to perform reasonably well even with relatively short pilot sequence lengths. The proposed signalling and DE schemes allow for non-orthogonal and overlapping pilots, which considerably reduces the resource coordination effort. Additionally, the decontamination ability of the proposed strategies are analysed with limited pilot resources. Finally, a centralized pilot allocation scheme was introduced to further enhance the pilot decontamination.

Numerical examples were considered to investigate the effect of interference seen in a dynamic TDD system and the effect of signalling overhead due to bi-directional signalling. The results demonstrate that the proposed training and estimation framework provides superior system performance over the uncoordinated scheme for different dynamic TDD network parameters and optimization objectives. Additionally, the performance was improved dramatically in a time-correlated fading with the use of periodic beamformer re- initialization.

3 Beamformer design for flexible TDD-based integrated access and backhaul

3.1 Introduction

Motivated by the concerns in Section 1.2.2, we consider a flexible TDD-based IAB network, such that in a given timeslot, BS and RNs operate in distinct UL/DL modes. For example, when BS is in the DL mode, RNs are in the UL mode and vice-versa, as illustrated in Fig. 19. Thereby, RNs are continuously in the two-way HD relaying mode, which significantly alleviates the HD loss in such a relaying setup. An iterative beamformer design with the WQM objective and resource allocation design are proposed to manage the resulting cross-channel interference and to allocate a wireless backhaul and access resources jointly over two consecutive data delivery intervals required for communications between the BS and UEs through HD RNs. From the queue minimization point of view, it is important to consider end-to-end data transmission. To this end, we introduce user-specific UL/DL queues to RNs, in addition to queues at UEs and BS, and incorporate them into the end-to-end WQM objective. Similar to DL only scenarios considered in [85, 86], the WQM problem in the considered IAB setup is solved via iterative evaluation of KKT conditions leading to a low complexity distributed algorithm with minimal queue state-related scalar information exchange between network nodes. Furthermore, the iterative design incorporates a water-filling type scheme to multiplex user-specific data streams over the backhaul in both DL and UL directions.

To facilitate practical implementation, we provide an over-the-air (OTA) signalling scheme as in [37, 39, 36], wherein precoded pilots are used to iteratively exchange the intermediate beamformers in both backward and forward directions. Then, direct beamformer estimation methods are applied to alleviate the pilot contamination effect, as in Section 2.4.1. In this chapter, we further propose a novel centralized approach to assign users into respective BS or RN by using path gain information and concerning potential practical constraints that are unique to IAB systems, such as limited spatial degrees of freedom in the BS-RN channel due to the line-of-sight (LOS) deployment and significant UL-to-DL interference of the nearby UE pairs. The user assignment is attained by solving a combinatorial optimization problem, which is in an integer linear

programming (ILP) form. Since the complexity of ILP increases exponentially, we propose two approximate approaches to solve it efficiently: 1) Direct linear program (LP) solution; and 2) SCA based LP solution [144].

Major contributions of this chapter are summarized as follows:

- An iterative beamformer design is proposed for the flexible TDD-based IAB system by assuming two consecutive data delivery intervals and user-specific queues at each node with the end-to-end WQM objective.
- The end-to-end WQM problem is solved via iterative evaluation of KKT conditions and a water-filling type scheme is proposed to multiplex user-specific data over wireless backhaul links.
- OTA bi-directional signalling architecture and direct beamformer estimation techniques are proposed to provide a practical decentralized beamformer design implementation and to mitigate the pilot contamination effect.
- A centralized user assignment algorithm is proposed for the considered IAB setting by using the long term channel statistics, nearby user information, and rank of the BS-RN channel.
- A thorough numerical study is carried out where the proposed flexible TDD-based IAB network is shown to significantly outperform the half duplex relaying reference case.

3.2 System model

We consider a flexible TDD based multi-user MIMO IAB system consisting of one BS and multiple DF RNs, as shown in Fig. 19. The set of UEs served by the BS or RN i is denoted by U_i. Here, for the simplicity of the notation, we use $i = 1$ for the BS and $i \in \{2,3,\ldots,N\} = \mathsf{B}_\mathrm{R}$ for RNs. The total number of UEs in the system is K and, the number of UEs served by the BS or RN i is $K_i = |\mathsf{U}_i|$. In addition, the serving BS/RN of the user k is denoted as i_k. Each UE k employs N_k antenna elements, while each BS/RN i employs M_i antenna elements. The maximum number of spatial data streams allocated to UE $k \in \mathsf{U}_i$ is denoted by $L_k \leq \min(M_i, N_k)$. In addition, the maximum number of spatial data streams between the BS and RN i is denoted as $\bar{L}_i \leq \min(M_i, M_1)$.

In the IAB system, we consider two-way HD relaying at RNs to eliminate the half-duplex loss effectively. Hence, in a given timeslot, BS and RNs operate in distinct UL/DL modes. Note that for UEs served by RN, data transmission from/to BS to/from UEs takes two timeslots. Therefore, we consider two timeslots to model the end-to-end

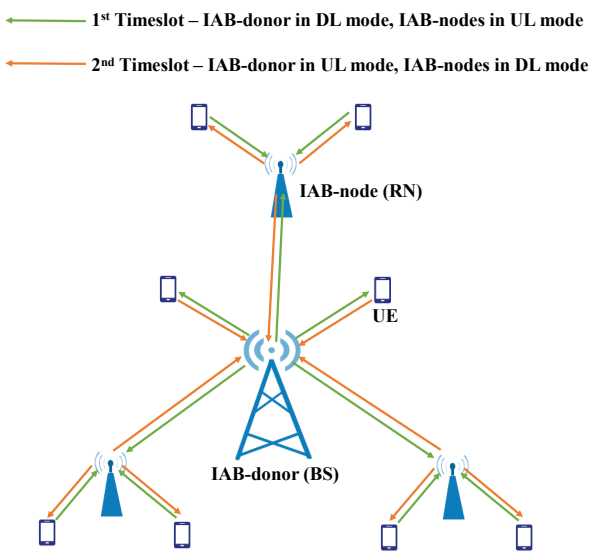

Fig. 19. Flexible TDD-based IAB Network with two-way HD relaying (Under CC BY 4.0 license from [134] ©2020 Authors).

system behaviour. In the first time slot, the BS is in DL mode while RNs are in UL mode (multiple access stage). In the second time slot, the BS is in UL mode, and RNs are in DL mode (broadcasting stage). Therefore, the following transmissions and transmit precoders are applied during the first timeslot;

- Tx1 : The BS transmits data to DL UEs. Transmit precoder for DL UE $k \in \mathsf{U}_1$ via l^{th} spatial stream is $\mathbf{m}_{k,l}^{(\mathrm{dl},1)} \in \mathbb{C}^{M_1}$.
- Tx2 : UL UEs transmits data to the serving RN. Transmit precoder from UL UE $k \in \mathsf{U}_i$ via l^{th} spatial stream is $\mathbf{m}_{k,l}^{(\mathrm{ul},1)} \in \mathbb{C}^{N_k}$.
- Tx3 : The BS wirelessly backhaul data to each RN to serve their DL UEs in the next timeslot. Transmit precoder for RN i at BS, via l^{th} spatial stream is $\mathbf{v}_{i,l}^{(\mathrm{dl})} \in \mathbb{C}^{M_1}$.

Due to the above transmissions in the first timeslot, the received signal $\mathbf{x}_k^{(\mathrm{dl},1)} \in \mathbb{C}^{N_k}$ at DL UE $k \in \mathsf{U}_1$ can be expressed as

$$\begin{aligned}\mathbf{x}_k^{(\mathrm{dl},1)} =& \mathbf{H}_{1,k}\Big(\sum_{j\in\mathsf{U}_1}\sum_{n=1}^{L_j}\mathbf{m}_{j,n}^{(\mathrm{dl},1)}d_{j,n}^{(\mathrm{dl},1)} + \sum_{i=2}^{N}\sum_{n=1}^{\bar{L}_i}\mathbf{v}_{i,n}^{(\mathrm{dl})}d_{i,n}^{(\mathrm{dl})}\Big) \\ &+ \sum_{i=2}^{N}\sum_{j\in\mathsf{U}_i}\sum_{n=1}^{L_j}\tilde{\mathbf{H}}_{j,k}\mathbf{m}_{j,n}^{(\mathrm{ul},1)}d_{j,n}^{(\mathrm{ul},1)} + \mathbf{z}_k, \end{aligned} \tag{53}$$

where $\mathbf{H}_{i,k} \in \mathbb{C}^{N_k \times M_i}$ is the channel matrix between BS/RN i and UE k, $\tilde{\mathbf{H}}_{j,k} \in \mathbb{C}^{N_k \times N_j}$ is the UE-UE interference channel matrix between UE j and UE k. All transmit data symbols $d_{j,n}^{(\mathrm{dl},1)}$, $d_{j,n}^{(\mathrm{ul},1)}$ and $d_{i,n}^{(\mathrm{dl})}$ $(\forall j,n,i)$ are assumed to be independent and identically distributed (i.i.d.) with $\mathbb{E}\{|d_{j,n}^{(\mathrm{dl},1)}|^2\} = 1$, $\mathbb{E}\{|d_{j,n}^{(\mathrm{ul},1)}|^2\} = 1$ and $\mathbb{E}\{|d_{i,n}^{(\mathrm{dl})}|^2\} = 1$. We assume complex white Gaussian noise $\mathbf{z}_k \in \mathbb{C}^{N_k}$ with variance N_0 per element. Similarly, the received signal $\mathbf{x}_i^{(\mathrm{ul},1)} \in \mathbb{C}^{M_i}$ at RN i can be expressed as

$$\begin{aligned}\mathbf{x}_i^{(\mathrm{ul},1)} =& \hat{\mathbf{H}}_{1,i}\Big(\sum_{j\in\mathsf{U}_1}\sum_{n=1}^{L_j}\mathbf{m}_{j,n}^{(\mathrm{dl},1)}d_{j,n}^{(\mathrm{dl},1)} + \sum_{r=2}^{N}\sum_{n=1}^{\bar{L}_r}\mathbf{v}_{r,n}^{(\mathrm{dl})}d_{r,n}^{(\mathrm{dl})}\Big) \\ &+ \sum_{r=2}^{N}\sum_{j\in\mathsf{U}_r}\sum_{n=1}^{L_j}\mathbf{H}_{i,j}^{\mathrm{H}}\mathbf{m}_{j,n}^{(\mathrm{ul},1)}d_{j,n}^{(\mathrm{ul},1)} + \mathbf{z}_i, \end{aligned} \tag{54}$$

where $\hat{\mathbf{H}}_{1,i} \in \mathbb{C}^{M_i \times M_1}$ is the channel matrix between the BS and RN i. To decode the received data, the following linear receivers are employed at the receiver nodes;

- Rx1 : The DL UE $k \in \mathsf{U}_1$ employs linear receiver $\mathbf{u}_{k,l}^{(\mathrm{dl},1)} \in \mathbb{C}^{N_k}$. Then the estimated data for l^{th} spatial stream is $\hat{d}_{k,l}^{(\mathrm{dl},1)} = (\mathbf{u}_{k,l}^{(\mathrm{dl},1)})^{\mathrm{H}}\mathbf{x}_k^{(\mathrm{dl},1)}$.
- Rx2 : The i^{th} RN employs linear receiver $\mathbf{u}_{k,l}^{(\mathrm{ul},1)} \in \mathbb{C}^{M_i}$ to decode the data from UL UE $k \in \mathsf{U}_i$ via l^{th} spatial stream. Then the estimated data is $\hat{d}_{k,l}^{(\mathrm{ul},1)} = (\mathbf{u}_{k,l}^{(\mathrm{ul},1)})^{\mathrm{H}}\mathbf{x}_i^{(\mathrm{ul},1)}$.
- Rx3 : The RN i employs $\mathbf{w}_{i,l}^{(\mathrm{dl})} \in \mathbb{C}^{M_i}$ to decode backhaul data from BS via l^{th} spatial stream. Then the estimated data is $\hat{d}_{i,l}^{(\mathrm{dl})} = (\mathbf{w}_{i,l}^{(\mathrm{dl})})^{\mathrm{H}}\mathbf{x}_i^{(\mathrm{ul},1)}$.

Similarly, the following transmissions and transmit precoders are used in the second timeslot;

- Tx4 : UL UEs transmit data to BS. The transmit precoder of UL UE $k \in \mathsf{U}_1$ in l^{th} spatial stream is $\mathbf{m}_{k,l}^{(\mathrm{ul},2)} \in \mathbb{C}^{N_k}$.
- Tx5 : Each RN transmit data to DL UEs. The transmit precoder for DL UE $k \in \mathsf{U}_i$ via l^{th} spatial stream is $\mathbf{m}_{k,l}^{(\mathrm{dl},2)} \in \mathbb{C}^{M_i}$.

– Tx6 : Relaying the received UL UE data to the BS by each RN. The transmit precoder of the RN i to BS, via l^{th} spatial stream is $\mathbf{v}_{i,l}^{(\mathrm{ul})} \in \mathbb{C}^{M_i}$.

Then, the received signal $\mathbf{x}_1^{(\mathrm{ul},2)} \in \mathbb{C}^{M_1}$ at the BS can be expressed as

$$\mathbf{x}_1^{(\mathrm{ul},2)} = \sum_{i=2}^{N} \hat{\mathbf{H}}_{1,i}^{\mathrm{T}} \Big(\sum_{n=1}^{\bar{L}_i} \mathbf{v}_{i,n}^{(\mathrm{ul})} d_{i,n}^{(\mathrm{ul})} + \sum_{j \in \mathsf{U}_i} \sum_{n=1}^{L_j} \mathbf{m}_{j,n}^{(\mathrm{dl},2)} d_{j,n}^{(\mathrm{dl},2)} \Big) + \sum_{j \in \mathsf{U}_1} \sum_{n=1}^{L_j} \mathbf{H}_{1,j}^{\mathrm{H}} \mathbf{m}_{j,n}^{(\mathrm{ul},2)} d_{j,n}^{(\mathrm{ul},2)} + \mathbf{z}_1, \tag{55}$$

where $d_{j,n}^{(\mathrm{dl},2)}$, $d_{j,n}^{(\mathrm{ul},2)}$ and $d_{i,n}^{(\mathrm{ul})}$ $(\forall j,n,i)$ are the transmit data symbols, which are i.i.d. with $\mathbb{E}\{|d_{j,n}^{(\mathrm{dl},2)}|^2\} = 1$, $\mathbb{E}\{|d_{j,n}^{(\mathrm{ul},2)}|^2\} = 1$ and $\mathbb{E}\{|d_{i,n}^{(\mathrm{ul})}|^2\} = 1$.

Similarly, the received signal $\mathbf{x}_k^{(\mathrm{dl},2)} \in \mathbb{C}^{N_k}$ at DL UE $k \in \mathsf{U}_i$ can be expressed as,

$$\mathbf{x}_k^{(\mathrm{dl},2)} = \sum_{r=2}^{N} \mathbf{H}_{r,k} \Big(\sum_{n=1}^{\bar{L}_i} \mathbf{v}_{i,n}^{(\mathrm{ul})} d_{i,n}^{(\mathrm{ul})} + \sum_{j \in \mathsf{U}_r} \sum_{n=1}^{L_j} \mathbf{m}_{j,n}^{(\mathrm{dl},2)} d_{j,n}^{(\mathrm{dl},2)} \Big) + \sum_{j \in \mathsf{U}_1} \sum_{n=1}^{L_j} \tilde{\mathbf{H}}_{j,k}^{\mathrm{T}} \mathbf{m}_{j,n}^{(\mathrm{ul},2)} d_{j,n}^{(\mathrm{dl},2)} + \mathbf{z}_k. \tag{56}$$

To decode each of the received data, we employ the following linear receivers at the receiver node.

– Rx4 : The BS employs $\mathbf{u}_{k,l}^{(\mathrm{ul},2)} \in \mathbb{C}^{M_1}$ to decode data from l^{th} spatial stream of UL UE $k \in \mathsf{U}_1$. Then the estimated data is $\hat{d}_{k,l}^{(\mathrm{ul},2)} = (\mathbf{u}_{k,l}^{(\mathrm{ul},2)})^{\mathrm{H}} \mathbf{x}_1^{(\mathrm{ul},2)}$.
– Rx5 : The DL UE $k \in \mathsf{U}_i$ employs $\mathbf{u}_{k,l}^{(\mathrm{dl},2)} \in \mathbb{C}^{N_k}$ to decode the received data via spatial stream l. Then the estimated data is $\hat{d}_{k,l}^{(\mathrm{dl},2)} = (\mathbf{u}_{k,l}^{(\mathrm{dl},2)})^{\mathrm{H}} \mathbf{x}_k^{(\mathrm{dl},2)}$.
– Rx6 : The BS employs $\mathbf{w}_{i,l}^{(\mathrm{ul})} \in \mathbb{C}^{M_1}$ to decode the relaying data from RN i via l^{th} spatial stream. Then the estimated data is $\hat{d}_{i,l}^{(\mathrm{ul})} = (\mathbf{w}_{i,l}^{(\mathrm{ul})})^{\mathrm{H}} \mathbf{x}_1^{(\mathrm{ul},2)}$.

Here, the corresponding user-specific MSE for UL/DL data detection is denoted in a common form as $\varepsilon_{k,l}^{(a,s)} = \mathbb{E}[|\hat{d}_{k,l}^{(a,s)} - d_{k,l}^{(a,s)}|^2]$ with $a = \{\mathrm{ul}, \mathrm{dl}\}$ and $s = \{1,2\}$. In addition, MSE for the data detection corresponding to backhaul traffic is denoted as $\varepsilon_{i,l}^{(a)} = \mathbb{E}[|\hat{d}_{i,l}^{(a)} - d_{i,l}^{(a)}|^2]$. Hence, the user-specific MSE value corresponding to Rx1 can be obtained as

$$\varepsilon_{k,l}^{(\mathrm{dl},1)} = 1 - 2\Re((\mathbf{u}_{k,l}^{(\mathrm{dl},1)})^{\mathrm{H}} \mathbf{H}_{1,k} \mathbf{m}_{k,l}^{(\mathrm{dl},1)}) + (\mathbf{u}_{k,l}^{(\mathrm{dl},1)})^{\mathrm{H}} \mathbf{M}_k^{(\mathrm{dl},1)} \mathbf{u}_{k,l}^{(\mathrm{dl},1)}, \tag{57}$$

$$\mathbf{M}_k^{(\mathrm{dl},1)} = \mathbf{H}_{1,k}\Big(\sum_{j\in\mathsf{U}_1}\sum_{n=1}^{L_j}\mathbf{m}_{j,n}^{(\mathrm{dl},1)}(\mathbf{m}_{j,n}^{(\mathrm{dl},1)})^{\mathrm{H}} + \sum_{r=2}^{N}\sum_{n=1}^{\bar{L}_r}\mathbf{v}_{r,n}^{(\mathrm{dl})}(\mathbf{v}_{r,n}^{(\mathrm{dl})})^{\mathrm{H}}\Big)\mathbf{H}_{1,k}^{\mathrm{H}} + \sum_{r=2}^{N}\sum_{j\in\mathsf{U}_r}\sum_{n=1}^{L_j}\tilde{\mathbf{H}}_{j,k}\mathbf{m}_{j,n}^{(\mathrm{ul},1)}(\tilde{\mathbf{H}}_{j,k}\mathbf{m}_{j,n}^{(\mathrm{ul},1)})^{\mathrm{H}} + \mathsf{N}_0\mathbf{I} \tag{58}$$

where $\mathbf{M}_k^{(\mathrm{dl},1)} = \mathbb{E}[\mathbf{x}_k^{(\mathrm{dl},1)}(\mathbf{x}_k^{(\mathrm{dl},1)})^{\mathrm{H}}]$ is the received signal covariance matrices for DL UE k. The expression for $\mathbf{M}_k^{(\mathrm{dl},1)}$ is given in (58) on top of the next page. Then, the MMSE receiver corresponding to Rx1 is given by

$$\tilde{\mathbf{u}}_{k,l}^{(\mathrm{dl},1)} = (\mathbf{M}_k^{(\mathrm{dl},1)})^{-1}\mathbf{H}_{1,k}\mathbf{m}_{k,l}^{(\mathrm{dl},1)}. \tag{59}$$

The reader is referred to Appendix A for the MSE, received signal covariance and MMSE receiver expressions corresponding to the receiver types from Rx2 to Rx6.

3.3 Precoder design

In this section, we present an iterative transmit/receive beamformer design with the WQM objective for the considered flexible TDD based IAB system. For UEs served by the RNs, it minimally takes two timeslots for the end-to-end data delivery. Hence, in the WQM objective, we jointly consider queue states at each node during both timeslots. For a successful IAB communication, the following UL/DL queues are required at each node;

- At the BS, DL UE queues ($Q_k^{(\mathrm{dl})}$) are required for, both, directly serving and relaying UEs as all DL traffic passes through the BS.
- At each UE, UL queues ($Q_k^{(\mathrm{ul})}$) are maintained to send UL traffic to the serving BS/RN.
- At the RNs, user-specific UL ($\bar{Q}_k^{(\mathrm{ul})}$) and DL ($\bar{Q}_k^{(\mathrm{dl})}$) queues are employed to store/relay access and backhaul data, hence to guarantee end-to-end data delivery.

Note that the DL UE queues at RN are filled up as backhaul traffic arrives from the BS during the first timeslot, and emptied when serving DL UEs during the second timeslot. Similarly, the UL UE queues at RN grow due to the received UL UE data during the first timeslot, and drain when relaying the data to the BS during the second timeslot. Hence, from the overall queue minimization perspective, it is crucial to consider the traffic

dynamic at each node over two timeslots. Then, we can define a queue deviation metric $\Psi_k^{(\mathrm{dl})}$ for all DL UE queues at the BS, after two timeslots, as

$$\Psi_k^{(\mathrm{dl})} = \begin{cases} Q_k^{(\mathrm{dl})} - \sum_{l=1}^{L_k} R_{k,l}^{(\mathrm{dl},1)} & k \in \mathsf{U}_1, \\ Q_k^{(\mathrm{dl})} - \sum_{l=1}^{L_i} a_k^{(\mathrm{dl})} R_{i,l}^{(\mathrm{dl})} & k \in \mathsf{U}_i, i \in \mathsf{B}_\mathrm{R}, \end{cases} \tag{60}$$

where $R_{k,l}^{(a,s)}$ denotes the number of transmitted bits over the l^{th} spatial stream to/from UE k. The backhaul rate over the l^{th} spatial stream to/from BS to RN i is denoted as $R_{i,l}^{(a)}$. Moreover, by assuming MMSE receivers are employed at each receiver node, the instantaneous rate can be expressed as $R_{k,l}^{(a,s)} = -\log_2(\varepsilon_{k,l}^{(a,s)})$ and $R_{i,l}^{(a)} = -\log_2(\varepsilon_{i,l}^{(a)})$ [37]. Here, the backhaul streams are multiplexed with data from several UEs and, $a_k^{(a)}$ is the multiplexed rate portion for each UE k ($0 \leq a_k^{(a)} \leq 1$). Moreover, at each UL UE, the queue deviation metric $\Psi_k^{(\mathrm{ul})}$ for the UL queues, after two timeslots, is given by

$$\Psi_k^{(\mathrm{ul})} = \begin{cases} Q_k^{(\mathrm{ul})} - \sum_{l=1}^{L_k} R_{k,l}^{(\mathrm{ul},2)} & k \in \mathsf{U}_1, \\ Q_k^{(\mathrm{ul})} - \sum_{l=1}^{L_k} R_{k,l}^{(\mathrm{ul},1)} & k \in \mathsf{U}_i, i \in \mathsf{B}_\mathrm{R}. \end{cases} \tag{61}$$

Similarly, the queue deviation metric $\bar{\Psi}_k^{(\mathrm{dl})}$ and $\bar{\Psi}_k^{(\mathrm{ul})}$ for DL and UL UE queues at the RN i_k, after two timeslots are given by

$$\bar{\Psi}_k^{(\mathrm{dl})} = \bar{Q}_k^{(\mathrm{dl})} + \sum_{l=1}^{L_i} a_k^{(\mathrm{dl})} R_{i,l}^{(\mathrm{dl})} - \sum_{l=1}^{L_k} R_{k,l}^{(\mathrm{dl},2)}, \tag{62a}$$

$$\bar{\Psi}_k^{(\mathrm{ul})} = \bar{Q}_k^{(\mathrm{ul})} + \sum_{l=1}^{L_k} R_{k,l}^{(\mathrm{ul},1)} - \sum_{l=1}^{L_i} a_k^{(\mathrm{ul})} R_{i,l}^{(\mathrm{ul})}. \tag{62b}$$

In order to simplify the notation, let $\tilde{\boldsymbol{\Psi}}^{(a)}$ and $\tilde{\bar{\boldsymbol{\Psi}}}^{(a)}$ denote vectors with elements $\tilde{\Psi}_k^{(a)} \triangleq \alpha_k^{1/q} \Psi_k^{(a)}$ and $\tilde{\bar{\Psi}}_k^{(a)} \triangleq \alpha_k^{1/q} \bar{\Psi}_k^{(a)}$, respectively. Here, α_k is a weighting factor, reflecting user specific priorities.

Note that, before the precoder/decoder design, we assume UEs are already assigned to a particular BS or RN by using the user assignment algorithm, which is explained in detail in Section III.C. Here, we define the weighted ℓ_q-norm queue minimization of the UL and DL users during two timeslots with sum transmit power constraints at the

transmitters as

$$\min_{\mathsf{M},\mathsf{W}} \sum_{a\in\{\mathrm{ul},\mathrm{dl}\}} \|\tilde{\boldsymbol{\Psi}}^{(a)}\|_q + \|\tilde{\bar{\boldsymbol{\Psi}}}^{(a)}\|_q \tag{63a}$$

$$\text{s. t.} \quad \sum_{l=1}^{L_k} \|\mathbf{m}_{k,l}^{(\mathrm{ul},1)}\|^2 \le P_k^{(\mathrm{ul})} \qquad \forall k \in \mathsf{U}_i, i \neq 1, \tag{63b}$$

$$\sum_{k\in\mathsf{U}_1}\sum_{l=1}^{L_k} \|\mathbf{m}_{k,l}^{(\mathrm{dl},1)}\|^2 + \sum_{i=2}^{N}\sum_{l=1}^{\bar{L}_i} \|\mathbf{v}_{i,l}^{(\mathrm{dl})}\|^2 \le P_1^{(\mathrm{dl})}, \tag{63c}$$

$$\sum_{l=1}^{L_k} \|\mathbf{m}_{k,l}^{(\mathrm{ul},2)}\|^2 \le P_k^{(\mathrm{ul})} \qquad \forall k \in \mathsf{U}_1, \tag{63d}$$

$$\sum_{k\in\mathsf{U}_i}\sum_{l=1}^{L_k} \|\mathbf{m}_{k,l}^{(\mathrm{dl},2)}\|^2 + \sum_{l=1}^{\bar{L}_i} \|\mathbf{v}_{i,l}^{(\mathrm{ul})}\|^2 \le P_i^{(\mathrm{dl})} \quad \forall i \in \mathbb{B}_{\mathrm{R}}, \tag{63e}$$

where M represents the set of all transmit precoders and W represents the set of all receive beamformers. The maximum transmit power at BS/RN i is denoted as $P_i^{(\mathrm{dl})}$ and the maximum transmit power at UE k denoted as $P_k^{(\mathrm{ul})}$.

The WQM problem in (63) is proposed to design precoders to minimize the total number of backlogged packets in the IAB network over two consecutive timeslots by optimizing transmit and receive beamformers at each node. An intriguing relationship can be obtained between WQM and WSRM formulations by considering a special case of l_q-norm in the objective (assuming large queues at each node and q=1) [86]. Moreover, both WSRM and WQM problems are known to be NP-hard even for the single antenna case[145, 146, 147]. However, computationally efficient solutions can be found by iterative alternating optimization (AO), similar to [85, 86]. First, by re-writing the rate terms using the corresponding MSE terms and introducing auxiliary MSE constraints as in [85] to (63), we can construct an approximated optimization problem

as

$$\min_{\mathsf{M},\mathsf{W},\mathsf{T}} \quad \sum_{k\in\mathsf{U}_1}\Big(\alpha_k^{(\mathrm{dl})}(Q_k^{(\mathrm{dl})}-\sum_{l=1}^{L_k}J_0t_{k,l}^{(\mathrm{dl},1)})^q+\alpha_k^{(\mathrm{ul})}(Q_k^{(\mathrm{ul})}-\sum_{l=1}^{L_k}J_0t_{k,l}^{(\mathrm{ul},2)})^q\Big)$$
$$+\sum_{i=2}^{N}\sum_{k\in\mathsf{U}_i}\Big(\alpha_k^{(\mathrm{ul})}(Q_k^{(\mathrm{ul})}-\sum_{l=1}^{L_k}J_0t_{k,l}^{(\mathrm{ul},1)})^q+\alpha_k^{(\mathrm{dl})}(Q_k^{(\mathrm{dl})}-\sum_{l=1}^{\bar{L}_i}a_k^{(\mathrm{dl})}J_0t_{i,l}^{(\mathrm{dl})})^q$$
$$+\alpha_k^{(\mathrm{dl})}(\bar{Q}_k^{(\mathrm{dl})}+\sum_{l=1}^{\bar{L}_i}a_k^{(\mathrm{dl})}J_0t_{i,l}^{(\mathrm{dl})}-\sum_{l=1}^{L_k}J_0t_{k,l}^{(\mathrm{dl},2)})^q$$
$$+\alpha_k^{(\mathrm{ul})}(\bar{Q}_k^{(\mathrm{ul})}+\sum_{l=1}^{L_k}J_0t_{k,l}^{(\mathrm{ul},1)}-\sum_{l=1}^{\bar{L}_i}a_k^{(\mathrm{ul})}J_0t_{i,l}^{(\mathrm{ul})})^q\Big), \tag{64a}$$

$$\text{s. t.} \quad \varepsilon_{k,l}^{(a,s)}\le\beta^{-t_{k,l}^{(a,s)}} \quad \forall(k,l),a\in\{\mathrm{dl},\mathrm{ul}\},s\in\{1,2\}, \tag{64b}$$

$$\varepsilon_{i,l}^{(a)}\le\beta^{-t_{i,l}^{(a)}} \quad \forall i\in\mathbb{B}_{\mathrm{R}}\&\forall l,a\in\{\mathrm{dl},\mathrm{ul}\}, \tag{64c}$$

$$(63\mathrm{b}),\ (63\mathrm{c}),\ (63\mathrm{d}),\ (63\mathrm{e}),$$

where T represents the set of the newly introduced auxiliary variables $t_{k,l}^{(a,s)}(\forall a,s,k,l), t_{i,l}^{(a)}(\forall a,i,l)$. In addition, $J_0=\log_2(\beta)$ and β is a predefined constant to adjust the approximation function such that $\beta>0$ [85]. By introducing these MSE constraints, the objective becomes a convex function of auxiliary variables $t_{k,l}^{(a,s)}, t_{i,l}^{(a)}$. However, the MSE constraints in (64b) and (64c) are still non-convex, and that non-convexity is handled by applying the successive convex approximation (SCA) method iteratively by using a first-order Taylor series approximation [85]. For example, (64b) can be approximated as,

$$\beta^{-t_{k,l}^{(a,s)}}=-J_1t_{k,l}^{(a,s)}+J_2, \tag{65}$$

where $J_1=\beta^{-\bar{t}_{k,l}^{(a,s)}}\log(\beta)$, $J_2=\beta^{-\bar{t}_{k,l}^{(a,s)}}+\bar{t}_{k,l}^{(a,s)}J_1$ and $\bar{t}_{k,l}^{(a,s)}$ is the point of approximation. For (64c), the same approximation is applied as in (65). Then, by substituting approximated expressions in (65) to (64b) and (64c), the optimization problem in (64) can be efficiently solved using the KKT optimality conditions with the iterative AO method[86].

3.3.1 Alternating optimization method

Here, we present the iterative AO method using the KKT optimality conditions as follows: we begin by fixing the transmit precoders and solving for the receive beamformers and

other variables (auxiliary and dual). First, we calculate the MMSE receivers using (59) and (88), then the corresponding MSE values are obtained from (57) and (86). By using the complementary slackness of (64b) and (64c), we can update auxiliary variables $t_{k,l}^{(a,s)}, t_{i,l}^{(a)}$ as

$$t_{k,l}^{(a,s)} = \bar{t}_{k,l}^{(a,s)} + \frac{1}{\log(\beta)}\left(1 - \varepsilon_{k,l}^{(a,s)}\beta^{\bar{t}_{k,l}^{(a,s)}}\right), \tag{66}$$

where $\bar{t}_{k,l}^{(a,s)}$ denotes $t_{k,l}^{(a,s)}$ from the previous iteration. This corresponds to a sub-gradient update of dual variable $t_{k,l}^{(a,s)}$ with step size $1/\log(\beta)$. Hence, for the faster convergence, we can experiment with the step size as in [85]. Next, dual variables $\omega_{k,l}^{(a,s)}, \omega_{i,l}^{(a)}$ corresponding to (64b) and (64c) are obtained as

$$\omega_{k,l}^{(a,s)} = (1-\rho)\bar{\omega}_{k,l}^{(a,s)} + \rho\,\tfrac{qJ_0}{J_1}\Upsilon, \tag{67}$$

where $\bar{\omega}_{k,l}^{(a,s)}$ denotes fixed $\omega_{k,l}^{(a,s)}$ from the previous iteration. Here, $\rho \in (0,1)$ controls the rate of convergence and is used to prevent over-allocation. For Rx1, Υ is given by

$$\Upsilon = \alpha_k^{(\mathrm{dl})}[(Q_k^{(\mathrm{dl})} - \sum_{l=1}^{L_k} J_0 t_{k,l}^{(\mathrm{dl},1)})^{q-1}]^+, \tag{68}$$

where $[x]^+ \triangleq \max\{x, 0\}$. For Rx2-Rx6, expressions for Υ are given in Appendix A.

Next, we fix the MMSE receivers and solve for the transmit precoders. The transmit precoders can be derived from the first-order optimality conditions of (64). Hence, transmit precoders for Tx1 transmitter type can be obtained as

$$\mathbf{m}_{k,l}^{(\mathrm{dl},1)} = \left(\mathbf{\Phi}_1^{(\mathrm{dl},1)} + \nu_1^{(\mathrm{dl},1)}\mathbf{I}\right)^{-1} \omega_{k,l}^{(\mathrm{dl},1)}\mathbf{H}_{1,k}^{\mathrm{H}}\mathbf{u}_{k,l}^{(\mathrm{dl},1)}, \tag{69}$$

where $\mathbf{\Phi}_1^{(\mathrm{dl},1)}$ is the weighted transmit co-variance matrix and the expression for $\mathbf{\Phi}_1^{(\mathrm{dl},1)}$ is obtained as in (70) at the top of the next page. In addition, $\nu_1^{(\mathrm{dl},1)}$, is the dual variable corresponding to the power constraint in (63c). Hence, the transmit beamformers can efficiently solved from (69) by a bisection search over the dual variables to satisfy the power constraint. For Tx2-Tx6, the transmit precoder expressions are provided in Appendix A. Finally, we repeat the above precoder/decoder optimization until the convergence of the objective function.

$$\mathbf{\Phi}_1^{(\mathrm{dl},1)} = \sum_{k\in\mathsf{U}_1}\sum_{l=1}^{L_j}\omega_{k,l}^{(\mathrm{dl},1)}\mathbf{H}_{1,k}^{\mathrm{H}}\mathbf{u}_{k,l}^{(\mathrm{dl},1)}(\mathbf{H}_{1,k}^{\mathrm{H}}\mathbf{u}_{k,l}^{(\mathrm{dl},1)})^{\mathrm{H}} + \sum_{i=2}^{N}\hat{\mathbf{H}}_{1,i}^{\mathrm{H}}(\sum_{l=1}^{\bar{L}_i}\omega_{i,l}^{(\mathrm{dl})}\mathbf{w}_{i,l}^{(\mathrm{dl})}(\mathbf{w}_{i,l}^{(\mathrm{dl})})^{\mathrm{H}}$$
$$+\sum_{k\in\mathsf{U}_i}\sum_{l=1}^{L_j}\omega_{k,l}^{(\mathrm{ul},1)}\mathbf{u}_{k,l}^{(\mathrm{ul},1)}(\mathbf{u}_{k,l}^{(\mathrm{ul},1)})^{\mathrm{H}})\hat{\mathbf{H}}_{1,i}. \tag{70}$$

3.3.2 Multiplexing backhaul data

In the proposed beamformer design, we consider that a backhaul carries multiple UE data at the same time either in UL or DL direction. Therefore, we define multiplexing factors $a_k^{(a)}$ to obtain individual user-specific rates via the backhaul link. Here, the multiplexing of user specific data over $\bar{L}_i$ backhaul streams assigned to RN i can be carried out using conventional approaches such as frequency-division-multiplexing (FDM) or time-division-multiplexing (TDM). In this subsection, we propose two approaches to calculate these multiplexing factors $a_k^{(a)}$: 1) a KKT-based solution; 2) the Heuristic method.

KKT-based solution

We can model these multiplexing factors $a_k^{(a)}$ as optimization variables in the original optimization problem in (64). In general, for any value of q in (64a), it is a tedious task to obtain a generalized closed-form solution for $a_k^{(a)}$ from KKT conditions as we have to find the roots of a polynomial equation. However, for the specific case with $q = 2$, we can obtain optimized $a_k^{(a)}$ values by iteratively evaluating their corresponding KKT conditions (assuming the fixed receive beamformers and auxiliary variables from the previous section). Note that $q > 2$ cases are left for future work. To this end, we introduce the following additional boundary constraints to the original optimization problem (64).

$$\sum_{k=1}^{|\mathsf{U}_i|} a_k^{(a)} = 1 \qquad \forall i, \tag{71a}$$

$$a_k^{(a)} \geq 0 \qquad \forall k. \tag{71b}$$

Then, by differentiating the modified Lagrangian (with $q = 2$) w.r.t to $a_k^{(a)}$ and applying the complementary slackness to the boundary constraints (71), we can obtain the

following closed-form solution

$$a_k^{(a)} = [Z_k^{(a)} - v_i^{(a)}]^+, \tag{72}$$

where $v_i^{(a)}$ is the scaled dual variable corresponding to equality constraint (71a), and $Z_k^{(a)}$ is given by

$$Z_k^{(\mathrm{dl})} = (Q_k^{(\mathrm{dl})} - \bar{Q}_k^{(\mathrm{dl})} + \sum_{l=1}^{L_k} J_0 t_{k,l}^{(\mathrm{dl},2)})/2 \sum_{l=1}^{\bar{L}_i} J_0 t_{i,l}^{(\mathrm{dl})}. \tag{73a}$$

$$Z_k^{(\mathrm{ul})} = (\bar{Q}_k^{(\mathrm{ul})} + \sum_{l=1}^{L_k} J_0 t_{k,l}^{(\mathrm{ul},1)})/\sum_{l=1}^{\bar{L}_i} J_0 t_{i,l}^{(\mathrm{ul})}. \tag{73b}$$

Here, $v_i^{(a)}, a_k^{(a)}$ are obtained by using a water-filling type algorithm such that $\sum_{k=1}^{|\mathsf{U}_i|} [Z_k^{(a)} - v_i^{(a)}]^+ = 1$. From the above solution, it is obvious that more backhaul resources are allocated to UEs with larger $Z_k^{(a)}$ values while no data is delivered to users with $Z_k^{(a)} - v_i^{(a)} < 0$. In each iteration $Z_k^{(a)}$ values change due to the iterative evaluation of the auxiliary variables. Thus, $a_k^{(a)}$ must be re-evaluated in each iteration until convergence.

Heuristic method

In this method, we assign multiplexing factors $a_k^{(a)}$ based on the queue state of the UL and DL traffic and consider those as fixed values in the optimization problem (64). The proposed heuristic method is essential when we are unable to find an optimization solution to $a_k^{(a)}$ (cases that $q \geq 3$) or when we need a simple practical solution.

For the heuristic assignment of $a_k^{(a)}$, we make an assumption that the generated traffic in the system is delivered to the destination within two timeslots (no backlogged packets in the relay nodes). In such a case, we may assume that $\bar{Q}_k^{(a)} = 0$, $\sum_{l=1}^{L_k} J_0 t_{k,l}^{(\mathrm{dl},2)} = Q_k^{(\mathrm{dl})}$, $\sum_{l=1}^{L_k} J_0 t_{k,l}^{(\mathrm{ul},1)} = Q_k^{(\mathrm{ul})}$ and $\sum_{l=1}^{\bar{L}_i} J_0 t_{i,l}^{(a)} = \sum_{k=1}^{|\mathsf{U}_i|} Q_k^{(a)}$. Then, by substituting these values to (73)–(72) and applying boundary conditions, we can obtain $a_k^{(a)}$ simply as

$$a_k^{(a)} = \frac{Q_k^{(a)}}{\sum_{j=1}^{|\mathsf{U}_i|} Q_j^{(a)}}, \qquad i \in \mathbb{B}_{\mathrm{R}}. \tag{74}$$

Finally, the complete iterative beamformer design with the proposed backhaul multiplexing schemes is summarized in Algorithm 3.

Algorithm 3 Iterative Beamformer Design

Initializing feasible transmit beamformers $\mathbf{m}_{k,l}^{(a,s)}, \mathbf{v}_{i,l}^{(a)}$.
Calculate multiplexing factors $a_k^{(a)}$ for each UE using (74) (Heuristic method).
repeat
    Estimate MMSE receivers $\mathbf{u}_{k,l}^{(a,s)}, \mathbf{w}_{i,l}^{(a)}$ by using (59) and (88).
    Calculate MSE values $\varepsilon_{k,l}^{(a,s)}, \varepsilon_{i,l}^{(a)}$ from (57) and (86).
    Calculate auxiliary variables $t_{k,l}^{(a,s)}, t_{i,l}^{(a)}$ from (66).
    Calculate multiplexing factors $a_k^{(a)}$ for each UE from (72) (KKT based method).
    Calculate dual variables $\omega_{k,l}^{(a,s)}, \omega_{i,l}^{(a)}$ using (67), (68) and (89).
    Estimate transmit precoders $\mathbf{m}_{k,l}^{(a,s)}, \mathbf{v}_{i,l}^{(a)}$ from (69) and (90).
until convergence.

3.3.3 User assignment

In this subsection, we propose a novel centralized approach to assign UEs into a particular BS or RN. Typically, UEs are assigned to their respective serving nodes based on the strongest received signal strength indicator (RSSI) value. However, that approach is not always a viable option for the IAB system, due to the asymmetric DL and UL data transmission and the spatial degree of freedom limitations for the BS-RN backhaul links. For example, two nearby UEs may be assigned to two different serving BS/RNs based on their RSSI values. Then, both UEs may suffer from significant UL-to-DL interference due to the different (UL and DL) transmission modes at BS, and RNs. To avoid this, we aim to assign nearby users into the same serving node. Moreover, RNs are often deployed in such a way that the BS-RN channel has a line of sight (LOS) path. Hence, the fading channels between BS-RNs experience Rician fading statistics due to the dominant LOS component. With the LOS deployment, we may be able to have a reliable wireless backhaul between BS and RNs. However, at the same time, the number of parallel spatial streams available for the backhaul link is limited. The limited backhaul capacity may constitute a bottleneck for UEs served by RNs, as their incoming/outgoing traffic is relayed through the wireless in-band backhaul links. Therefore, such practical constraints unique to IAB systems are also considered in the proposed user assignment algorithm.

In the proposed user assignment approach, the BS collects the following information,

– Exact RSSI values between BS-UE and RN-UE links.

– The number of antennas and maximum transmit powers at each terminal.
– The multiplexing order of the BS-RN channels.
– Neighbouring UE information from each UEs based on the measured RSSI values between UE-UE links.

Initially, we calculate the individual utility value $g_{i,k}$ for assigning an UE k to a particular BS or RN i. The cost value $g_{i,k}$ is expressed as

$$g_{i,k} = \log_2(1 + \frac{P_i^{(\mathrm{dl})} S_{i,k}}{M_i \mathsf{N}_0}), \tag{75}$$

where $S_{i,k}$ is the path gain between BS/RN i and UE k. The cost value $g_{i,k}$ represents a coarse prediction for the DL rate of UE k if served by BS/RN i. Next, the rank of the BS-RN channel for each backhaul link i is defined as

$$D_i = \mathrm{rank}(\hat{\mathbf{H}}_{1,i}) \qquad i \in \mathbb{B}_{\mathrm{R}}. \tag{76}$$

In addition, the nearby UE set Y_k for each UE k potentially constituting high cross-link interference is given as

$$\mathsf{Y}_k = \{ j \mid S_{j,k} > S_{\mathrm{th}} \quad \text{for } j = 1, ..., K \}, \tag{77}$$

where $S_{j,k}$ is the path gain between UE j and k, and S_{th} is a design parameter controlling the size $|\mathsf{Y}_k|$.

Each element $c_{i,k} \in \{0,1\}$ in UE allocation matrix $\mathbf{C} \in \mathbb{B}^{N \times K}$ matrix represents the assignment value of the UE k into BS/RN i, where $c_{i,k} = 1$ if the kth UE assigned into ith BS/RN, otherwise $c_{i,k} = 0$. Finally, the user assignment problem for the IAB system can be formulated as

$$\max_{\mathbf{C}, A_i} \quad \sum_{i=1}^{N} \sum_{k=1}^{K} c_{i,k} g_{i,k} - \sum_{i=2}^{N} \zeta_i A_i \tag{78a}$$

$$\text{s. t. } A_i - (\sum_{k=1}^{K} c_{i,k} - D_i) \geq 0 \qquad i \in \mathbb{B}_{\mathrm{R}}, \tag{78b}$$

$$A_i \geq 0 \qquad i \in \mathbb{B}_{\mathrm{R}}, \tag{78c}$$

$$\sum_{i=1}^{N} c_{i,k} = 1 \qquad \forall k, \tag{78d}$$

$$c_{i,k} = \{0,1\} \qquad \forall i,k, \tag{78e}$$

$$c_{i,k} - c_{i,x} = 0 \qquad \forall k, x \in \mathsf{Y}_k. \tag{78f}$$

where A_i denotes the number of UEs exceeding the spatial multiplexing capabilities of BS-RN link i and $\zeta_i > 0$ is a penalty value limiting the allocation of UEs to a specific RN much beyond the rank of the corresponding BS-RN channel. In the objective, we aim to find an optimal $c_{i,k} \in \{0,1\}$ allocation to maximize the sum utility while penalizing the over-allocation of users into the RNs. Inequality constraints (78b) and (78c) make sure that the over-allocation penalty is always non-negative. The equality constraint (78d) guarantees that each UE is allocated into one serving BS/RN, while the equality constraint (78f) aims to avoid large cross-link interference by forcing nearby users into the same BS/RN. Different approaches to solve the proposed user assignment problem are discussed below.

Direct LP solution

The user assignment problem in (78) is a combinatorial integer linear programming (ILP) problem [148]. The computational complexity of ILP increases exponentially with the number of BSs/RNs and UEs. However, we can find an approximated solution with greatly reduced complexity by relaxing the binary variable $c_{i,k}$ as a continuous variable $0 \leq c_{i,k} \leq 1$ and solving it as an LP problem. However, it is crucial to define nearby users set Y_k with properly planned interference threshold S_{th} to avoid assigning fractional $c_{i,k}$ values.

SCA based LP solution

As previously stated, there is a chance to obtain fractional valued assignment matrix $\mathbf{C}$ from the direct LP solution due to an inadequate parameter setting or unfavorable user distribution. Hence, here we present a complementary method for the user assignment, which is still less complex than the ILP method but more scrupulous than the direct LP solution. In addition to relaxing the binary variables as continuous variables as in the direct LP solution, we introduce the following well-known sparsity inducing penalty function to the objective to enforce a binary solution [144]

$$f(\mathbf{C}) = \sum_{i=1}^{B} \sum_{k=1}^{K} \log(c_{i,k} + \delta), \tag{79}$$

where δ is a small positive constant used to limit the dynamic range of the log function. Moreover, to adapt the objective to the SCA framework, we linearize the penalty

function by using first-order Taylor series approximation as[144]

$$f(\mathbf{C}^{(n+1)}) = f(\mathbf{C}^{(n)}) + \sum_{i=1}^{B}\sum_{k=1}^{K} \frac{c_{i,k} - c_{i,k}^{(n)}}{c_{i,k}^{(n)} + \delta}. \tag{80}$$

Now, with the linearized penalty (80) appended to the objective, the optimization problem in (78) can be solved as an iterative LP.

3.4 Practical implementation

In the previous section, we proposed an iterative precoder/decoder design with the WQM objective for the IAB system for a given user assignment. In principle, the proposed design summarized in Algorithm 3 can be implemented either in a centralized or decentralized manner. A specific challenge for the centralized implementation is the CSI acquisition of the cross-link interference channels, e.g., among mutually interfering user terminals. Explicit feedback of the UE-to-UE and RN-to-UE channels to the BS would be required to enable optimal beamformer design, which would make the centralized implementation infeasible in practice. In contrast, the proposed coordinated node specific beamformer design can be implemented in a decentralized manner by employing bi-directional F-B training via spatially precoded OTA pilot signalling [37, 39, 36]. Here, our primary focus is on the detailed analysis of the decentralized implementation of the beamformer design in both ideal and non-ideal conditions.

3.4.1 Training and signalling

The 5G 3GPP NR standard allows a large degree of flexibility to define application-specific frame structures. Specifically, due to the minislot concept introduced in NR, greatly expedited OTA information exchange is possible in both directions, as already shown in our previous work [133].

For the decentralized design, we use a specific TDD frame structure, as shown in Fig. 20. The TDD frame is divided into two portions: 1) beamformer signalling; 2) data transmission. In the beamformer signalling phase, we employ precoded pilot sequences to exchange initial/intermediate beamformers and user-specific weights between coordinated nodes in both forward and backward directions iteratively. There, each node estimates their precoder/decoder based on the received forward/backward training sequences and the estimated precoder/decoder as the precoder for the next

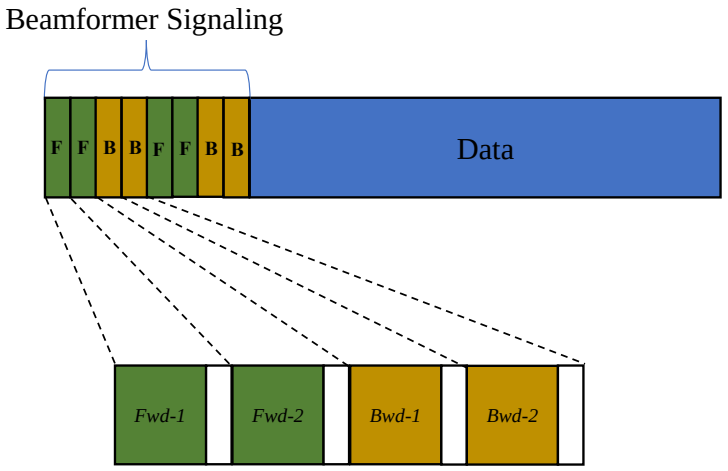

Fig. 20. TDD frame structure (Under CC BY 4.0 license from [134] ©2020 Authors).

iteration forward/backward training. The forward and backward phases refer to the directions where the pilot training is aligned with or opposed to the data transmission, respectively. In the data transmission phase, the transmit precoders and receive decoders acquired after the last bi-directional training iteration are used for transmitting and receiving the data symbols.

There are two different beamformer estimation strategies, which can be used with bi-directional OTA signalling to obtain the transmit/receive beamformers: 1) the direct beamformer estimation (DE), and 2) the stream specific estimation (SSE). In the DE method, the received precoded pilot training matrix is directly applied to estimate the required beamformer. In contrast, in the SSE, each stream specific pilot sequence is decoded separately. Then, the estimated stream specific equivalent channels are used to construct the beamformers. Both schemes perform equally well in ideal conditions, such as employing orthogonal pilot sequences at each node with high SNR for estimation. However, the orthogonal pilot allocation is not typically possible for practical dense network deployments, especially with decentralized resource scheduling. Since the DE approach has shown good resilience to non-ideal conditions [149], in this study, we focus on the DE method only.

Table 2. Pilot precoders and local feedbacks used during OTA bi-directional training (Under CC BY 4.0 license from [134] ©2020 Authors).

Label	Tx nodes	OTA pilot precoders	Local feedbacks
Fwd-1	BS	$\mathbf{m}_{k,l}^{(\mathrm{dl},1)}$, $\mathbf{v}_{i,l}^{(\mathrm{dl})}$	$t_{i,l}^{(\mathrm{ul})}$,$t_{k,l}^{(\mathrm{dl},2)}$
	UEs served by RNs	$\mathbf{m}_{k,l}^{(\mathrm{ul},1)}$	NA
Fwd-2	UEs served by BS	$\mathbf{m}_{k,l}^{(\mathrm{ul},2)}$	NA
	RNs	$\mathbf{m}_{k,l}^{(\mathrm{dl},2)}$, $\mathbf{v}_{i,l}^{(\mathrm{ul})}$	$t_{i,l}^{(\mathrm{dl})}$,$t_{k,l}^{(\mathrm{ul},1)}$
Bwd-1	UEs served by BS	$\sqrt{\omega_{k,l}^{(\mathrm{dl},1)}}\mathbf{u}_{k,l}^{(\mathrm{dl},1)}$	$\omega_{k,l}^{(\mathrm{dl},1)}$
	RNs	$\sqrt{\omega_{i,l}^{(\mathrm{dl})}}\mathbf{w}_{i,l}^{(\mathrm{dl})}$, $\sqrt{\omega_{k,l}^{(\mathrm{ul},1)}}\mathbf{u}_{k,l}^{(\mathrm{ul},1)}$	$\omega_{i,l}^{(\mathrm{dl})}$, $\omega_{k,l}^{(\mathrm{ul},1)}$
Bwd-2	BS	$\sqrt{\omega_{i,l}^{(\mathrm{ul})}}\mathbf{w}_{i,l}^{(\mathrm{ul})}$, $\sqrt{\omega_{k,l}^{(\mathrm{dl},2)}}\mathbf{u}_{k,l}^{(\mathrm{dl},2)}$	$\omega_{i,l}^{(\mathrm{ul})}$, $\omega_{k,l}^{(\mathrm{dl},2)}$
	UEs served by RNs	$\sqrt{\omega_{k,l}^{(\mathrm{ul},2)}}\mathbf{u}_{k,l}^{(\mathrm{ul},2)}$	$\omega_{k,l}^{(\mathrm{ul},2)}$

3.4.2 Decentralized beamformer estimation

For the DE method, pilot precoders used for OTA bi-directional training and local scalar feedbacks are summarized in Table 2. In addition to the aforementioned OTA signalling, control feedback channels are used to explicitly exchange limited scalar-valued parameters related to initial queue states and the auxiliary variables of the local nodes (local nodes are referred to as immediate parent-child BS-RN, BS-UE and RN-UE pairs, and UE-UE pairs are not considered local nodes). Details of the beamformer design steps at the transmit and receive nodes using OTA training and additional local feedback channels with minimal signalling are presented below.

Receive beamformer and weight estimation

The received precoded pilots information and explicit scalar valued local feedback information during *Fwd-1* and *Fwd-2* are used to estimate the receive beamformers, MSE values, user-specific weights, and auxiliary variables corresponding to the first and second timeslots, respectively.

Let $\mathbf{b}_{k,l}^{(a,s)} \in \mathbb{C}^S$ and $\mathbf{b}_{i,l}^{(s)} \in \mathbb{C}^S$ denote the pilot training sequences for l^{th} data stream corresponding to UE (UL or DL) k and RN i, respectively. Here, S is the length of

the pilot sequence. In the forward training, the pilots are precoded with the transmit precoders $\mathbf{m}_{k,l}^{(a,s)}$ and $\mathbf{v}_{i,l}^{(a)}$. Then, the received precoded pilot training matrix at DL UE $k \in \mathsf{U}_1$ during *Fwd-1* is given by

$$\begin{aligned}\mathbf{T}_k^{(\mathrm{dl},1)} =& \mathbf{H}_{1,k}\Big(\sum_{j\in\mathsf{U}_1}\sum_{n=1}^{L_j}\mathbf{m}_{j,n}^{(\mathrm{dl},1)}\mathbf{b}_{j,n}^{(\mathrm{dl},1)} + \sum_{i=2}^{N}\sum_{n=1}^{\bar{L}_i}\mathbf{v}_{i,n}^{(\mathrm{dl})}\mathbf{b}_{i,n}^{(\mathrm{dl})}\Big) \\ &+ \sum_{i=2}^{N}\sum_{j\in\mathsf{U}_i}\sum_{n=1}^{L_j}\tilde{\mathbf{H}}_{j,k}\mathbf{m}_{j,n}^{(\mathrm{ul},1)}\mathbf{b}_{j,n}^{(\mathrm{ul},1)} + \mathbf{N}_k, \end{aligned} \tag{81}$$

where $\mathbf{N}_k \in \mathbb{C}^{N_k \times S}$ is the estimation noise matrix for all pilot symbols. Then, by using the received composite channel information $\mathbf{T}_k^{(\mathrm{dl},1)}$ and own pilot training sequence $\mathbf{b}_{k,l}^{(\mathrm{dl},1)}$ we can directly estimate the MMSE receivers as

$$\mathbf{u}_{k,l}^{(\mathrm{dl},1)} = \left(\mathbf{T}_k^{(\mathrm{dl},1)}\mathbf{T}_k^{(\mathrm{dl},1)^{\mathrm{H}}} + \mathsf{N}_0\mathbf{I}\right)^{-1}\mathbf{T}_k^{(\mathrm{dl},1)}\mathbf{b}_{k,l}^{(\mathrm{dl},1)^{\mathrm{H}}}. \tag{82}$$

Note that, the estimated MMSE receiver and the exact expression in (59) become identical, when training sequences are orthogonal, and SNR is high [133] (estimation noise vanishes). Next, the corresponding MSE can be estimated as

$$\varepsilon_{k,l}^{(\mathrm{dl},1)} = 1 - \mathbf{u}_{k,l}^{(\mathrm{dl},1)^{\mathrm{H}}}\mathbf{T}_k^{(\mathrm{dl},1)}\mathbf{b}_{k,l}^{(\mathrm{dl},1)^{\mathrm{H}}}. \tag{83}$$

Similarly, for Rx2-Rx6, the received precoded matrices $\mathbf{T}_k^{(a,s)}\ \forall\, a,s,k$ and local stream specific pilot sequences $\mathbf{b}_{k,l}^{(a,s)}\ \forall\, a,s,k,l$ are used to estimate the corresponding MMSE receiver and MSE similar to (82) and (83). Then, we can calculate node specific auxiliary variables $t_{k,l}^{(a,s)}$ as in (66), by using the estimated MSE values. Finally, the user-specific weights $\omega_{k,l}^{(a,s)}$ are estimated using (67) and, (69) or (90). However, to do this, in addition to the OTA precoded information, we need explicit information on initial queues and auxiliary variables ($t_{k,l}^{(a,s)}, t_{i,l}^{(a)}$) from the local nodes. We assume this to be information exchange to happen over separate control feedback channels established among the local nodes. However, note that some of the feedback information can be outdated due to the inherent latency in the decentralized estimation.

Transmit precoder estimation

The received precoded pilot information and local feedback information during *Bwd-1* and *Bwd-2* are used to estimate the transmit beamformers corresponding to the first and second timeslots, respectively.

During the backward training, the pilots are precoded with the weighted receivers $\sqrt{\omega_{k,l}^{(a,s)}}\mathbf{u}_{k,l}^{(a,s)}$ and $\sqrt{\omega_{i,l}^{(a)}}\mathbf{w}_{i,l}^{(a)}$. Then, the received precoded pilot training matrix at the BS during *Bwd-1* is given by

$$\mathbf{R}_1^{(\mathrm{dl},1)} = \sum_{i=2}^{N} \hat{\mathbf{H}}_{1,i}^{\mathrm{H}} \Big(\sum_{j\in\mathsf{U}_i} \sum_{n=1}^{L_j} \sqrt{\omega_{j,n}^{(\mathrm{ul},1)}}\mathbf{u}_{j,n}^{(\mathrm{ul},1)}\mathbf{b}_{j,n}^{(\mathrm{ul},1)} + \sum_{n=1}^{\bar{L}_i} \sqrt{\omega_{i,n}^{(\mathrm{dl})}}\mathbf{w}_{i,n}^{(\mathrm{dl})}\mathbf{b}_{i,n}^{(\mathrm{dl})} \Big) + \sum_{j\in\mathsf{U}_1} \sum_{n=1}^{L_j} \mathbf{H}_{1,j}^{\mathrm{H}} \sqrt{\omega_{j,n}^{(\mathrm{dl},1)}}\mathbf{u}_{j,n}^{(\mathrm{dl},1)}\mathbf{b}_{j,n}^{(\mathrm{dl},1)} + \mathbf{N}_1, \tag{84}$$

where $\mathbf{N}_1 \in \mathbb{C}^{M_1\times S}$ is the estimation noise matrix for all pilot symbols. Note that the forward and backward sequences are assumed to be the same for any particular user. With the knowledge of the received training matrices, feedback information on local user-specific weights ($\omega_{k,l}^{(a,s)}, \omega_{i,l}^{(a)}$), and training sequences assigned to each locally served user, each transmit node can locally estimate their corresponding transmit beamformers. For example, the transmit precoder for UE $k \in \mathsf{U}_1$ can be obtained in a closed-form expression as

$$\mathbf{m}_{k,l}^{(\mathrm{dl},1)} = \left(\mathbf{R}_1^{(\mathrm{dl},1)}\mathbf{R}_1^{(\mathrm{dl},1)^{\mathrm{H}}} + \mathbf{I}\nu_1^{(\mathrm{dl},1)} \right)^{-1} \sqrt{\omega_{k,l}^{(\mathrm{dl},1)}}\mathbf{R}_1^{(\mathrm{dl},1)}\mathbf{b}_{k,l}^{(\mathrm{dl},1)^{\mathrm{H}}}, \tag{85}$$

where the optimal $\nu_1^{(\mathrm{dl},1)}$ is found by bisection search to satisfy the power constraints (63c). Similarly, for Tx2-Tx6, the received precoded training matrices $\mathbf{R}_k^{(a,s)}, \mathbf{R}_i^{(a,s)}$, local stream specific pilot sequences $\mathbf{b}_{k,l}^{(a,s)}, \mathbf{b}_{i,l}^{(a)}$ and user-specific weights $\omega_{k,l}^{(a,s)}, \omega_{i,l}^{(a)}$ received over the feedback channels are used to estimate the transmit precoders. This transmit and receiver precoder estimation is carried out iteratively as in the previous case. Finally, we can summarize the proposed decentralized beamformer design as in Algorithm 4.

3.4.3 Complexity study

In this subsection, we study the computational complexity of the proposed decentralized beamformer design. Since the complexity is linearly proportional to the number of OTA signalling rounds, we consider a single iteration only. The complexity at each node during the beamformer estimation is composed of the following.

– At the BS, both transmit and receive beamformers are estimated. For the transmit beamformer, the dominant operation is the matrix inversion in (85). In addition, there

Algorithm 4 Decentralized Beamformer design assist with bi-directional training and local feedbacks

1: Initialize transmit precoders $(\mathbf{m}_{k,l}^{(a,s)}, \mathbf{v}_{i,l}^{(a)})$.
2: Calculate multiplexing factors $a_k^{(a)}$ for each UE using (74) (Heuristic method).
3: Exchange UL/DL queues $(Q_k^{(a)}, \bar{Q}_k^{(a)})$, prioritizing weights $(\alpha_k^{(a)})$, initial auxiliary variables $(t_{i,l}^{(a)}, t_{k,l}^{(a,s)})$ and multiplexing factors $(a_k^{(a)})$ between local nodes via feedback channels.
4: **repeat**
5: *Fwd-1*: BS and UEs served by RNs send OTA pilots precoded with transmit beamformers $\mathbf{m}_{k,l}^{(a,1)}, \mathbf{v}_{i,l}^{(\mathrm{dl})}$. Exchange auxiliary variables $t_{i,l}^{(\mathrm{ul})}, t_{k,l}^{(\mathrm{dl},2)}$ (initial or previously calculated during *Fwd-2*) to local nodes via feedback.
6: RNs and UEs served by BS estimate MMSE receivers $\mathbf{u}_{k,l}^{(a,1)}, \mathbf{w}_{i,l}^{(\mathrm{dl})}$ from (82), and calculate auxiliary variables $t_{k,l}^{(a,1)}, t_{i,l}^{(\mathrm{dl})}$ from (66) and user-specific weights $\omega_{k,l}^{(a,1)}, \omega_{i,l}^{(\mathrm{dl})}$ from (67).
7: *Fwd-2*: RNs and UEs served by BS send OTA pilots precoded with transmit beamformers $\mathbf{m}_{k,l}^{(a,2)}, \mathbf{v}_{i,l}^{(\mathrm{ul})}$. Exchange auxiliary variables $t_{i,l}^{(\mathrm{dl})}, t_{k,l}^{(\mathrm{ul},1)}$ (calculated during *Fwd-1*) to local nodes via feedback.
8: BS and UEs served by RNs estimate MMSE receivers $\mathbf{u}_{k,l}^{(a,2)}, \mathbf{w}_{i,l}^{(\mathrm{ul})}$ from (82) and calculate auxiliary variables $t_{k,l}^{(a,2)}, t_{i,l}^{(\mathrm{ul})}$ from (66) and user-specific weights $\omega_{k,l}^{(a,2)}, \omega_{i,l}^{(\mathrm{ul})}$ from (67).
9: *Bwd-1*: RNs and UEs served by BS send OTA pilots precoded with weighted MMSE receivers $\sqrt{\omega_{k,l}^{(a,1)}}\mathbf{u}_{k,l}^{(a,1)}, \sqrt{\omega_{i,l}^{(\mathrm{dl})}}\mathbf{w}_{k,l}^{(\mathrm{dl})}$. Exchange user-specific weights $\omega_{k,l}^{(a,1)}, \omega_{i,l}^{(\mathrm{dl})}$ to local nodes via feedback.
10: BS and UEs served by RNs estimate transmit precoders $\mathbf{m}_{k,l}^{(a,1)}, \mathbf{v}_{i,l}^{(\mathrm{dl})}$ from (85).
11: *Bwd-2*: The BS and UEs served by RNs send OTA pilots precoded with intermediate weighted MMSE receivers $\sqrt{\omega_{k,l}^{(a,2)}}\mathbf{u}_{k,l}^{(a,2)}, \sqrt{\omega_{i,l}^{(\mathrm{ul})}}\mathbf{w}_{k,l}^{(\mathrm{ul})}$. Exchange user-specific weights $\omega_{k,l}^{(a,2)}, \omega_{i,l}^{(\mathrm{ul})}$ to local nodes via feedback.
12: RNs and UEs served by BS estimate transmit precoders $\mathbf{m}_{k,l}^{(a,2)}, \mathbf{v}_{i,l}^{(\mathrm{ul})}$ from (85).
13: **until** convergence.

is a dual variable that is found by bisection search to satisfy the power constraint. Hence, the complexity is $\mathsf{O}(M_1^3\Delta(K_1L_k+\sum_{i=2}^{N}\bar{L}_i))$, where Δ is the number bisection iterations required to satisfy the power constraint. Moreover, for receiver estimation, the dominant operation is the matrix product operation within the inverse matrix in (82). Hence the complexity is $\mathsf{O}(M_1^2S)$.

– At the UEs, the transmitter estimation complexity is $\mathsf{O}(N_k^3\Delta L_k)$ and the receiver estimation complexity is $\mathsf{O}(N_k^2S)$.
– Similarly, At RNs, the transmitter estimation complexity is $\mathsf{O}(M_i^3\Delta(K_iL_k+\bar{L}_i))$ and the receiver estimation complexity is $\mathsf{O}(M_i^2S)$.

According to the complexity study, the BS should have a higher computational capability compared to UEs and RNs. Note that due to the decentralized and parallel computation of the precoders at BS and RNs, the computational complexity per one OTA signalling cycle considerably is in the same range as any other multiuser MIMO MMSE-type single-hop beamformer designs[85, 86, 80].

3.5 Numerical examples

In the simulation model, we consider a symmetric IAB model with one BS and four RNs, with 200m distance between BS and each RN. The number of BS, RN and UE antennas is $M_1 = 20$, $M_i = 8$ and $N_k = 2$, respectively. The power constraint for BS is normalized to $P_1 = 10$, and power constraints at RNs and UEs are $P_i = P_1/4$ and $p_k = P_1/20$ (to have similar UL and DL power levels in both timeslots), respectively. Noise power (N_0) is obtained assuming the cell edge (100m from BS) SNR for BS transmission to be 10 dB (SNR = $S_{1,k}P_1^{(\mathrm{dl})}/\mathsf{N}_0$). In addition, the path loss exponent is 3.67. We consider uncorrelated i.i.d fading for BS-UE and RN-UE channels. The BS-RN channels in Figs. 21 and 22 are modelled as uncorrelated i.i.d while correlated Rician fading is assumed for the rest of the figures. In addition, for Figs. 25 to 27, we consider $D_i = 2\,\forall i \in \mathbb{B}_{\mathrm{R}}$ and path gain threshold for nearby user set $S_{\mathrm{th}} = 15^{-3.67}$. We consider the Poisson arrival process to generate the traffic in the network, where $\lambda_k^{(\mathrm{a})}(\tau) \sim \mathbf{Pois}(A_k^{(\mathrm{a})})$ is the generated traffic for DL/UL UE k in time instance τ. Here, $A_k^{(\mathrm{a})} = \mathbb{E}_\tau\{\lambda_k^{(\mathrm{a})}\}$ are the average number of packet arrivals in bits for the corresponding UL/DL UEs. Then, the total number of queued packets in each UL/DL queue at $(\tau+1)^{th}$ time instant is given by $Q_k^{(a)}(\tau+1) = \left[Q_k^{(a)}(\tau) - R_k^{(a)}(\tau)\right]^+ + \lambda_k^{(a)}(\tau)$, where $R_k^{(a)}$ is the transmission rate to/from UE k. In addition, the user priority weights (α_k) are assumed

to be 1. Except for Fig. 23, the rest of the figures are limited to 10 beamformer iterations per scheduling interval (TDD frame) due to practical limitations in OTA beamformer training process.

It should be noted that the choice of the symmetric placement of RNs was fairly arbitrary and mainly based on the ability to reproduce the results easily. However, the proposed beamformer design is independent of the simulation setup and works for any asymmetric deployment as well. Indeed, the user-specific rates and backhaul rates depend on the link distance given a limited power budget at each node. Hence, from the queue minimization perspective, given the same traffic arrival rate per user, the weakest backhaul links would dominate the accumulated total backlog packets in the network. In practice, the arrival rate should be adjusted for users served by more distant RNs. The optimal placement of RNs is given practical constraints imposed by the proposed IAB setup is an interesting idea for future extension of the current work.

The average total backlogged packets after 1000 traffic arrivals (which is equivalent to 2000 timeslots) in the system queues versus average traffic arrival rate is shown in Fig. 21, where UEs are randomly placed within 50m from the serving BS/RN. As the reference case, we consider a conventional HD relaying system, which takes two timeslots for each UL and DL data transmission. In the HD system, we assume that for 50% of the time, it is in DL mode, while for the rest of the time, it is in UL mode. We can observe that, despite the increased cross-link interference, flexible TDD based IAB system always performs much better in comparison to the HD relaying system in all traffic arrival rates. The IAB system becomes unstable after the arrival rate reaches 0.9 (after that queues grow linearly with the arrival rate), while the HD case becomes saturated with much lower arrival rates. In addition, we can observe that RN queues are in general less congested than the queues at UEs and at BS. Hence, the RNs can potentially have smaller buffer sizes without deteriorating the system performance. Fig. 22 illustrates the total backlogged packets in the IAB system with the number of packet arrivals. For the arrival rate 0.8, the system is in a stable region where the total number of backlogged traffic fluctuate around 200 bits. However, when the average arrival rate is at 0.9, the IAB system becomes unstable and queues grow without limit. Thus, for the considered simulation model, the proposed WQM based beamformer design is able to optimally utilize network resources up to arrival rate 0.8 while satisfying all the UE demands.

It should be noted that the beamformers are designed to follow the dynamic traffic arrival process, where each node is assigned resources based on their instantaneous

queue states both in UL and DL. Therefore, in such a dynamic environment, the beamformers never really converge but keep adapting to the instantaneous traffic load while minimizing the total (weighted) queues in the network over time. However, for a static snapshot of the dynamic process, the convergence behaviour of the proposed beamformer design can be studied. Fig. 23 illustrates the convergence of the algorithm at one particular time instance (with 0.8 arrival rate) averaged over a large number of channel realizations. The results demonstrate that even though it takes about 20 iterations to reach a point where the objective is not improved anymore, most of the improvement occurs during thew first few iterations. This a desired feature for an algorithm which aims at following a dynamic traffic arrival process.

The performance of the IAB system for different antenna configurations are represented in Fig. 24. As expected, the stable region increases with the number of antennas both at BS and RNs. Again, in all the cases, IAB system shows superior performance in comparison to the reference case with HD relays. The performance of the proposed user assignment algorithm with $K = 20$ after 1000 random user drops is presented in Fig. 25. Those results are generated using the direct LP solution that we have proposed to the optimization problem in (78) (Note that the SCA based LP solution provides quite similar results for the chosen parameter set). The left figure shows the average number of UEs assigned to BS and each RN. There, on average, half of the UEs are assigned to BS while the other half is assigned to the rest of the RNs. Due to the symmetrical placement of the RNs around the BS, on average, the UEs are equally assigned to RNs. In addition, when a UE drops in the middle of the BS and a RN, that particular UE is most likely assigned to BS. The right figure illustrates CDF of the assignment values ($c_{i.k}$). We can observe that 80% of the time the $c_{i.k}$ value takes 0, and for the rest of the time, it takes 1. We hardly observe any fractional values are assigned to $c_{i.k}$. Hence, the proposed design assigns only 0s and 1s to the assignment matrix as desired.

The performance of the IAB system after 1000 traffic arrivals with the proposed user assignment algorithm is shown in Fig. 26. The proposed user assignment algorithm is labelled as 'UA'. In the reference case, labelled as C-UE, UEs are assigned to BS or RN based on the strongest RSSI value. We can observe that with the proposed user assignment method, the performance of the system is improved compared to the traditional RSSI based user assignment for all $K = \{15, 20, 25\}$. Increasing the total number of UEs K, the stable region of the IAB system is decreased due to the limited power budget and degrees of freedom.

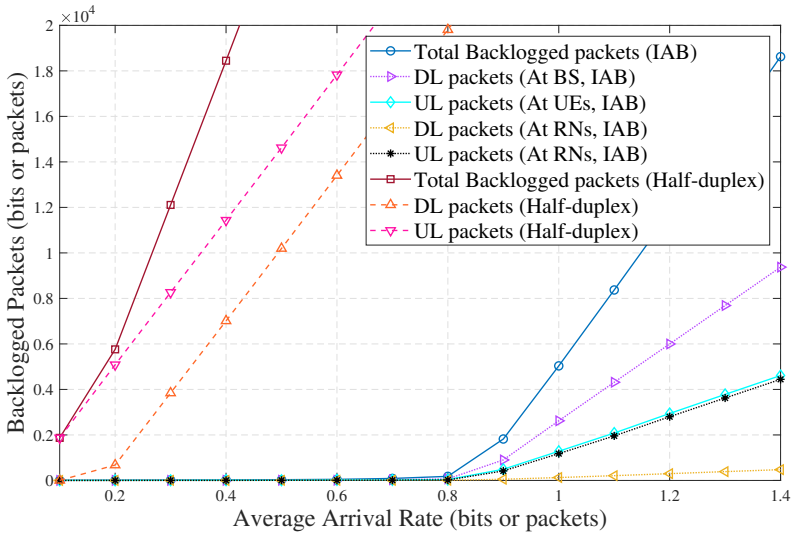

Fig. 21. Comparison of an IAB model with a conventional HD relaying system after 1000 traffic arrivals for $K_i = 4\,\forall i$ (Under CC BY 4.0 license from [134] ©2020 Authors).

In Fig. 27, the performance of the IAB system is shown after 1000 traffic arrivals when employing non-orthogonal random pilots for OTA training with the decentralized beamformer implementation. In addition, a 10 dB pilot boost is used in the simulations. For the considered model, ideally 48 orthogonal pilot sequences (2 for each user and 2 for each BS-RN link) would be required to carry out the OTA bi-directional training without any pilot contamination (assuming the same pilot is used for forward and backward training). Therefore, we can observe that the decentralized random pilot allocation is greatly deteriorated if shorter sequence lengths ($S = 16, 32$) are used due to the high level of pilot contamination. However, the decentralized pilot assignment starts to perform reasonably well with $S = 48$, and with $S = 96$, it can withstand about 80% of the traffic load provided by the centralized (orthogonal) pilot allocation.

3.6 Summary and discussion

In this chapter, a flexible TDD-based IAB system consisting of a BS, multiple single-hop RNs, and UEs was investigated with complex interference conditions due to simultaneous UL/DL traffic, in-band access, and backhaul traffic. In the considered flexible TDD mode, RNs and BS are assigned to distinct UL or DL transmission modes to mitigate

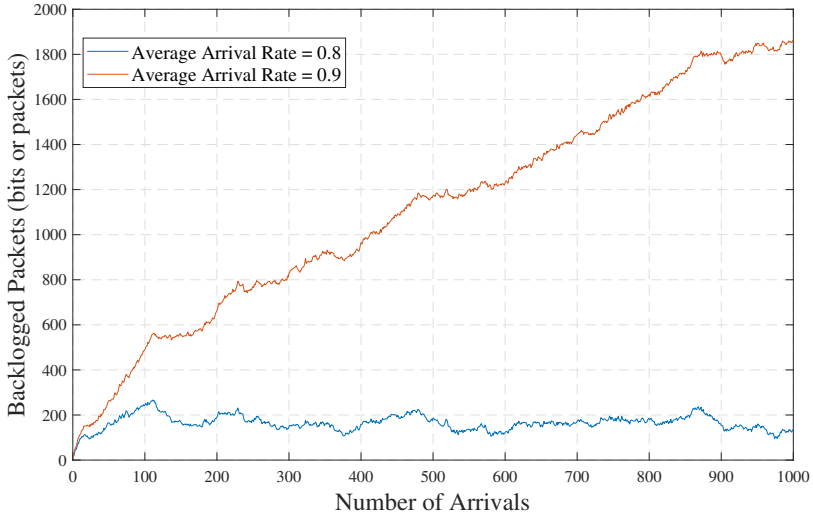

Fig. 22. Total backlogged packets in the IAB system with the number of traffic arrivals for $K_i = 4 \, \forall i$ (Under CC BY 4.0 license from [134] ©2020 Authors).

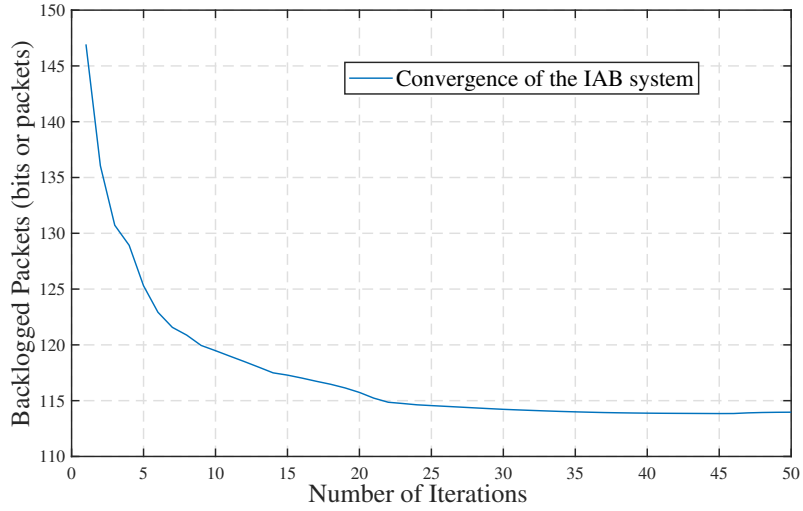

Fig. 23. Convergence behaviour of the proposed iterative beamformer design for IAB system with $K_i = 4 \, \forall i$ (Under CC BY 4.0 license from [134] ©2020 Authors).

conventional HD loss at RNs. An iterative beamformer design with WQM objective was proposed to manage the resulting cross-channel interference and to allocate a wireless

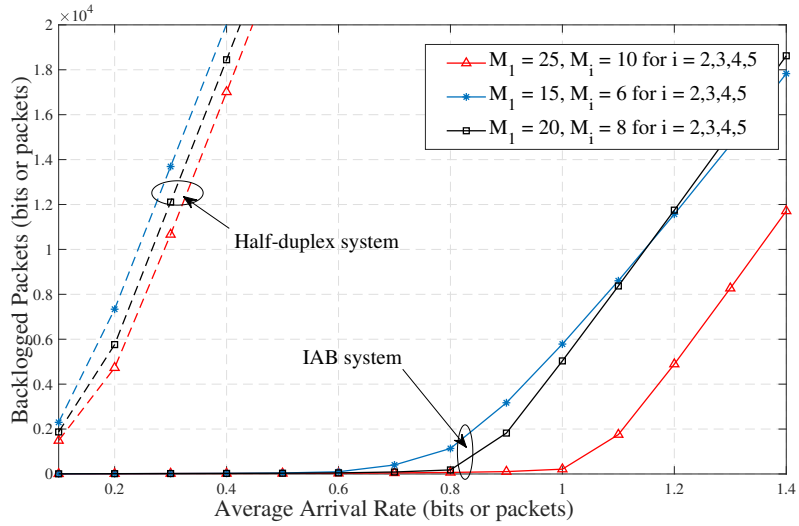

Fig. 24. IAB system performance for different antenna configurations at BS and RNs with $K_i = 4\,\forall i$ (Under CC BY 4.0 license from [134] ©2020 Authors).

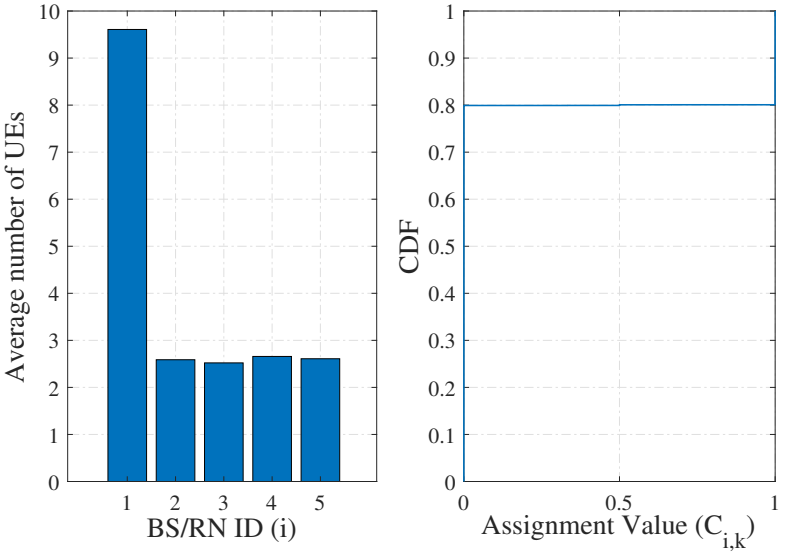

Fig. 25. Performance of the user assignment algorithm with $K = 20$; Left figure: Average number of UEs assigned into each BS/RN; Right figure: CDF of the assignment values $c_{i,k}$ (Under CC BY 4.0 license from [134] ©2020 Authors).

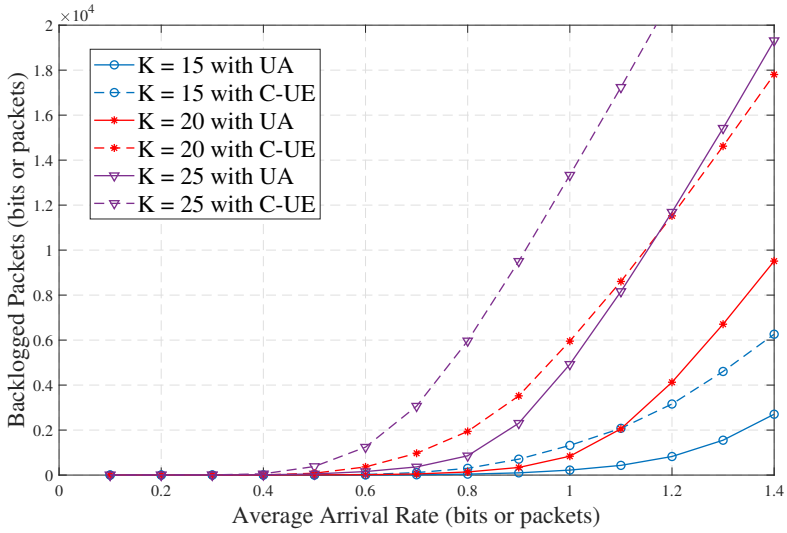

Fig. 26. Average total backlogged packets of the system with the user assignment algorithm (Under CC BY 4.0 license from [134] ©2020 Authors).

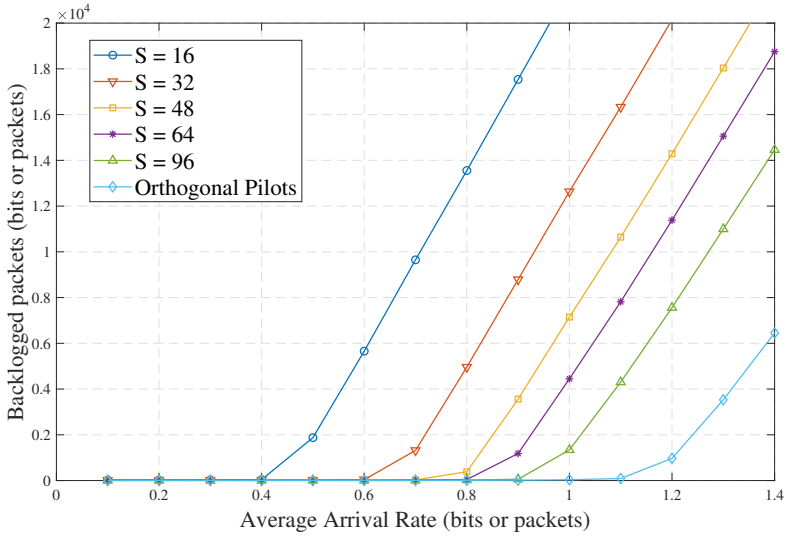

Fig. 27. IAB system performance of the decentralized implementation by using OTA bi-directional training with non-orthogonal pilot sequences for $K = 20$ (Under CC BY 4.0 license from [134] ©2020 Authors).

backhaul and access resources jointly over two consecutive data delivery intervals required for communications between the BS and UEs through HD RNs. Dynamic

traffic behaviour in the IAB system is handled via the WQM objective, and user-specific UL/DL queues are also introduced at RNs to guarantee reliable end-to-end data delivery. The original NP-hard optimization problem was solved to obtain a computationally efficient solution by using the iterative AO method. Backhaul rate multiplexing was introduced to the original optimization problem and corresponding rate multiplexing terms were solved either directly via KKT-based algorithm or via a simple heuristic method.

Bi-directional forward-backward training via spatially precoded over-the-air pilot signalling is employed to allow decentralized beamformer design across all the nodes. A novel user allocation method was proposed by solving a combinatorial optimization problem to assign UEs to BS or RNs based only on long-term channel statistics and some practical IAB limitations. The numerical examples illustrate the superior system performance of the considered flexible IAB in comparison to the conventional HD relaying system. Furthermore, IAB-nodes can potentially be equipped with smaller buffer sizes without compromising the system performance. Finally, a DE based coordinated beamformer design was proposed using precoded pilots in OTA bi-directional signalling and explicit scalar feedbacks. This was shown to perform reasonably well by alleviating the pilot contamination even with relatively short non-orthogonal pilot sequence lengths.

4 Conclusions and future work

This chapter summarizes the major contributions and most important results of this thesis, as well as some future research directions.

4.1 Conclusions

The focus of this thesis is to investigate two types of heterogeneous wireless communication systems, namely dynamic TDD systems and IAB systems. Particular attention was given to decentralized beamforming design, bidirectional signalling, and pilot decontamination strategies. In Chapter 1, the motivation for the research was presented, followed by a review of related prior studies. Chapter 2 focused on MIMO-based multi-user multi-cell dynamic TDD systems and the designing of the distributed framework for beamforming and bi-directional transmissions. The focus of Chapter 3 was on studying a flexible TDD-based IAB system that can be used to minimize HD loss at IAB nodes and the employment of joint beamformer design for access and backhaul traffic delivery with the assistance of bidirectional signalling. The bidirectional signalling framework was emphasized in both chapters to direct pilot decontamination techniques.

Multiantenna interference management for dynamic TDD systems was discussed in Chapter 2 in conjunction with several network optimization objectives such as WQM, (Q)WSR, and SMSE. The original NP-hard optimization problem was solved by applying a fast converging KKT-based iterative AO method, and the solution was evaluated in a distributed manner. The OTA bi-directional signalling and training framework was developed to facilitate transmit and receive beamformers in UL and DL to be optimized iteratively. The distributed fast converging beamformer approach based on the WQM criterion was shown to be the best solution for both dynamic traffic variations and difficult interference scenarios. A new set of DE strategies based on OTA bidirectional signalling techniques was proposed to address contamination resulting from the use of overlapping and non-orthogonal pilots. In the case of relatively short pilot sequences, both strategies A and B demonstrated promising results. Additionally, a centralized pilot allocation scheme was adopted to further improve the pilot decontamination process. The numerical results demonstrate that the proposed training and estimation framework

provides superior system performance over the uncoordinated scheme for different dynamic TDD network parameters and optimization objectives.

In Chapter 3, a flexible TDD-based IAB system was investigated under complex interference conditions caused by simultaneous UL/DL traffic, in-band access, and backhaul traffic. The decentralized multiantenna beamforming techniques were used to mitigate interference with the WQM objective. In the beamformer design, the queue dynamics across two timeslots were taken into account. In order to obtain a computationally efficient solution, an iterative AO method was employed to solve the original NP-hard optimization problem. An optimization problem involving backhaul rate multiplexing was formulated and the rates were solved either directly by KKT-based algorithms or by simple heuristic approaches. A practical, centralized user assignment algorithm was developed, using combinatorial optimization techniques, to meet the needs of IAB functionality and WQM. Distributed implementation of the beamformer design was carried out by using the OTA bi-directional signalling framework and robust LS-based direct beamformer estimation. In numerical examples, the flexible TDD-based IAB system with the proposed beamformer design user assignment scheme showed superior performance in comparison to the conventional HD relaying system. Furthermore, IAB-nodes can potentially be equipped with smaller buffer sizes without compromising the system performance. Finally, DE based coordinated beamformer design was proposed using precoded pilots in OTA bi-directional signalling and explicit scalar feedbacks. It was shown to perform reasonably well by alleviating the pilot contamination even with relatively short non-orthogonal pilot sequence lengths.

4.2 Future directions

Flexible TDD is considered in 5G and even in future releases of the 3GPP standards since its flexible frame structure encourages the use of TDD for different models of wireless systems that require low latency, efficient spectrum use, and minimal synchronization overhead. These flexible TDD-based studies conducted considering dynamic TDD systems and IAB systems can be extended, and the results of these studies are essential for the development of future wireless systems. With the provision of MIMO for both dynamic TDD and IAB systems, interference can be mitigated while optimally managing network utilities with different precoder design objectives. The proposed MIMO solutions and algorithms can be extended or reused to different types

of heterogeneous systems such as underlying D2D, cell-free massive MIMO, multi-TRP and, etc.

The proposed decentralization framework for beamformer estimation and signalling exchange in limited pilot environments is an important area of interest. It is envisioned that multipoint transmission and reception (multi-TRP), cell-free massive MIMO will be crucial for future networks to improve reliability, coverage, and capacity performance [150, 151]. Distributed resource allocation, encoding, and decoding are essential parts of those systems. Accordingly, [152] investigated a distributed framework for the cooperative precoding design in cell-free massive MIMO using OTA signalling mechanism, and [153] proposed two practical explicit CSI feedback schemes, following CSI feedback framework from NR Rel. 15. Hence, multi-TRP and cell-free massive MIMO systems can thus be studied more in-depth using a modified OTA bidirectional signalling framework that was proposed in Chapters 2 and 3.

The ongoing 5G and beyond system implementations are not that advanced in radio resource management to enable decentralized beamforming, in which still beamformer implementation follows a centralized design [154]. There is a dire need to simplify the decentralized beamformer designs such that the required control signalling overhead would not harm overall network performance. However, it may be possible to implement decentralized beamformer designs based on a fast-converging and efficient OTA signalling framework. This thesis presents algorithms that speed up the convergence of the beamformer design so that minimal OTA iterations are required to achieve the desired results. Despite this, there is enough room for further improvements to allow fast convergence or explore solutions that rely on closed-form expressions. Additionally, 5G and LTE still adhere to a predefined slot allocation policy, which is inefficient for highly dense small cell deployments and asymmetric traffic. Despite 5G's ability to offer application-specific frames, network vendors may still be reluctant to implement these additional functionalities due to the tedious effort that is required to be put into the implementation process not yet economical for them [155, 156]. Therefore, further studies can be carried out on both dynamic TDD and IAB systems to optimize time-slot allocation by considering dynamic traffic conditions.

The WQM-based beamformer design is unique among all other beamforming methods, since it takes instant network behaviour into account, delivering traffic with a minimum delay to minimize the total number of backlogged packets in the network. Furthermore, WQM addresses important future network requirements, such as low latency, network congestion, and spectral efficiency to enhance capacity. In Chapters 2

and 3, WQM-based beamformer designs were developed which demonstrated how to derive (Q)WSR and SMSE-based beamformers by applying special conditions to derived expressions. Thus, WQM can be used as the starting point to analyse different wireless networks, as it can be transformed to obtain a better insight on other network utilities as well. In addition, there is plenty of room for modifying proposed solutions by fine-tuning some of the parameters that produce fast convergence or by using novel methods to obtain desired solutions. Additionally, joint beamformer design is another interesting approach to optimize network utilities, in which precoders by combining multiple timeslots or both UL/DL precoders are calculated using a common optimization objective. The proposed approach of combining all UL/DL precoders over two timeslots using the WQM objective, as discussed in Chapter 3, proved to be much more effective as transmissions in both timeslots are required for determining total packet delivery. This particular approach can be used as a guideline for optimizing more complicated system models. Furthermore, we have exploited convex optimization tools and heuristic approaches to optimize resource scheduling in both dynamic TDD and IAB systems. The proposed algorithms and procedures are not only limited to wireless communication systems, but they can also be tailored to solve different optimization problems in a wide range of domains.

The pilot contamination phenomenon will be prevalent in future wireless networks, particularly in massive-MIMO and densified small cell networks. Hence, it is crucial to explore various methods through which to deal with this concern, such as utilizing advanced detection schemes or pilot reuse/scheduling methods. It was demonstrated in Chapters 2 and 3 that DE provided better decontamination in both dynamic TDD systems and IAB systems. This DE method with different bi-directional OTA signalling methods can be further developed for different system models under contaminated conditions. In addition, further studies can be conducted to improve decontamination by designing pilot precoders so that noise and interference have a minimal impact on DE output. Moreover, the proposed pilot reuse design in Chapter 2 reduces pilot contamination considerably in dynamic TDD systems. The literature places a greater emphasis on centralized pilot reuse methods that are based on massive MIMO scenarios since they are relatively easy to implement in practice. However, these algorithms can be further developed or extended to employ hybrid decontamination techniques to reduce contamination to a greater extent.

Recent studies on dynamic TDD systems have been focused on different research directions such as mmWave based hybrid beamforming [157, 158], joint UL/DL cell

mode selection [159, 160], and employing low-precision ADCs/DACs [161, 162]. With hybrid beamforming, it is possible to suppress interference significantly in both the analog and digital domains. However, specific challenges may arise during CSI acquisition (applicable to precoded pilots based OTA bi-directional training as well) due to the choice of the analog and digital beamformers. Therefore, further studies can be carried out on hybrid beamforming especially considering the OTA signalling requirements to reduce the complexity and overhead. The key benefit of dynamic TDD over synchronous TDD is the advancement in spectral efficiency at the expense of the complexity associated with handling the additional interference. Hence, the objective of the UL/DL mode selection at a given time should be matched to the optimization objectives of beamformer design and resource allocation while considering dynamic traffic conditions and other priority concerns in the network to gain most of the benefits offered by the dynamic TDD system. Furthermore, there can be further studies on joint UL/DL selection, beamformer design, and resource allocation within the available time/frequency/space dimensions. Moreover, with the advent of mmWave communication and massive MIMO, dynamic TDD systems can be investigated for low-bit ADCs/DACs on both the transmitter and receiver sides. Using low-bit ADCs and DACs with massive MIMO-based dynamic TDD, reasonable performance can be achieved with minimal power consumption and costs.

IAB is an ongoing research topic for 5G and beyond wireless networks. There are several use cases and topologies defined in 3GPP, with a focus on improving coverage through the implementation of small cells while utilizing the benefits of high bandwidth mm-Wave systems. Numerous research efforts are being conducted for the IAB since it could be vital for future communication systems. Resource scheduling, backhaul management, interference management, meeting the latency requirements, complexity at IAB-nodes, and user assignments are the key considerations of IAB systems. In Chapter 3, many of the aforementioned challenges have been addressed, considering multi-node single-hop IAB network topology. It is possible to extend this study to multi-hop systems by modifying the beamformer design according to the IAB model and traffic flow. It is also possible to study the robustness of the IAB systems since their performance can be vulnerable to different weather and deployment parameters [51]. Moreover, mm-Wave communication plays an important role in achieving the anticipated network performance and communication tasks of 5G and 6G. System architectures such as IAB systems and small cell systems, hybrid beamforming techniques, massive MIMO, and machine learning-based systems are being developed with mm-Wave. System models in

Chapters 2 and 3, can be further analysed for massive-MIMO using the tools of random matrix theory and for hybrid beamforming techniques assuming mm-Wave systems.

References

[1] L. J. Vora, "Evolution of mobile generation technology: 1g to 5g and review of upcoming wireless technology 5g," *International journal of modern trends in engineering and research*, vol. 2, no. 10, pp. 281–290, 2015.

[2] Y. Tamirat, "The role of nanotechnology in semiconductor industry: Review article," *Journal of Material Science & Nanotechnology*, vol. 5, no. 2, p. 202, 2017.

[3] M. Haenlein and A. Kaplan, "A brief history of artificial intelligence: On the past, present, and future of artificial intelligence," *California management review*, vol. 61, no. 4, pp. 5–14, 2019.

[4] S. Lindgren, *Digital media and society*. Sage, 2017.

[5] C. Systems. Cisco Visual Networking Index: Forecast and Methodology, 2016-2021. [Online Sep. 2017], https://www.cisco.com/c/en/us/solutions/collateral/service-provider/visual-networking-index-vni/complete-white-paper-c11-481360.pdf.

[6] E. Oughton, Z. Frias, T. Russell, D. Sicker, and D. D. Cleevely, "Towards 5g: Scenario-based assessment of the future supply and demand for mobile telecommunications infrastructure," *Technological Forecasting and Social Change*, vol. 133, pp. 141–155, 2018.

[7] H. Holma, A. Toskala, and T. Nakamura, *5G technology: 3GPP new radio*. John Wiley & Sons, 2020.

[8] A. Osseiran, J. F. Monserrat, and P. Marsch, *5G mobile and wireless communications technology*. Cambridge University Press, 2016.

[9] T. Nakamura, "5g evolution and 6g," in *2020 IEEE Symposium on VLSI Technology*. IEEE, 2020, pp. 1–5.

[10] J. G. Andrews, S. Buzzi, W. Choi, S. V. Hanly, A. Lozano, A. C. K. Soong, and J. C. Zhang, "What will 5G be?" *IEEE Journal on selected areas in communications*, vol. 32, no. 6, pp. 1065–1082, 2014.

[11] M. Series, "Imt vision–framework and overall objectives of the future development of imt for 2020 and beyond," *Recommendation ITU*, vol. 2083, 2015.

[12] P. Rost, A. Banchs, I. Berberana, M. Breitbach, M. Doll, H. Droste, C. Mannweiler, M. A. Puente, K. Samdanis, and B. Sayadi, "Mobile network architecture evolution toward 5g," *IEEE Communications Magazine*, vol. 54, no. 5, pp. 84–91, 2016.

[13] E. Dahlman, G. Mildh, S. Parkvall, J. Peisa, J. Sachs, Y. Selén, and J. Sköld, "5g wireless access: requirements and realization," *IEEE Communications Magazine*, vol. 52, no. 12, pp. 42–47, 2014.

[14] C. Bockelmann, N. Pratas, H. Nikopour, K. Au, T. Svensson, C. Stefanovic, P. Popovski, and A. Dekorsy, "Massive machine-type communications in 5g: Physical and mac-layer solutions," *IEEE Communications Magazine*, vol. 54, no. 9, pp. 59–65, 2016.

[15] A. Ghosh, A. Maeder, M. Baker, and D. Chandramouli, "5G Evolution: A View on 5G Cellular Technology beyond 3GPP Release 15," *IEEE Access*, vol. 7, pp. 127 639–127 651, 2019.

[16] 3GPP, "Technical report 38.802: Study on new radio access technology physical layer aspects v.2.0.0," 3rd Generation Partnership Project 3GPP, www.3gpp.org, Tech. Rep., Mar. 2017.

[17] ——, “ User Equipment (UE) Radio Frequency (RF) requirements for Frequency Range 2 (FR2) ,” 3rd Generation Partnership Project 3GPP, www.3gpp.org, Tech. Rep., 2019.

[18] Ericsson, “Ericsson mobility report june 2021,” *Ericsson com*, 2021.

[19] D. Tse and P. Viswanath, *Fundamentals of wireless communication*. Cambridge university press, 2005.

[20] F. Rusek, D. Persson, B. K. Lau, E. G. Larsson, T. L. Marzetta, O. Edfors, and F. Tufvesson, “Scaling up mimo: Opportunities and challenges with very large arrays,” *IEEE signal processing magazine*, vol. 30, no. 1, pp. 40–60, 2012.

[21] 3GPP, “ Study on New Radio (NR) access technology (3GPP TR 38.912 version 15.0.0 Release 15) ,” 3rd Generation Partnership Project 3GPP, www.3gpp.org, Tech. Rep., 2019.

[22] ——, “ NR; User Equipment (UE) Multiple Input Multiple Output (MIMO) Over-the-Air (OTA) performance requirements TS 38.151,” 3rd Generation Partnership Project 3GPP, www.3gpp.org, Tech. Rep., 2021.

[23] A. Z. Yonis, M. F. L. Abdullah, and M. F. Ghanim, “Lte-fdd and lte-tdd for cellular communications,” *Proceeding, Progress in*, 2012.

[24] S. Chen, S. Sun, Y. Wang, G. Xiao, and R. Tamrakar, “A comprehensive survey of TDD-based mobile communication systems from TD-SCDMA 3G to TD-LTE (A) 4G and 5G directions,” *China Communications*, vol. 12, no. 2, pp. 40–60, 2015.

[25] M. Shafi, A. F. Molisch, P. J. Smith, T. Haustein, P. Zhu, P. De Silva, F. Tufvesson, A. Benjebbour, and G. Wunder, “5g: A tutorial overview of standards, trials, challenges, deployment, and practice,” *IEEE journal on selected areas in communications*, vol. 35, no. 6, pp. 1201–1221, 2017.

[26] T. L. Marzetta, “Noncooperative cellular wireless with unlimited numbers of base station antennas,” *IEEE Trans. Wireless Commun.*, vol. 9, no. 11, pp. 3590–3600, Oct. 2010.

[27] P. Omiyi, H. Haas, and G. Auer, “Analysis of TDD cellular interference mitigation using busy-bursts,” *IEEE Trans. Wireless Commun.*, vol. 6, no. 7, pp. 2721–2731, Jul. 2007.

[28] H. Pennanen, A. Tolli, and M. Latva-Aho, “Decentralized coordinated downlink beamforming via primal decomposition,” *IEEE Signal Processing Letters*, vol. 18, no. 11, pp. 647–650, 2011.

[29] H. Pennanen, A. Tölli, and M. Latva-aho, “Multi-cell beamforming with decentralized coordination in cognitive and cellular networks,” *IEEE transactions on signal processing*, vol. 62, no. 2, pp. 295–308, 2013.

[30] X. Jiang, A. Decurninge, K. Gopala, F. Kaltenberger, M. Guillaud, D. Slock, and L. Deneire, “A framework for over-the-air reciprocity calibration for tdd massive mimo systems,” *IEEE Transactions on Wireless Communications*, vol. 17, no. 9, pp. 5975–5990, 2018.

[31] 3GPP, “ NR; Base Station (BS) radio transmission and reception. TS 38.104,” 3rd Generation Partnership Project 3GPP, www.3gpp.org, Tech. Rep., 2019.

[32] ——, “ NR; Requirements for support of radio resource management. TS 38.133,” 3rd Generation Partnership Project 3GPP, www.3gpp.org, Tech. Rep., 2019.

[33] Z. Shen, A. Khoryaev, E. Eriksson, and X. Pan, “Dynamic uplink-downlink configuration and interference management in TD-LTE,” *IEEE Commun. Mag.*, vol. 50, no. 11, pp. 51–59, Nov. 2012.

[34] T. Nakamura, S. Nagata, A. Benjebbour, Y. Kishiyama, T. Hai, S. Xiaodong, Y. Ning, and L. Nan, “Trends in small cell enhancements in LTE advanced,” *IEEE Commun. Mag.*, vol. 51, no. 2, pp. 98–105, Feb. 2013.

[35] Y. Kishiyama, A. Benjebbour, T. Nakamura, and H. Ishii, "Future steps of lte-a: evolution toward integration of local area and wide area systems," *IEEE wireless communications*, vol. 20, no. 1, pp. 12–18, 2013.

[36] A. Tolli, H. Ghauch, J. Kaleva, P. Komulainen, M. Bengtsson, M. Skoglund, M. Honig, E. Lahetkangas, E. Tiirola, and K. Pajukoski, "Distributed coordinated transmission with forward-backward training for 5g radio access," *IEEE Communications Magazine*, vol. 57, no. 1, pp. 58–64, 2019.

[37] P. Komulainen, A. Tölli, and M. Juntti, "Effective CSI signaling and decentralized beam coordination in TDD multi-cell MIMO systems," *IEEE Trans. Signal Processing*, vol. 61, no. 9, pp. 2204–2218, May. 2013.

[38] D. A. Schmidt, C. Shi, R. A. Berry, M. L. Honig, and W. Utschick, "Distributed resource allocation schemes," *IEEE Signal Processing Magazine*, vol. 26, no. 5, pp. 53–63, 2009.

[39] C. Shi, R. A. Berry, and M. L. Honig, "Bi-Directional Training for Adaptive Beamforming and Power Control in Interference Networks," *IEEE Trans. Signal Processing*, vol. 62, pp. 607–618, Feb. 2014.

[40] M. Xu, D. Guo, and M. Honig, "Distributed bi-directional training of nonlinear precoders and receivers in cellular networks," *IEEE Transactions on Signal Processing*, vol. 63, no. 21, pp. 5597–5608, 2015.

[41] 3GPP, " NR; Physical channels and modulation ," 3rd Generation Partnership Project 3GPP, www.3gpp.org, Tech. Rep., 2019.

[42] N. Bhushan, J. Li, D. Malladi, R. Gilmore, D. Brenner, A. Damnjanovic, R. T. Sukhavasi, C. Patel, and S. Geirhofer, "Network densification: the dominant theme for wireless evolution into 5g," *IEEE Communications Magazine*, vol. 52, no. 2, pp. 82–89, 2014.

[43] X. Ge, S. Tu, G. Mao, C. X. Wang, and T. Han, "5g ultra-dense cellular networks," *IEEE Wireless Communications*, vol. 23, no. 1, pp. 72–79, 2016.

[44] C. Dehos, J. L. González, A. De Domenico, D. Ktenas, and L. Dussopt, "Millimeter-wave access and backhauling: the solution to the exponential data traffic increase in 5g mobile communications systems?" *IEEE Communications Magazine*, vol. 52, no. 9, pp. 88–95, 2014.

[45] Y. Li, E. Pateromichelakis, N. Vucic, J. Luo, W. Xu, and G. Caire, "Radio resource management considerations for 5g millimeter wave backhaul and access networks," *IEEE Communications Magazine*, vol. 55, no. 6, pp. 86–92, 2017.

[46] S. Parkvall, Y. Blankenship, R. Blasco, E. Dahlman, G. Fodor, S. Grant, E. Stare, and M. Stattin, "5g nr release 16: Start of the 5g evolution," *IEEE Communications Standards Magazine*, vol. 4, no. 4, pp. 56–63, 2020.

[47] 3GPP, " Study on Integrated Access and Backhaul for NR TR 38.874," 3rd Generation Partnership Project 3GPP, www.3gpp.org, Tech. Rep., 2018.

[48] ——, " NR; Background for integrated access and backhaul radio transmission and reception ," 3rd Generation Partnership Project 3GPP, www.3gpp.org, Tech. Rep., 2020.

[49] ——, " NR; Integrated Access and Backhaul (IAB) radio transmission and reception ," 3rd Generation Partnership Project 3GPP, www.3gpp.org, Tech. Rep., 2019.

[50] M. Polese, M. Giordani, T. Zugno, A. Roy, S. Goyal, D. Castor, and M. Zorzi, "Integrated access and backhaul in 5g mmwave networks: Potential and challenges," *IEEE Communications Magazine*, vol. 58, no. 3, pp. 62–68, 2020.

[51] C. Madapatha, B. Makki, C. Fang, O. Teyeb, E. Dahlman, M. S. Alouini, and T. Svensson, "On integrated access and backhaul networks: Current status and potentials," *IEEE Open Journal of the Communications Society*, vol. 1, pp. 1374–1389, 2020.

[52] C. Saha, M. Afshang, and H. S. Dhillon, "Integrated mmWave Access and Backhaul in 5G: Bandwidth Partitioning and Downlink Analysis," in *IEEE Int. Conf. on Commun. (ICC)*. IEEE, May. 2018, pp. 1–6.

[53] J. A. Stankovic, "Research Directions for the Internet of Things," *IEEE Internet Things J.*, vol. 1, no. 1, pp. 3–9, Mar. 2014.

[54] Y. Siriwardhana, C. De Alwis, G. Gür, M. Ylianttila, and M. Liyanage, "The fight against the covid-19 pandemic with 5g technologies," *IEEE Engineering Management Review*, vol. 48, no. 3, pp. 72–84, 2020.

[55] P. Mogensen, K. Pajukoski, E. Tiirola, E. Lähetkangas, J. Vihriälä, S. Vesterinen, M. I. Laitila, G. Berardinelli, G. W. O. Da Costa, L. G. U. Garcia *et al.*, "5g small cell optimized radio design," in *2013 IEEE Globecom Workshops (GC Wkshps)*. IEEE, 2013, pp. 111–116.

[56] I. Hwang, B. Song, and S. S. Soliman, "A holistic view on hyper-dense heterogeneous and small cell networks," *IEEE Communications Magazine*, vol. 51, no. 6, pp. 20–27, 2013.

[57] B. Yang, G. Mao, M. Ding, X. Ge, and X. Tao, "Dense small cell networks: From noise-limited to dense interference-limited," *IEEE Transactions on Vehicular Technology*, vol. 67, no. 5, pp. 4262–4277, 2018.

[58] J. Liu, M. Sheng, L. Liu, and J. Li, "Network densification in 5g: From the short-range communications perspective," *IEEE Communications Magazine*, vol. 55, no. 12, pp. 96–102, 2017.

[59] S. Chen and J. Zhao, "The requirements, challenges, and technologies for 5G of terrestrial mobile telecommunication," *IEEE Commun. Mag.*, vol. 52, no. 5, pp. 36–43, May. 2014.

[60] M. Ding, D. Lopez-Perez, H. Claussen, and M. A. Kaafar, "On the fundamental characteristics of ultra-dense small cell networks," *IEEE Network*, vol. 32, no. 3, pp. 92–100, 2018.

[61] J. Li, S. Farahvash, M. Kavehrad, and R. Valenzuela, "Dynamic TDD and fixed cellular networks," *IEEE Commun. Lett.*, vol. 4, no. 7, pp. 218–220, Jul. 2000.

[62] B. Yu, S. Mukherjee, H. Ishii, and L. Yang, "Dynamic TDD support in the LTE-B enhanced Local Area architecture," in *IEEE Globecom Workshops*, 2012, pp. 585–591.

[63] 3GPP TSG RAN WG1, "Study on scenarios and requirements for next generation access technologies TR 38.913," 3rd Generation Partnership Project 3GPP, www.3gpp.org, Tech. Rep., 2017.

[64] E. Lahetkangas, K. Pajukoski, J. Vihriala, G. Berardinelli, M. Lauridsen, E. Tiirola, and P. Mogensen, "Achieving low latency and energy consumption by 5G TDD mode optimization," in *IEEE Int. Conf. Commun. Workshops (ICC)*. IEEE, jun. 2014, pp. 1–6.

[65] M. S. ElBamby, M. Bennis, W. Saad, and M. Latva-aho, "Dynamic Uplink-Downlink Optimization in TDD-based Small Cell Networks," in *IEEE Int. Symposium on Wireless Communication Systems (ISWCS)*, 2014.

[66] Y. Choi, I. Sohn, and K. B. Lee, "A novel decentralized time slot allocation algorithm in dynamic TDD system," in *IEEE Consumer Communications and Networking Conference (CCNC)*, vol. 2, 2006, pp. 1268–1272.

[67] I. Sohn, K. B. Lee, and Y. Choi, "Comparison of decentralized time slot allocation strategies for asymmetric traffic in TDD systems," *IEEE Trans. Wireless Commun.*, vol. 8, no. 6, pp. 2990–3003, Jun. 2009.

[68] H. Chung, M. Kim, N. Kim, and S. Yun, "Time slot allocation based on region and time partitioning for dynamic TDD-OFDM systems," in *IEEE Vehi. Tech. Conf. (VTC)*, vol. 5, 2006, pp. 2459–2463.

[69] K. Lee, Y. Park, M. Na, H. Wang, and D. Hong, "Aligned Reverse Frame Structure for Interference Mitigation in Dynamic TDD Systems," *IEEE Trans. Wireless Commun.*, vol. 16, no. 10, pp. 6967–6978, Aug. 2017.

[70] H. Zhang and H. Dai, "Cochannel interference mitigation and cooperative processing in downlink multicell multiuser mimo networks," *EURASIP Journal on Wireless Communications and Networking*, vol. 2004, no. 2, pp. 1–14, 2004.

[71] K. Hosseini, W. Yu, and R. S. Adve, "Large-scale mimo versus network mimo for multicell interference mitigation," *IEEE Journal of Selected Topics in Signal Processing*, vol. 8, no. 5, pp. 930–941, 2014.

[72] E. G. Larsson, O. Edfors, F. Tufvesson, and T. L. Marzetta, "Massive MIMO for next generation wireless systems," *IEEE Commun. Mag.*, vol. 52, no. 2, pp. 186–195, Feb. 2014.

[73] E. Björnson, J. Hoydis, and L. Sanguinetti, "Pilot contamination is not a fundamental asymptotic limitation in massive mimo," in *2017 IEEE International Conference on Communications (ICC)*. IEEE, 2017, pp. 1–6.

[74] L. Sanguinetti, A. L. Moustakas, and M. Debbah, "Interference management in 5G reverse TDD HetNets with wireless backhaul: A large system analysis," *IEEE journal on Sel. Areas in Commun.*, vol. 33, no. 6, pp. 1187–1200, Mar. 2015.

[75] M. Ding, D. L. Perez, A. V. Vasilakos, and W. Chen, "Dynamic TDD transmissions in homogeneous small cell networks," in *IEEE Int. Conf. Commun. Workshops (ICC)*. IEEE, 2014, pp. 616–621.

[76] C. Yoon and D. H. Cho, "Energy efficient beamforming and power allocation in dynamic TDD based C-RAN system," *IEEE Commun. Lett.*, vol. 19, no. 10, pp. 1806–1809, Aug. 2015.

[77] R. A. Berry and E. M. Yeh, "Cross-layer wireless resource allocation," *IEEE Signal Processing mag.*, vol. 21, no. 5, pp. 59–68, Aug. 2004.

[78] M. Chiang, S. H. Low, A. R. Calderbank, and J. C. Doyle, "Layering as optimization decomposition: A mathematical theory of network architectures," *Proceedings of the IEEE*, vol. 95, no. 1, pp. 255–312, Mar. 2007.

[79] M. C. Filippou, P. De Kerret, D. Gesbert, T. Ratnarajah, A. Pastore, and G. A. Ropokis, "Coordinated shared spectrum precoding with distributed CSIT," *IEEE Trans. on Wireless Commun.*, vol. 15, no. 8, pp. 5182–5192, Apr. 2016.

[80] S. S. Christensen, R. Agarwal, E. Carvalho, and J. M. Cioffi, "Weighted sum-rate maximization using weighted MMSE for MIMO-BC beamforming design," *IEEE Trans. Wireless Commun.*, vol. 7, no. 12, pp. 4792–4799, Dec. 2008.

[81] Q. Shi, M. Razaviyayn, Z. Luo, and C. He, "An iteratively weighted MMSE approach to distributed sum-utility maximization for a MIMO interfering broadcast channel," *IEEE Trans. Signal Processing*, vol. 59, no. 9, pp. 4331–4340, Sept. 2011.

[82] F. Negro, I. Ghauri, and D. Slock, "Sum rate maximization in the noisy mimo interfering broadcast channel with partial csit via the expected weighted mse," in *2012 International Symposium on Wireless Communication Systems (ISWCS)*, 2012, pp. 576–580.

[83] D. A. Schmidt, C. Shi, R. A. Berry, M. L. Honig, and W. Utschick, "Comparison of distributed beamforming algorithms for MIMO interference networks," *IEEE Trans. Signal Processing*, vol. 61, no. 13, pp. 3476–3489, Jul. 2013.

[84] O. Tervo, L. N. Tran, and M. Juntti, "Optimal energy-efficient transmit beamforming for multi-user MISO downlink," *IEEE Trans. Signal Processing*, vol. 63, no. 20, pp. 5574–5588, Jul. 2015.

[85] J. Kaleva, A. Tölli, and M. Juntti, "Decentralized sum rate maximization with QoS constraints for interfering broadcast channel via successive convex approximation," *IEEE Trans. Signal Processing*, vol. 64, no. 11, pp. 2788–2802, Jun. 2016.

[86] G. Venkatraman, A. Tölli, M. Juntti, and L. N. Tran, "Traffic aware resource allocation schemes for multi-cell MIMO-OFDM systems," *IEEE Trans. Signal Processing*, vol. 64, no. 11, pp. 2730–2745, Jun. 2016.

[87] J. Jose, A. Ashikhmin, P. Whiting, and S. Vishwanath, "Channel estimation and linear precoding in multiuser multiple-antenna TDD systems," *IEEE Trans. Vehi. Tech.*, vol. 60, no. 5, pp. 2102–2116, Apr. 2011.

[88] M. Biguesh and A. B. Gershman, "Training-based MIMO channel estimation: a study of estimator tradeoffs and optimal training signals," *IEEE Trans. Signal Processing*, vol. 54, no. 3, pp. 884–893, Feb. 2006.

[89] R. Brandt and M. Bengtsson, "Distributed CSI acquisition and coordinated precoding for TDD multicell MIMO systems," *IEEE Trans. Vehi. Tech.*, vol. 65, no. 5, pp. 2890–2906, May. 2016.

[90] R. R. Müller, L. Cottatellucci, and M. Vehkaperä, "Blind pilot decontamination," *IEEE J. Select Topics Signal Processing*, vol. 8, no. 5, pp. 773–786, Mar. 2014.

[91] E. Björnson, E. De Carvalho, J. H. Sørensen, E. G. Larsson, and P. Popovski, "A random access protocol for pilot allocation in crowded massive mimo systems," *IEEE Transactions on Wireless Communications*, vol. 16, no. 4, pp. 2220–2234, 2017.

[92] H. Q. Ngo, T. L. Marzetta, and E. G. Larsson, "Analysis of the pilot contamination effect in very large multicell multiuser MIMO systems for physical channel models," in *IEEE Int. Conf. Acoustics, Speech and Signal Processing (ICASSP)*, 2011, pp. 3464–3467.

[93] J. Jose, A. Ashikhmin, T. L. Marzetta, and S. Vishwanath, "Pilot contamination and precoding in multi-cell TDD systems," *IEEE Trans. Wireless Commun.*, vol. 10, no. 8, pp. 2640–2651, Aug. 2011.

[94] J. H. Sørensen and E. De Carvalho, "Pilot decontamination through pilot sequence hopping in massive mimo systems," in *2014 IEEE Global Communications Conference*. IEEE, 2014, pp. 3285–3290.

[95] H. Yin, D. Gesbert, M. C. Filippou, and Y. Liu, "Decontaminating pilots in massive MIMO systems," in *IEEE Int. Conf. Commun. (ICC)*. IEEE, 2013, pp. 3170–3175.

[96] H. Xu, C. Pan, W. Xu, G. L. Stuber, J. Shi, and M. Chen, "Robust Beamforming with Pilot Reuse Scheduling in a Heterogeneous Cloud Radio Access Network," *IEEE Trans. Vehi. Tech.*, Apr. 2018.

[97] R. Gholami, L. Cottatellucci, and D. Slock, "Tackling pilot contamination in cell-free massive mimo by joint channel estimation and linear multi-user detection," in *2021 IEEE International Symposium on Information Theory (ISIT)*, 2021, pp. 2828–2833.

[98] N. N. Moghadam, H. Shokri-Ghadikolaei, G. Fodor, M. Bengtsson, and C. Fischione, "Pilot precoding and combining in multiuser mimo networks," *IEEE Journal on Selected Areas in Communications*, vol. 35, no. 7, pp. 1632–1648, 2017.

[99] V. Saxena, G. Fodor, and E. Karipidis, "Mitigating pilot contamination by pilot reuse and power control schemes for massive mimo systems," in *2015 IEEE 81st Vehicular Technology Conference (VTC Spring)*. IEEE, 2015, pp. 1–6.

[100] W. Saad, M. Bennis, and M. Chen, "A vision of 6g wireless systems: Applications, trends, technologies, and open research problems," *arXiv preprint arXiv:1902.10265*, Feb. 2019.

[101] D. Hui and J. Axnäs, "Joint routing and resource allocation for wireless self-backhaul in an indoor ultra-dense network," in *IEEE Int. Symp. on Personal, Indoor, and Mobile Radio Commun. (PIMRC)*. IEEE, Nov. 2013, pp. 3083–3088.

[102] R. Baldemair, T. Irnich, K. Balachandran, E. Dahlman, G. Mildh, Y. Selén, S. Parkvall, M. Meyer, and A. Osseiran, "Ultra-dense networks in millimeter-wave frequencies," *IEEE Commun. Mag.*, vol. 53, no. 1, pp. 202–208, Jan. 2015.

[103] 3GPP, " Study on security aspects of Integrated Access and Backhaul (IAB) for Next Radio (NR) TR 33.824," 3rd Generation Partnership Project 3GPP, www.3gpp.org, Tech. Rep., 2019.

[104] J. N. Laneman, D. Tse, and G. W. Wornell, "Cooperative diversity in wireless networks: Efficient protocols and outage behavior," *IEEE Trans on Information theory*, vol. 50, no. 12, pp. 3062–3080, Dec. 2004.

[105] G. Kramer, M. Gastpar, and P. Gupta, "Cooperative strategies and capacity theorems for relay networks," *IEEE Trans. on Information Theory*, vol. 51, no. 9, pp. 3037–3063, Sep. 2005.

[106] A. Sendonaris, E. Erkip, and B. Aazhang, "User cooperation diversity. Part I. System description," *IEEE Trans. Commun.*, vol. 51, no. 11, pp. 1927–1938, Nov. 2003.

[107] R. Nabar, H. Bolcskei, and F. Kneubuhler, "Fading relay channels: Performance limits and space-time signal design," *IEEE J. Select. Areas Commun.*, vol. 22, no. 6, pp. 1099–1109, Aug. 2004.

[108] P. Jayasinghe, L. K. S. Jayasinghe, M. Juntti, and M. Latva-Aho, "Performance analysis of optimal beamforming in fixed-gain AF MIMO relaying over asymmetric fading channels," *IEEE Trans. on commun.*, vol. 62, no. 4, pp. 1201–1217, Feb. 2014.

[109] U. Siddique, H. Tabassum, and E. Hossain, "Downlink spectrum allocation for in-band and out-band wireless backhauling of full-duplex small cells," *IEEE Transactions on Communications*, vol. 65, no. 8, pp. 3538–3554, Aug. 2017.

[110] H. Shen, W. Xu, S. Gong, Z. He, and C. Zhao, "Statistically robust beamforming optimization for multi-antenna full-duplex df relaying," *IEEE Access*, vol. 7, pp. 175 564–175 575, Dec. 2019.

[111] Y. Cai, Y. Xu, Q. Shi, B. Champagne, and L. Hanzo, "Robust joint hybrid transceiver design for millimeter wave full-duplex mimo relay systems," *IEEE Transactions on Wireless Communications*, vol. 18, no. 2, pp. 1199–1215, Feb. 2019.

[112] R. Gupta and S. Kalyanasundaram, "Resource allocation for self-backhauled networks with half-duplex small cells," in *IEEE Int. Conf. on Commun. Workshops (ICC Workshops)*. IEEE, May. 2017, pp. 198–204.

[113] S. Hong, J. Brand, J. I. Choi, M. Jain, J. Mehlman, S. Katti, and P. Levis, "Applications of self-interference cancellation in 5g and beyond," *IEEE Commun. Mag.*, vol. 52, no. 2, pp. 114–121, Feb. 2014.

[114] B. Rankov and A. Wittneben, "Spectral efficient protocols for half-duplex fading relay channels," *IEEE Journal on selected Areas in Communications*, vol. 25, no. 2, pp. 379–389, Feb. 2007.

[115] S. S. Ikki and S. Aissa, "Performance analysis of two-way amplify-and-forward relaying in the presence of co-channel interferences," *IEEE Transactions on Communications*, vol. 60, no. 4, pp. 933–939, Apr. 2012.

[116] K. Jayasinghe, P. Jayasinghe, N. Rajatheva, and M. Latva-Aho, "Secure beamforming design for physical layer network coding based mimo two-way relaying," *IEEE Communications Letters*, vol. 18, no. 7, pp. 1270–1273, Jul. 2014.

[117] J. Kaleva, A. Tölli, and M. Venkatraman, G.and Juntti, "Downlink precoder design for coordinated regenerative multi-user relaying," *IEEE Trans. signal processing*, vol. 61, no. 5, pp. 1215–1229, Mar. 2013.

[118] M. Heino, D. Korpi, T. Huusari, E. Antonio-Rodriguez, S. Venkatasubramanian, T. Riihonen, L. Anttila, C. Icheln, K. Haneda, R. Wichman, and M. Valkama, "Recent advances in antenna design and interference cancellation algorithms for in-band full duplex relays," *IEEE Communications Magazine*, vol. 53, no. 5, pp. 91–101, May. 2015.

[119] A. Sabharwal, P. Schniter, D. Guo, D. W. Bliss, S. Rangarajan, and R. Wichman, "In-band full-duplex wireless: Challenges and opportunities," *IEEE Journal on selected areas in communications*, vol. 32, no. 9, pp. 1637–1652, Jun. 2014.

[120] A. Sharma, R. K. Ganti, and J. K. Milleth, "Joint backhaul-access analysis of full duplex self-backhauling heterogeneous networks," *IEEE Transactions on Wireless Communications*, vol. 16, no. 3, pp. 1727–1740, Mar. 2017.

[121] Z. Zhang, Z. Ma, M. Xiao, G. K. Karagiannidis, Z. Ding, and P. Fan, "Two-Timeslot Two-Way Full-Duplex Relaying for 5G Wireless Communication Networks," *IEEE Transactions on Communications*, vol. 64, no. 7, pp. 2873–2887, Jul. 2016.

[122] R. H. Y. Louie, Y. Li, and B. Vucetic, "Practical physical layer network coding for two-way relay channels: performance analysis and comparison," *IEEE Transactions on Wireless Communications*, vol. 9, no. 2, pp. 764–777, Feb. 2010.

[123] R. Zhang, Y. Liang, C. C. Chai, and S. Cui, "Optimal beamforming for two-way multi-antenna relay channel with analogue network coding," *IEEE Journal on Selected Areas in Communications*, vol. 27, no. 5, pp. 699–712, Jun. 2009.

[124] A. Y. Panah and P. Sartori, "System and method for two-way relaying with beamforming," Apr. 2019, uS Patent 10,256,873.

[125] V. Havary-Nassab, S. Shahbazpanahi, and A. Grami, "Optimal distributed beamforming for two-way relay networks," *IEEE Transactions on Signal Processing*, vol. 58, no. 3, pp. 1238–1250, Mar. 2010.

[126] O. P. Adare, H. Babbili, C. Madapatha, B. Makki, and T. Svensson, "Uplink power control in integrated access and backhaul networks," *arXiv preprint arXiv:2110.07704*, 2021.

[127] C. Madapatha, B. Makki, A. Muhammad, E. D., M. S. Alouini, and T. Svensson, "On topology optimization and routing in integrated access and backhaul networks: A genetic algorithm-based approach," *arXiv preprint arXiv:2102.07252*, 2021.

[128] E. Björnson, J. Hoydis, and L. Sanguinetti, "Pilot contamination is not a fundamental asymptotic limitation in massive mimo," in *2017 IEEE International Conference on Communications (ICC)*. IEEE, 2017, pp. 1–6.

[129] P. Jayasinghe, A. Tölli, J. Kaleva, and M. Latva-aho, "Bi-directional signaling for dynamic TDD with decentralized beamforming," in *IEEE Int. Conf. Commun. Workshop (ICC)*, 2015, pp. 185–190.

[130] P. Jayasinghe, A. Tölli, and M. Latva-aho, "Bi-directional signaling strategies for dynamic TDD networks," in *IEEE Int. Workshp Signal Processing Advances Wireless Commun. (SPAWC)*, 2015, pp. 540–544.

[131] P. Jayasinghe, A. Tölli, J. Kaleva, and M. Latva-aho, "Direct beamformer estimation for dynamic TDD networks with forward-backward training," in *IEEE Int. Workshp Signal Processing Advances Wireless Commun. (SPAWC)*. IEEE, Jul. 2017, pp. 1–6.

[132] P. Jayasinghe, A. Tölli, J. Kaleva, G. Venkatraman, and M. Latva-aho, "Traffic aware pilot de-contamination for multi-cell MIMO systems," in *European Conference on Networks and Communications (EuCNC)*. IEEE, Jun. 2017, pp. 1–6.

[133] P. Jayasinghe, A. Tölli, J. Kaleva, and M. Latva-aho, "Bi-Directional Beamformer Training for Dynamic TDD Networks," *IEEE Trans. Signal Processing*, vol. 66, no. 23, pp. 6252–6267, Dec. 2018.

[134] P. Jayasinghe, A. Tölli, J. Kaleva, and M. Latva-Aho, "Traffic aware beamformer design for flexible tdd-based integrated access and backhaul," *IEEE Access*, vol. 8, pp. 205 534–205 549, 2020.

[135] P. Jayasinghe, A. Tölli, J. Kaleva, and M. Latva-aho, "Traffic aware beamformer design for integrated access and backhaul with flexible tdd," in *2020 IEEE Wireless Communications and Networking Conference (WCNC)*, 2020, pp. 1–6.

[136] K. Jayasinghe, P. Jayasinghe, N. Rajatheva, and M. Latva-Aho, "Linear Precoder-Decoder Design of MIMODevice-to-Device Communication Underlaying Cellular Communication," *IEEE Trans. Commun.*, vol. 62, no. 10, pp. 4304–4319, Dec. 2014.

[137] ——, "Secure beamforming design for physical layer network coding based mimo two-way relaying," *IEEE Communications Letters*, vol. 18, no. 7, pp. 1270–1273, 2014.

[138] K. Jayasinghe, P. Jayasinghe, N. Rajatheva, and M. Latva-aho, "Physical layer security for relay assisted mimo d2d communication," in *2015 IEEE International Conference on Communication Workshop (ICCW)*. IEEE, 2015, pp. 651–656.

[139] A. Roivainen, P. Jayasinghe, J. Meinila, V. Hovinen, and M. Latva-aho, "Vehicle-to-vehicle radio channel characterization in urban environment at 2.3 ghz and 5.25 ghz," in *2014 IEEE 25th Annual International Symposium on Personal, Indoor, and Mobile Radio Communication (PIMRC)*, 2014, pp. 63–67.

[140] P. Jayasinghe, L. K. S. Jayasinghe, M. Juntti, and M. Latva-aho, "Relay selection on dual hop af mimo with ostbc over asymmetric fading channels," in *2014 IEEE Wireless Communications and Networking Conference (WCNC)*, 2014, pp. 1170–1175.

[141] ——, "Effect of cci and feedback delay on the multi-antenna af relaying over asymmetric fading channels," in *2014 IEEE Wireless Communications and Networking Conference (WCNC)*, 2014, pp. 1303–1308.

[142] L. K. S. Jayasinghe, P. Jayasinghe, N. Rajatheva, and M. Latva-aho, "Mimo physical layer network coding based underlay device-to-device communication," in *2013 IEEE 24th Annual International Symposium on Personal, Indoor, and Mobile Radio Communications (PIMRC)*, 2013, pp. 89–94.

[143] P. Jayasinghe, L. S. Jayasinghe, M. Juntti, and M. Latva-aho, "Performance analysis of optimal beamforming in af mimo relaying over asymmetric fading channels," in *2013 IEEE 24th Annual International Symposium on Personal, Indoor, and Mobile Radio Communications (PIMRC)*, 2013, pp. 708–712.

[144] G. Venkatraman, A. Tölli, M. Juntti, and L. Tran, "Multigroup multicast beamformer design for miso-ofdm with antenna selection," *IEEE Transactions on Signal Processing*, vol. 65, no. 22, pp. 5832–5847, Nov. 2017.

[145] C. T. K. Ng and H. Huang, "Linear precoding in cooperative MIMO cellular networks with limited coordination clusters," *IEEE Journal on Selected Areas in Communications*, vol. 28, no. 9, pp. 1446–1454, Dec. 2010.

[146] Z. Q. Luo and S. Zhang, "Dynamic Spectrum Management: Complexity and Duality," *IEEE Journal of Selected Topics in Signal Processing*, vol. 2, no. 1, pp. 57–73, Feb.2008.

[147] S. Shi, M. Schubert, and H. Boche, "Downlink MMSE transceiver optimization for multiuser MIMO systems: Duality and sum-MSE minimization," *IEEE Transactions on Signal Processing*, vol. 55, no. 11, pp. 5436–5446, Nov.2007.

[148] S. Boyd and L. Vandenberghe, *Convex optimization*. Cambridge university press, 2004.

[149] J. Kaleva, A. Tölli, M. Juntti, R. A. Berry, and M. L. Honig, "Decentralized joint precoding with pilot-aided beamformer estimation," *IEEE Transaction on Signal Processing*, vol. 66, no. 9, pp. 2330–2341, Mar. 2018.

[150] J. Peisa, P. Persson, S. Parkvall, E. Dahlman, A. Grovlen, C. Hoymann, and D. Gerstenberger, "5G evolution: 3GPP releases 16 & 17 overview," *Ericsson Technology Review*, vol. 6, pp. 2–13, 2020.

[151] H. Q. Ngo, A. Ashikhmin, H. Yang, E. G. Larsson, and T. L. Marzetta, "Cell-free massive mimo versus small cells," *IEEE Transactions on Wireless Communications*, vol. 16, no. 3, pp. 1834–1850, 2017.

[152] I. Atzeni, B. Gouda, and A. Tölli, "Distributed precoding design via over-the-air signaling for cell-free massive mimo," *IEEE Transactions on Wireless Communications*, vol. 20, no. 2, pp. 1201–1216, Oct. 2020.

[153] R. Ahmed, K. Jayasinghe, and T. Wild, "Comparison of explicit csi feedback schemes for 5g new radio," in *2019 IEEE 89th Vehicular Technology Conference (VTC2019-Spring)*, 2019, pp. 1–5.

[154] R. P. Antonioli, G. Fodor, P. Soldati, and T. F. Maciel, "Decentralized joint beamforming, user scheduling, and qos management in 5g and beyond systems," *IEEE Communications Standards Magazine*, vol. 5, no. 1, pp. 62–69, 2021.

[155] M. Taheribakhsh, A. H. Jafari, M. M. Peiro, and N. Kazemifard, "5g implementation: Major issues and challenges," in *2020 25th International Computer Conference, Computer Society of Iran (CSICC)*, 2020, pp. 1–5.

[156] F. Qamar, M. U. A. Siddiqui, M. H. D. Hindia, R. Hassan, and Q. N. Nguyen, "Issues, challenges, and research trends in spectrum management: A comprehensive overview and new vision for designing 6g networks," *Electronics*, vol. 9, no. 9, p. 1416, 2020.

[157] A. Tölli, J. Kaleva, G. Venkatraman, and D. Gesbert, "Joint ul/dl mode selection and transceiver design for dynamic tdd systems," in *2016 IEEE Global Conference on Signal and Information Processing (GlobalSIP)*, 2016, pp. 630–634.

[158] A. Arvola, S. Joshi, and A. Tölli, "Dynamic ul/dl mode selection and resource allocation in multi-cell mimo tdd systems," in *2019 53rd Asilomar Conference on Signals, Systems, and Computers*, 2019, pp. 1936–1940.

[159] L. Wei, M. Ma, Z. Guo, Y. Fei, and B. Jiao, "Hybrid beamforming design and implementation for mitigating inter-cell interference in flexible duplex cellular system," in *2019 IEEE 30th International Symposium on Personal, Indoor and Mobile Radio Communications (PIMRC Workshops)*, 2019, pp. 1–6.

[160] P. K. Shah, K. Joshi, S. Joshi, A. Tolli, and K. Umebayashi, “Direct beamformer estimation for hybrid architecture in mmwave dynamic tdd system,” in *2020 IEEE Wireless Communications and Networking Conference Workshops (WCNCW)*, 2020, pp. 1–6.

[161] I. Atzeni and A. Tölli, “Uplink data detection analysis of 1-bit quantized massive mimo,” in *2021 IEEE 22nd International Workshop on Signal Processing Advances in Wireless Communications (SPAWC)*, 2021, pp. 371–375.

[162] C. K. Wen, C. J. Wang, S. Jin, K. K. Wong, and P. Ting, “Bayes-optimal joint channel-and-data estimation for massive mimo with low-precision adcs,” *IEEE Transactions on Signal Processing*, vol. 64, no. 10, pp. 2541–2556, 2016.

Appendix 1

1.0.1 MSE, received signal covariance and MMSE receiver expressions for Rx2-Rx6

MSE expressions for receiver type Rx2-Rx6 given by

$$\varepsilon_{k,l}^{(s,a)}/\varepsilon_{i,l}^{(a)} = \begin{cases} 1-2\Re(\mathbf{u}_{k,l}^{(\mathrm{ul},1)^{\mathrm{H}}}\mathbf{H}_{i,k}^{\mathrm{H}}\mathbf{m}_{k,l}^{(\mathrm{ul},1)})+\mathbf{u}_{k,l}^{(\mathrm{ul},1)^{\mathrm{H}}}\mathbf{M}_{i}^{(\mathrm{ul},1)}\mathbf{u}_{k,l}^{(\mathrm{ul},1)}, & \mathrm{Rx2} \\ 1-2\Re(\mathbf{w}_{i,l}^{(\mathrm{dl})^{\mathrm{H}}}\hat{\mathbf{H}}_{1,i}\mathbf{v}_{i,l}^{(\mathrm{dl})})+\mathbf{w}_{i,l}^{(\mathrm{dl})^{\mathrm{H}}}\mathbf{M}_{i}^{(\mathrm{ul},1)}\mathbf{w}_{i,l}^{(\mathrm{dl})}, & \mathrm{Rx3} \\ 1-2\Re(\mathbf{u}_{k,l}^{(\mathrm{ul},2)^{\mathrm{H}}}\mathbf{H}_{1,k}^{\mathrm{H}}\mathbf{m}_{k,l}^{(\mathrm{ul},2)})+\mathbf{u}_{k,l}^{(\mathrm{ul},2)^{\mathrm{H}}}\mathbf{M}_{1}^{(\mathrm{ul},2)}\mathbf{u}_{k,l}^{(\mathrm{ul},2)}, & \mathrm{Rx4} \\ 1-2\Re(\mathbf{u}_{k,l}^{(\mathrm{dl},2)^{\mathrm{H}}}\mathbf{H}_{i,k}\mathbf{m}_{k,l}^{(\mathrm{dl},2)})+\mathbf{u}_{k,l}^{(\mathrm{dl},2)^{\mathrm{H}}}\mathbf{M}_{k}^{(\mathrm{dl},2)}\mathbf{u}_{k,l}^{(\mathrm{dl},2)}, & \mathrm{Rx5} \\ 1-2\Re(\mathbf{w}_{i,l}^{(\mathrm{ul})^{\mathrm{H}}}\hat{\mathbf{H}}_{1,i}^{\mathrm{H}}\mathbf{v}_{i,l}^{(\mathrm{ul})})+\mathbf{w}_{k,l}^{(\mathrm{ul})^{\mathrm{H}}}\mathbf{M}_{1}^{(\mathrm{ul},2)}\mathbf{w}_{i,l}^{(\mathrm{ul})}, & \mathrm{Rx6} \end{cases} \tag{86}$$

where $\mathbf{M}_{i}^{(\mathrm{ul},1)} = \mathbb{E}[\mathbf{x}_{i}^{(\mathrm{ul},1)}(\mathbf{x}_{i}^{(\mathrm{ul},1)})^{\mathrm{H}}]$, $\mathbf{M}_{1}^{(\mathrm{ul},2)} = \mathbb{E}[\mathbf{x}_{1}^{(\mathrm{ul},2)}(\mathbf{x}_{1}^{(\mathrm{ul},2)})^{\mathrm{H}}]$, and $\mathbf{M}_{k}^{(\mathrm{dl},2)} = \mathbb{E}[\mathbf{x}_{k}^{(\mathrm{dl},2)}(\mathbf{x}_{k}^{(\mathrm{dl},2)})^{\mathrm{H}}]$ are the received signal covariance matrices at each node, which are given in (87).

$$\begin{aligned} \mathbf{M}_{i}^{(\mathrm{ul},1)} =& \hat{\mathbf{H}}_{1,i}\Big(\sum_{j\in\mathsf{U}_1}\sum_{n=1}^{L_j}\mathbf{m}_{j,n}^{(\mathrm{dl},1)}(\mathbf{m}_{j,n}^{(\mathrm{dl},1)})^{\mathrm{H}}+\sum_{r=2}^{N}\sum_{n=1}^{\bar{L}_r}\mathbf{v}_{r,n}^{(\mathrm{dl})}(\mathbf{v}_{r,n}^{(\mathrm{dl})})^{\mathrm{H}}\Big)\hat{\mathbf{H}}_{1,i}^{\mathrm{H}} \\ &+\sum_{r=2}^{N}\sum_{j\in\mathsf{U}_r}\sum_{n=1}^{L_j}\mathbf{H}_{i,j}^{\mathrm{H}}\mathbf{m}_{j,n}^{(\mathrm{ul},1)}(\mathbf{H}_{i,j}^{\mathrm{H}}\mathbf{m}_{j,n}^{(\mathrm{ul},1)})^{\mathrm{H}}+\mathsf{N}_0\mathbf{I}. \\ \mathbf{M}_{1}^{(\mathrm{ul},2)} =& \sum_{r=2}^{N}\hat{\mathbf{H}}_{1,r}^{\mathrm{H}}\Big(\sum_{n=1}^{\bar{L}_r}\mathbf{v}_{r,n}^{(\mathrm{ul})}(\mathbf{v}_{r,n}^{(\mathrm{ul})})^{\mathrm{H}}+\sum_{j\in\mathsf{U}_r}\sum_{n=1}^{L_j}\mathbf{m}_{j,n}^{(\mathrm{dl},2)}(\mathbf{m}_{j,n}^{(\mathrm{dl},2)})^{\mathrm{H}}\Big)\hat{\mathbf{H}}_{1,r} \\ &+\sum_{j\in\mathsf{U}_1}\sum_{n=1}^{L_j}\mathbf{H}_{1,j}^{\mathrm{H}}\mathbf{m}_{j,n}^{(\mathrm{ul},2)}(\mathbf{H}_{1,j}^{\mathrm{H}}\mathbf{m}_{j,n}^{(\mathrm{ul},2)})^{\mathrm{H}}+\mathsf{N}_0\mathbf{I}. \\ \mathbf{M}_{k}^{(\mathrm{dl},2)} =& \sum_{r=1}^{N}\mathbf{H}_{r,k}\Big(\sum_{n=1}^{\bar{L}_r}\mathbf{v}_{r,n}^{(\mathrm{ul})}(\mathbf{v}_{r,n}^{(\mathrm{ul})})^{\mathrm{H}}+\sum_{j\in\mathsf{U}_r}\sum_{n=1}^{L_j}\mathbf{m}_{j,n}^{(\mathrm{dl},2)}(\mathbf{m}_{j,n}^{(\mathrm{dl},2)})^{\mathrm{H}}\Big)\mathbf{H}_{r,k}^{\mathrm{H}} \\ &+\sum_{j\in\mathsf{U}_1}\sum_{n=1}^{L_j}\tilde{\mathbf{H}}_{j,k}^{\mathrm{H}}\mathbf{m}_{j,n}^{(\mathrm{ul},2)}(\tilde{\mathbf{H}}_{j,k}^{\mathrm{H}}\mathbf{m}_{j,n}^{(\mathrm{ul},2)})^{\mathrm{H}}+\mathsf{N}_0\mathbf{I}. \end{aligned} \tag{87}$$

Then, the corresponding MMSE receivers are given by

$$\tilde{\mathbf{u}}_{k,l}^{(a,s)}/\tilde{\mathbf{w}}_{i,l}^{(a)} = \begin{cases} (\mathbf{M}_i^{(\mathrm{ul},1)})^{-1}\mathbf{H}_{i,k}^{\mathrm{H}}\mathbf{m}_{k,l}^{(\mathrm{ul},1)}, & \text{Rx2} \\ (\mathbf{M}_i^{(\mathrm{ul},1)})^{-1}\hat{\mathbf{H}}_{1,i}\mathbf{v}_{i,l}^{(\mathrm{dl})}, & \text{Rx3} \\ (\mathbf{M}_1^{(\mathrm{ul},2)})^{-1}\mathbf{H}_{1,k}^{\mathrm{H}}\mathbf{m}_{k,l}^{(\mathrm{ul},2)}, & \text{Rx4} \\ (\mathbf{M}_k^{(\mathrm{dl},2)})^{-1}\mathbf{H}_{i,k}\mathbf{m}_{k,l}^{(\mathrm{dl},2)}, & \text{Rx5} \\ (\mathbf{M}_1^{(\mathrm{ul},2)})^{-1}\hat{\mathbf{H}}_{1,i}^{\mathrm{H}}\mathbf{v}_{i,l}^{(\mathrm{ul})}. & \text{Rx6} \end{cases} \tag{88}$$

1.0.2 Expressions for Υ

For Rx2-Rx6, Υ is given by

$$\Upsilon = \begin{cases} \alpha_k^{(\mathrm{ul})}[(Q_k^{(\mathrm{ul})} - \sum_{l=1}^{L_k} J_0 t_{k,l}^{(\mathrm{ul},1)})^{q-1} - (\bar{Q}_k^{(\mathrm{ul})} \\ + \sum_{l=1}^{L_k} J_0 t_{k,l}^{(\mathrm{ul},1)} - \sum_{l=1}^{\bar{L}_i} a_k^{(\mathrm{ul})} J_0 t_{i,l}^{(\mathrm{ul})})^{q-1}]^+, & \text{Rx2} \\ [\sum_{k\in\mathsf{U}_i} \alpha_k^{(\mathrm{dl})} a_k^{(\mathrm{dl})}((Q_k^{(\mathrm{dl})} - \sum_{l=1}^{\bar{L}_i} a_k^{(\mathrm{dl})} J_0 t_{i,l}^{(\mathrm{dl})})^{q-1} \\ -(\bar{Q}_k^{(\mathrm{dl})} + \sum_{l=1}^{\bar{L}_i} a_k^{(\mathrm{dl})} J_0 t_{i,l}^{(\mathrm{dl})} - \sum_{l=1}^{L_k} J_0 t_{k,l}^{(\mathrm{dl},2)})^{q-1})]^+, & \text{Rx3} \\ \alpha_k^{(\mathrm{ul})}[(Q_k^{(\mathrm{ul})} - \sum_{l=1}^{L_k} J_0 t_{k,l}^{(\mathrm{ul},2)})^{q-1}]^+, & \text{Rx4} \\ \alpha_k^{(\mathrm{dl})}[(\bar{Q}_k^{(\mathrm{dl})} + \sum_{l=1}^{\bar{L}_i} a_k^{(\mathrm{dl})} J_0 t_{i,l}^{(\mathrm{dl})} - \sum_{l=1}^{L_k} J_0 t_{k,l}^{(\mathrm{dl},2)})^{q-1}]^+, & \text{Rx5} \\ [\sum_{k\in\mathsf{U}_i} \alpha_k^{(\mathrm{ul})} a_k^{(\mathrm{ul})}((\bar{Q}_k^{(\mathrm{ul})} + \sum_{l=1}^{L_k} J_0 t_{k,l}^{(\mathrm{ul},1)} \\ - \sum_{l=1}^{\bar{L}_i} a_k^{(\mathrm{ul})} J_0 t_{i,l}^{(\mathrm{ul})})^{q-1})]^+, & \text{Rx6} \end{cases} \tag{89}$$

1.0.3 Transmit precoder expressions for Tx2-Tx6

Expressions for transmit precoders are given by

$$\mathbf{m}_{k,l}^{(a,s)}/\mathbf{v}_{i,l}^{(a)} = \begin{cases} \left(\mathbf{\Phi}_k^{(\mathrm{ul},1)} + \nu_k^{(\mathrm{ul},1))}\mathbf{I}\right)^{-1} \omega_{k,l}^{(\mathrm{ul},1))}\mathbf{H}_{i,k}\mathbf{u}_{k,l}^{(\mathrm{ul},1)}, & \text{Tx2} \\ \left(\mathbf{\Phi}_1^{(\mathrm{dl},1)} + \nu_1^{(\mathrm{dl},1)}\mathbf{I}\right)^{-1} \omega_{i,l}^{(\mathrm{dl})}\hat{\mathbf{H}}_{1,i}^{\mathrm{H}}\mathbf{w}_{i,l}^{(\mathrm{dl})}, & \text{Tx3} \\ \left(\mathbf{\Phi}_k^{(\mathrm{ul},2)} + \nu_k^{(\mathrm{ul},2)}\mathbf{I}\right)^{-1} \omega_{k,l}^{(\mathrm{ul},2)}\mathbf{H}_{1,k}\mathbf{u}_{k,l}^{(\mathrm{ul},2)}, & \text{Tx4} \\ \left(\mathbf{\Phi}_i^{(\mathrm{dl},2)} + \nu_i^{(\mathrm{dl},2)}\mathbf{I}\right)^{-1} \omega_{k,l}^{(\mathrm{dl},2)}\mathbf{H}_{i,k}^{\mathrm{H}}\mathbf{u}_{k,l}^{(\mathrm{dl},2)}, & \text{Tx5} \\ \left(\mathbf{\Phi}_i^{(\mathrm{dl},2)} + \nu_i^{(\mathrm{dl},2)}\mathbf{I}\right)^{-1} \omega_{i,l}^{(\mathrm{ul})}\mathbf{H}_{1,i}\mathbf{w}_{k,l}^{(\mathrm{ul})}. & \text{Tx6} \end{cases} \tag{90}$$

where $\mathbf{\Phi}_k^{(\mathrm{ul},1)}$, $\mathbf{\Phi}_k^{(\mathrm{ul},2)}$ and $\mathbf{\Phi}_i^{(\mathrm{dl},2)}$ are the weighted transmit covariance matrices, which are given in (91) . In addition, $v_k^{((\mathrm{ul},1)}$, $v_k^{(\mathrm{ul},2)}$ and $v_i^{(\mathrm{dl},2)}$ are the dual variables corresponding to the power constraints in (63b), (63d) and (63e), respectively.

$$
\begin{aligned}
\mathbf{\Phi}_k^{(\mathrm{ul},1)} &= \sum_{j\in\mathsf{U}_1}\sum_{l=1}^{L_j}\omega_{j,l}^{(\mathrm{dl},1)}\tilde{\mathbf{H}}_{j,k}^{\mathrm{H}}\mathbf{u}_{j,l}^{(\mathrm{dl},1)}(\tilde{\mathbf{H}}_{j,k}^{\mathrm{H}}\mathbf{u}_{j,l}^{(\mathrm{dl},1)})^{\mathrm{H}}+\sum_{i=2}^{N}\mathbf{H}_{i,k}(\sum_{l=1}^{\bar{L}_i}\omega_{i,l}^{(\mathrm{dl})}\mathbf{w}_{i,l}^{(\mathrm{dl})}(\mathbf{w}_{i,l}^{(\mathrm{dl})})^{\mathrm{H}} \\
&\quad+\sum_{j\in\mathsf{U}_i}\sum_{l=1}^{L_j}\omega_{j,l}^{(\mathrm{ul},1)}\mathbf{u}_{j,l}^{(\mathrm{ul},1)}(\mathbf{u}_{j,l}^{(\mathrm{ul},1)})^{\mathrm{H}})\mathbf{H}_{i,k}^{\mathrm{H}}. \\
\mathbf{\Phi}_k^{(\mathrm{ul},2)} &= \sum_{i=2}^{N}\sum_{j\in\mathsf{U}_i}\sum_{n=1}^{L_j}\omega_{j,l}^{(\mathrm{dl},2)}\tilde{\mathbf{H}}_{j,k}^{\mathrm{H}}\mathbf{w}_{j,l}^{(\mathrm{dl},2)}(\tilde{\mathbf{H}}_{j,k}^{\mathrm{H}}\mathbf{w}_{j,l}^{(\mathrm{dl},2)})^{\mathrm{H}}+\mathbf{H}_{1,k}(\sum_{i=2}^{N}\sum_{l=1}^{\bar{L}_i}\omega_{i,l}^{(\mathrm{ul})}\mathbf{w}_{i,l}^{(\mathrm{ul})}(\mathbf{w}_{i,l}^{(\mathrm{ul})})^{\mathrm{H}} \\
&\quad+\sum_{j\in\mathsf{U}_1}\sum_{l=1}^{L_j}\omega_{j,l}^{(\mathrm{ul},2)}\mathbf{u}_{j,l}^{(\mathrm{ul},2)}(\mathbf{u}_{j,l}^{(\mathrm{ul},2)})^{\mathrm{H}})\mathbf{H}_{1,k}^{\mathrm{H}}. \\
\mathbf{\Phi}_i^{(\mathrm{dl},2)} &= \sum_{r=2}^{N}\sum_{j\in\mathsf{U}_r}\sum_{n=1}^{L_j}\omega_{j,l}^{(\mathrm{dl},2)}\mathbf{H}_{i,j}^{\mathrm{H}}\mathbf{w}_{j,l}^{(\mathrm{dl},2)}(\mathbf{H}_{i,j}^{\mathrm{H}}\mathbf{w}_{j,l}^{(\mathrm{dl},2)})^{\mathrm{H}}+\mathbf{H}_{1,i}(\sum_{i=2}^{N}\sum_{l=1}^{\bar{L}_i}\omega_{i,l}^{(\mathrm{ul})}\mathbf{w}_{i,l}^{(\mathrm{ul})}(\mathbf{w}_{i,l}^{(\mathrm{ul})})^{\mathrm{H}} \\
&\quad+\sum_{j\in\mathsf{U}_1}\sum_{l=1}^{L_j}\omega_{j,l}^{(\mathrm{ul},2)}\mathbf{u}_{j,l}^{(\mathrm{ul},2)}(\mathbf{u}_{j,l}^{(\mathrm{ul},2)})^{\mathrm{H}})\mathbf{H}_{1,i}^{\mathrm{H}}.
\end{aligned}
\tag{91}
$$

816. Okwuibe, Jude (2021) Software-defined resource management for industrial internet of things

817. Luttinen, Esko (2022) Spectrum as a resource, spectrum as an asset : a techno-economic study

818. Darabi, Hamid (2022) Machine learning techniques for urban flood risk assessment

819. Tervo, Nuutti (2022) Concepts for radiated nonlinear distortion and spatial linearization in millimeter-wave phased arrays

820. Nissilä, Tuukka (2022) Ice-templated cellulose nanofiber structures as reinforcement material in composites

821. Yu, Zitong (2022) Physiological signals measurement and spoofing detection from face video

822. Chen, Haoyu (2022) Human gesture and micro-gesture analysis : datasets, methods, and applications

823. Khan, Iqra Sadaf (2022) Exploring Industry 4.0 and its impact on sustainability and collaborative innovation

824. Peng, Wei (2022) Automatic neural network learning for human behavior understanding

825. Zhang, Ruichi (2022) Vanadium removal and recovery from liquid waste streams

826. Väätäjä, Maria (2022) Prospects of the room temperature fabrication method for electroceramics : feasibility for printing techniques and integration with temperature-sensitive materials

827. Li, Yante (2022) Machine learning for perceiving facial micro-expression

828. Behzad, Muzammil (2022) Deep learning methods for analyzing vision-based emotion recognition from 3D/4D facial point clouds

829. Leppänen, Tero (2022) From industrial side streams to the circular economy business : value chain, business ecosystem and productisation approach

830. Tuomela, Anne (2022) Enhancing the safety and surveillance of tailings storage facilities in cold climates

831. Kumar, Dileep (2022) Latency and reliability aware radio resource allocation for multi-antenna systems

832. Niu, He (2022) Valorization of mining wastes in alkali-activated materials

Book orders:
Virtual book store
http://verkkokauppa.juvenesprint.fi

UNIVERSITY OF OULU P.O. Box 8000 FI-90014 UNIVERSITY OF OULU FINLAND

ACTA UNIVERSITATIS OULUENSIS

ISBN 978-952-62-3349-9 (Paperback)
ISBN 978-952-62-3350-5 (PDF)
ISSN 0355-3213 (Print)
ISSN 1796-2226 (Online)

UNIVERSITY OF OULU